

Continuum Mechanical Modeling of Dry Granular Systems: From Dilute Flow to Solid-Like Behavior

vom Fachbereich Maschinenbau und Verfahrenstechnik
der Technischen Universität Kaiserslautern
zur Verleihung des akademischen Grades
Doktor-Ingenieur (Dr.-Ing.)
genehmigte Dissertation

von
Dipl.-Ing. Clément Zémerli
aus Lyon

Hauptreferent: Prof. Arnulf Latz
Korreferenten: PD. Dr. Heiko Andrä
Prof. Dr.-Ing Ralf Müller
Vorsitzender: Prof. Dr.-Ing. Siegfried Ripperger
Dekan: Prof. Dr.-Ing. Bernd Sauer

Tag der Einreichung: 05.03.2013
Tag der mündlichen Prüfung: 05.07.2013

Kaiserslautern, 2013

Herausgeber

Lehrstuhl für Technische Mechanik
Technische Universität Kaiserslautern
Gottlieb-Daimler-Straße
Postfach 3049
67653 Kaiserslautern

© Clément Zémerli

Ich danke der Prof. Dr. Hans Georg und Liselotte Hahn Stiftung für die finanzielle Unterstützung bei der Drucklegung.

Druck

Technische Universität Kaiserslautern
ZTB – Abteilung Foto-Repro-Druck

Alle Rechte vorbehalten, auch das des auszugsweisen Nachdrucks, der auszugsweisen oder vollständigen Wiedergabe (Photographie, Mikroskopie), der Speicherung in Datenverarbeitungsanlagen und das der Übersetzung.

ISBN 978-3-942695-07-7

Foreword

I would like to express my deep and sincere gratitude to Prof. Dr. Arnulf Latz and PD Dr. Heiko Andrä for their guidance and support during these three years. The quality of their remarks and their wide knowledge have a significant value. I want to thank Prof. Dr.-Ing. Ralf Müller for the interesting remarks and suggestions about this work.

I want to express my sincere thanks to Dr. Konrad Steiner, head of the department Flow and Material Simulation (Fraunhofer ITWM, Kaiserslautern) who gave me the opportunity to do this PhD. I am grateful to Dr. Dariusz Niedziela and Dr. Sebastian Schmidt for their support and interesting discussions on the topic.

During these years, I have collaborated with many colleagues for whom I have great regard and I extend my thanks to all of them. Specially I thank all the researchers and students of the Fraunhofer Institute of Industrial Mathematics (ITWM, Kaiserslautern) and of the Institute of Applied Mechanics (University of Kaiserslautern). I have appreciated their engagement as well as the quality of their work.

Specially, I want to thank all the persons who supported and encouraged me during this period and they will recognize themselves. Particularly, I have appreciated the nice time spent with Екатерина Круглова, к. ф.-м. н. Галина Принцпар, Irene Hassinger, Dr. Zahra Lakdawala, Dr. Cornelia Kronsbein, к. ф.-м. н. Александра Кохендёрфер, Cornelia Förderer, Johannes Spahn, Тигран Нагапетян, Tobias Zangmeister, Cyril Triplet, Daniel Kössling, Michael Plucik, Dr. Younis Hijazi, Dr. Janis Sliseris, Fabien Séries and Karlos Aizpurua.

I warmly thank Dr. Johan de Kock, Matti Schneider, Dr. Marco Buck, David Neusius for their relectures on the manuscript.

Finally, my special gratitude is due to my parents, my sister, my brother for their support and encouragements

Zusammenfassung

Granulare Strömungen treten in sehr vielen industriellen und geophysikalischen Anwendungen auf, wobei sich die Fließeigenschaften des Materials während dieser komplexen Prozesse stark verändern können. Mit einer diskreten Betrachtung der einzelnen Partikel lassen sich solche Prozesse realitätsnah simulieren. Allerdings führt dieser mikroskalige Ansatz zu sehr hohen Rechenzeiten. Aufgrund des hohen Aufwandes sind diese Methoden für die Simulation realistischer komplexer industrieller Prozesse nicht umsetzbar. Eine interessante Alternative ist die Anwendung eines kontinuumsmechanischen Modells, bei dem die Gleichungen auf einer Mesoskala formuliert werden. Diese Modelle werden in der Literatur häufig angewendet, um ein spezielles Verhalten, wie zum Beispiel nicht-newtonsche Strömungen, oder das Festkörperverhalten zu simulieren. Es gibt trotzdem immer noch kein allgemeines hydrodynamisches Modell, das ein granulares System mit der gleichen Genauigkeit wie die Navier-Stokes-Theorie für einfache Flüssigkeiten modellieren kann. Wenngleich die Formulierung solcher Modelle eine große wissenschaftliche Herausforderung darstellt, zeigt sie ein großes Potenzial für Anwendungen in der industriellen Praxis auf.

In dieser Arbeit wird erstmals ein kinetisches Modell unter Berücksichtigung von Festkörperverhalten erweitert. Die kinetische Theorie granularer Gase wurde in den letzten Jahrzehnten erfolgreich entwickelt, indem die klassische kinetische Gastheorie durch die Betrachtung inelastischer Stöße erweitert wurde [1]. Die granulare Temperatur wurde als Durchschnitt der lokalen räumlichen Fluktuationen der Teilchen eingeführt. Kinetische Modelle wurden oft benutzt, um verdünnte granulare Systeme zu simulieren, wie zum Beispiel in der Wirbelschicht. Sie sind aber nicht mehr anwendbar, wenn die Dissipation größer wird, weil die Hypothese instantaner Stöße dort nicht mehr gültig ist. Experimente zeigen auch, dass die Viskosität im hohen Dichtebereich größer werden sollte, wenn die Dehnsrate kleiner wird [2].

Wie in der Arbeit von Latz und Schmidt [3,4] erweitern wir ein kinetisches Modell für dichte Strömungen durch eine Modifizierung des Drucks und der Transportkoeffizienten, sobald die Dichte einen kritischen Wert erreicht hat.

Dies ermöglicht die Entwicklung einer granularen Strömung vom schnellen kinetischen bis zum viskoplastischen Bereich. Die Transportkoeffizienten haben die gleichen Abhängigkeiten wie sie Savage gefunden hat [5], als er Dehnungsfluktuationen in einem kritischen Plastizitätsmodell hinzugefügt hat und diese mit der granularen Temperatur verbunden hat.

Dieser Ansatz wurde schon erfolgreich angewendet, um einige typische granulare Fließprozesse, wie die Aufschüttung eines Sandhaufens oder granulare Strömungen in Silos zu simulieren. In [3, 4] wurde eine Finite-Volumen-Methode entwickelt, um Näherungslösungen der numerischen Probleme zu finden. Die numerische Methode wurde in der Software CoRheoS [3, 4, 6] implementiert, die in dieser Arbeit benutzt wird, um Eigenschaften des Modells zu analysieren. Bemerkenswerterweise zeigen wir, dass das Minimum, welches man typischerweise in Druckprofilen von Sandhaufen beobachten kann, in unseren Modell reproduziert werden kann.

Im quasi-statischen Bereich, bei nahezu maximaler Dichte, ergibt sich ein langsames Fließverhalten, wobei allerdings kein absoluter Ruhezustand erreicht werden kann. Das Festkörperverhalten ist ein asymptotischer Grenzwert eines Fließmodells, bei dem die granulare Temperatur gegen Null geht. Für eine exakte Modellierung des Festkörperverhaltens muss das Modell um Zustände innerhalb der Fließfläche, d.h. im elastischen Bereich, erweitert werden. Dafür kann das hydrodynamische Modell mit dem hyperelastischen Stoffgesetz von Jiang-Liu kombiniert werden [7]. Es wurde gezeigt, wie man durch die Einführung einer elastischen Dehnung den kontinuierlichen Übergang zwischen kritischer Strömung und elastischem Festkörperverhalten realisieren kann. Die Einführung einer elastischen Dehnung ermöglicht es, reversible Effekte direkt zu betrachten, würde aber zu einem komplexen numerischen Problem führen.

Eine alternative Möglichkeit ist die Anwendung eines hypoplastischen Stoffgesetzes [8]. Diese konstitutiven Gleichungen haben einen einfachen Formalismus, berücksichtigen jedoch viele Effekte der granularen Festkörper. In dieser Arbeit erweitern wir unser hydrodynamisches Modell um einen hypoplastischen Bereich, der einen kontinuierlichen Übergang zum Festkörper ermöglicht.

Mit diesem Ansatz entwickeln wir ein allgemeines hydrodynamisches Modell, das alle wesentlichen Bereiche eines granularen Systems abbilden kann. Es enthält Bagnold-Scherströmung, viskoplastische Strömungen sowie das Festkörperverhalten. Das Modell kann somit für die numerische Simulation von komplexen industriellen oder geophysikalischen Prozessen angewendet werden, wie z.B. Lawinen, Strömungen in Silos oder die Bodenkompromierung. Die numerische Behandlung dieser Modelle stellt eine große Herausforderung da. In der Literatur werden oft numerische Methoden angewendet, die sich ausschließlich auf ein einzelnes Verhalten beschränken.

In dem letzten Teil der Arbeit entwickeln wir einen Algorithmus, um eine eindimensionale Version des kompletten Modells zu lösen. Die numerische Methode basiert auf einer räumlichen Diskretisierung mit finite Differenzen und einer expliziten Zeitdiskretisierung. Sie wurde im Computeralgebrasystem *Mathematica 8.0* implementiert. Anhand von numerischen Beispielen zeigen wir, dass neben qualitativen Füllungsprozessen auch der Übergang vom statischen zum fließenden Verhalten simuliert werden kann.

Abstract

Granular materials are present in a wide range of industrial or geophysical applications. They are often involved in complex processes, during which different regimes occur at the same time or consecutively. Generally they are simulated with discrete methods, but it leads to high computational costs. Thus, these methods cannot be used to simulate complex industrial processes. An alternative solution is to employ a hydrodynamic model, based on equations formulated on a meso-scale. In the literature continuum models have been successfully employed to describe some specific regimes, such as dense shear flows or solid-like behavior. However, there is still no general hydrodynamic theory which can model a granular system with the same accuracy as the Navier-Stokes theory for simple fluids. Building such a theory remains a big challenge but it would be very useful to optimize industrial processes.

In this work we start from a kinetic model valid for dilute granular flows and extend its applicability to dense flow and quasi-static behavior. Like in the model of Latz and Schmidt [3, 4], we extend the validity of a kinetic model to dense flow by modifying both pressure and transport coefficients above a cross-over volume fraction. This is a relevant choice to describe any granular system moving from rapid collisional flow to slow viscoplastic motion. It was already successfully employed to simulate some typical processes like the formation of sand pile or granular flows in silos. Remarkably, we also show that this model qualitatively reproduces the pressure dip in sand pile, one of the most striking features in the behavior of granular systems. In our simulation, the pressure dip is implied by the density inhomogeneities which occur during the sand pile formation.

However, in the quasi-static limit, the system is constrained to flow slowly at yield and cannot fully reach static states. The solid-like behavior is an asymptotic limit of a flow model for vanishing granular temperature. The model must be extended to fully account for the granular solid-like behavior. An interesting solution is to combine the flow model with the Jiang-Liu hyperelastic law [7]. We show how an initial elastic strain can be calculated to ensure a continuous transition to the quasi-elastic regime. Alternatively, one

can account for solid-like behavior with some hypoplastic relation [8]. These constitutive laws are based on a simple formalism but reproduce some salient features of the granular solid state. This is a convenient choice for practical applications. Thus, we extend our hydrodynamic model by including a hypoplastic regime, in a way which ensures a continuous transition from the flow behavior to a solid-like one.

Following this approach, we formulate a general hydrodynamic model valid at arbitrary deformation rates which can reproduce a lot of granular phenomena. It includes Bagnold scaling at high deformations, viscoplastic motion at smaller strain rates and a quasi-static behavior in the solid limit. It combines the most advanced continuum theories on granular systems. The mechanisms for the transition between the different regimes are specified. It emerges as an unified continuum model which can be applied to the simulation of complex industrial or geophysical processes. For instance, it can be employed to model avalanches, flow in silos or soil compactification.

Solving numerically such a problem is a great challenge from a mathematical point of view. Generally, numerical methods concentrate on only one specific regime. We develop an explicit flux-conservative numerical scheme to numerically solve a one dimensional version of the full hydrodynamic problem. The code is implemented in the computer algebra system *Mathematica 8.0*. Numerical tests show its capacity to qualitatively reproduce filling processes as well as the flow of a sand column on an inclined plane. Both simulations can reproduce the three regimes generally observed in granular systems, i.e the dilute flow, dense flow and solid-like behavior. Beside a more quantitative validation, the code can be employed to model industrial processes where compressive effects dominate.

Contents

1	Introduction	1
1.1	State of the art	1
1.2	About this work	11
1.2.1	Motivation and goals	11
1.2.2	Structure of the thesis	11
2	Some basics of continuum mechanics	13
2.1	Fluid kinematics	14
2.1.1	Lagrangian description	14
2.1.2	Eulerian description	14
2.2	Balance equations	15
2.2.1	Mass conservation	15
2.2.2	Momentum balance	15
2.2.3	General heat transfer equation in a viscous fluid	17
2.3	Some classical constitutive relations	18
2.3.1	Ideal gas	19
2.3.2	Newtonian fluid	19
2.3.3	Elastic solid	20
3	Extended Kinetic Model (EKM)	21
3.1	Kinetic model	22
3.1.1	Balance equations	22
3.1.2	Kinetic constitutive relations	23
3.2	Extension to dense flow	28
3.2.1	Combining dilute and dense flow	28
3.2.2	Extended kinetic model	29
4	Analysis of dense flow regimes	33
4.1	Flow regimes	33
4.2	Rapid dense shear flow	34
4.3	Quasi-static behavior in the dense slow regime	40

4.3.1	Stress-strain relation, yield surface and flow rule	41
4.3.2	Frictional properties	47
4.3.3	Asymptotic behavior	49
4.4	Limits of vanishing and increasing deformations	52
4.4.1	Asymptotic static limits	52
4.4.2	Yield surface evolution for increasing deformations . .	54
4.5	Shortcoming: discontinuous transition from loading to unloading	56
4.6	Some illustrative examples	57
4.6.1	1D-stationary extensional flow	57
4.6.2	Filling on a tube	62
4.6.3	Sand pile formation and pressure dip	63
4.7	Conclusion and discussion	74
5	From slow critical flow to static state	77
5.1	Transition to rigid solid behavior	78
5.2	Transition to quasi-elastic regime	80
5.2.1	Quasi-static limit of the EKM vs. yield in elasto- plasticity theories	80
5.2.2	Jiang-Liu hyperelastic law	80
5.2.3	Combining the plastic response of the EKM with the Jiang-Liu model	83
5.2.4	Initial conditions	86
5.2.5	Illustrative example	89
5.2.6	Summary and discussion	91
5.3	Transition to hypoplastic regime	94
5.3.1	Hypoplastic constitutive laws	94
5.3.2	Quasi-static limit of the EKM vs. hypoplastic law at yield	96
5.3.3	Hypoplastic law	97
5.3.4	Comparison with Wolffersdoff's law	99
5.3.5	Initial conditions	100
5.3.6	Illustrative example	101
5.4	Conclusion: General hydrodynamic model	101
6	Numerical applications	107
6.1	Numerical methods for filling and compression processes . . .	107
6.2	1D Model	109
6.2.1	Governing equations	109
6.2.2	Hypoplastic behavior at loading and unloading	113
6.3	Numerical method	114
6.3.1	Time discretization	114

6.3.2	Space discretization	116
6.3.3	Discretization of the balance equations	118
6.4	Implementation	121
6.5	Numerical tests	123
6.5.1	Stationary kinetic flow	123
6.5.2	Filling simulation	124
6.5.3	Sand flowing on an inclined plane	127
7	Conclusion	129
A	Some properties of the granular solid	133
A.1	Basic properties	133
A.2	Hypoplastic law of Wolffersdorff	136
B	Pressure profile in sand piles	139
	List of Symbols	141
	Bibliography	145

1

Introduction

1.1 State of the art

About granular matter Starting with the early works of Reynolds [9], Coulomb [10] and continuing until the most recent studies of the scientific community, granular materials have been investigated in a broad range of ways. Experimentalists can now measure grain motion with particle imaging techniques [11] and computational scientists run high-performance computations [4]. However, the study of granular systems is still in an early stage of development. This is probably because the physics of granular systems has received less attention than other disciplines like fluid dynamics, important for the oil industry in the 20th century. In a review about the statics of granular matter, the french Nobel laureate P.G. de Gennes said that the physics of granular matter was “in 1998 at the level of solid-state physics in 1930” [12]. From a physical point of view, it is a new type of condensed matter whose description is not consensual. Despite all the technological knowledge of our society and the progress made in the last three decades, these materials are still poorly understood and their description is still controversial.

Granular matter refers to any material composed of many individual solid particles whose size is greater than one micron [12]. It can be composed of grains having different shapes or sizes. These materials are everywhere in nature (soils, dunes ...) and represent (on a weight basis) one half of the products and at least three quarters of the raw material of the chemical industry [13]. On the whole, granular materials are the material which are second most manipulated material by man, after water [13]. They are involved in several applications. Civil engineers manipulate concrete or asphalt to construct buildings, aerospace engineers employ propellants for the propulsion of rockets, chemical engineers mix powders in fluidized beds [14, 15], agri-

culturists produce cereals, astrophysicists observe planet rings [16] around Saturn, etc. . . Additionally, complex processes have been developed to produce cosmetics and medication [17], where particles must be mixed to create some chemical reaction. From their extraction (for instance from a mine) to their industrial manipulation, the granular products must be transported and stored. Some of these operations are potentially very dangerous. The storage of grains in silos has led to dramatic accidents. For this reason, silos must be carefully designed [18, 19]. Additionally, phenomena such as avalanches [4, 20], debris-flow [21], dune displacement [22] or rupture of dams can be at the origin of human catastrophes. Earthquake excitations can lead to a sudden fluidization of the soil, rendering foundation of buildings unstable. The seismology and the study of stability of dikes [23] and their resistance to shocks [24] is also of crucial importance to avoid dramatic events.

Physical properties Some basic observations reveal that a granular system can behave like a solid, a fluid or a gas. In the Sahara silica grains form dunes and ripples. If some sand is put on a plate which is progressively inclined, the grains will start to roll upon a critical angle. The amount of grains flows like fluid. Granular gases can be formed by shaking sand in a bottle. Additionally, a high diversity of gaseous regimes like convection, undulations or bouncing beds were experimentally identified [25]. In fluidized beds (an important technology of the chemical industry), a pressurized fluid is injected into some particulate medium [14, 15] to make fluidization happen. Some of these phenomena and processes are illustrated in Figure 1.1.

Being aware of this behavior, it is tempting to test if the concepts or equations that were developed to model classical liquids, solids or gases also apply to granular systems [26]. In the literature three different regimes have been intensively studied [27]:

- the dilute or collisional flow during which particles interact essentially through collisions,
- the dense flow, an intermediate state between the dilute flow and the quasi-static one,
- the rate-independent quasi-static regime characterized by a slow motion and quasi-elastic properties.

This separation into regimes is not a strict result of a general theory on granular systems but a convenient phenomenological distinction due to the

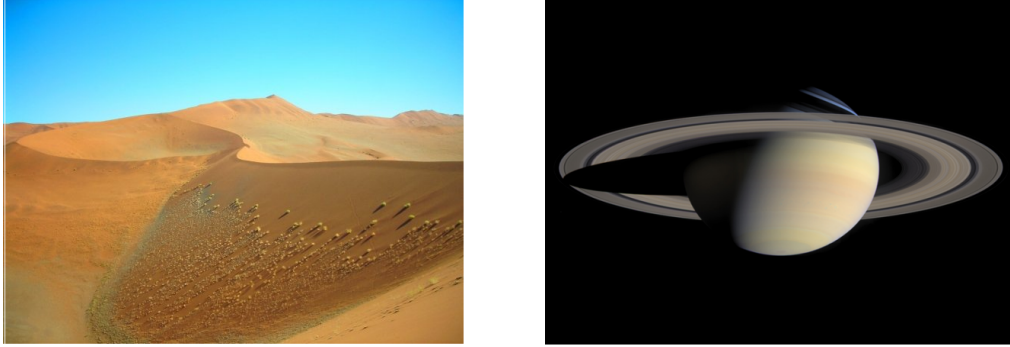


Figure 1.1: Left picture: sand dunes in Namib desert, Right: rings around Saturn (source NASA/JPL/Space Science Institute).

lack of a general consistent theory. The transition between these different states has been less investigated and remains an open problem. Experimentally, these different regimes are difficult to distinguish. Their boundaries are not clearly defined.

Because the size of the particles is greater than one micron, brownian motion is negligible and thermal fluctuations are not predominant [12,27]. This is not the case for other gases or liquids for which macroscopic quantities can be derived with statistical physics based on the interplay of thermal fluctuations and interactions between particles [26]. Another specific property is that no clear separation exists between a macroscopic and a microscopic scale, contrary to other gases or liquids. On a sand pile, small avalanches can occur at the free surface with a characteristic length of a few grains [1]. Granular systems are also dissipative, the presence of particles which interact through instantaneous inelastic collisions or friction facilitates the dissipation of kinetic energy [1,28,29].

Experimental investigations Civil engineers need a precise knowledge of the comportment of soils to design foundations. In the last century, a lot of experimental tests have been developed to characterize soils submitted to slow deformations [30]. The most employed experiment is the triaxial test which measures important material parameters like the angle of friction or the cohesion. The critical state friction angle can be determined by performing shear tests. The oedometric test is also widely employed and determines how a sample reacts under different applied loads. All these tests are based on the measurement of forces and displacements. This can easily be done if the distribution of stress and strain is homogeneous in the sample. But,

in reality, inhomogeneous deformations always occur during experiments involving granular systems. Element tests are thus evaluated as if the state were homogeneous during the test [8]. This induces some mistake on the measurement.

On the other side, fluid rheologists have performed experiments to characterize steady uniform flows on simple geometries. Velocity and density profiles have been investigated on configurations like shear cells, silos, inclined plane, chute flow or in sand piles [31]. Recently, more sophisticated experimental techniques like photo-elasticity, X-ray tomography [32], diffusive wave spectroscopy [33] or high speed camera [20,34] have been developed to measure micro-scale properties and especially velocity fluctuations. Photo-elasticity experiments showed the existence of contact networks in static sand piles [35,36] but also during dense flows [37]. Interesting experimental investigations have focused on sonic waves whose properties are linked to the elastic properties of the media [38,39]. A complete and precise set of data is however often difficult to obtain. Determining the best way to measure a physical quantity in a granular system is often subject to debates.

Modeling granular systems In the last decades, researchers have developed several approaches to model granular materials. We will pay attention to specify their interest for the numerical simulation of industrial processes. It must be pointed out that numerical simulations are not only a powerful tool to optimize industrial processes but also an important help in building theoretical models. Although they don't provide a substitute for experiments, they can significantly help to formulate constitutive equations or to better understand the physics underlying the models. Additionally, they give information that is sometimes not obtainable from experiments.

Discrete approach Granular materials are composed of several grains. It is thus tempting to describe them with discrete equations which relate some microscopic variables. This is the purpose of the Discrete Element Method, pioneered by the work of Cundall in 1971, see [40] for a review. A particle is described by its initial position and velocity and the Newtonian law is integrated in each time step to calculate its new position and velocity. Diverse interaction forces, contact models, rotational degrees of freedom or other dynamical parameters can be employed. It provides the possibility to model a very high diversity of materials (dry, wet) and behavior (segregation, shear banding) from assumptions made at the scale of the particles. Various branches have been successfully developed like the Generalized Discrete Element Method [41] or the Discontinuous Deformation Analysis [42]. A lot of

processes like flows in silo [43] and particle mixing [44] have been simulated in the last few years. This method is recognized as a very effective tool to simulate a wide range of problems concerning granular flows and soil mechanics. However, the number of particles that must be computed to simulate industrial processes is very high (several billions are not rare) leading to very long computation times. Although the simulation time can be reduced by using high performance computing and parallel processing, the cost of these simulations is still high.

Continuum mechanical modeling The continuum mechanical approach is based on the formulation of equations for variables such as density, velocity or temperature on a mesoscopic spatial scale. This approach remains valid as long as the flow is continuous. It requires that the medium contains a sufficient number of grains and does not include some irregularities such as voids or aggregates. When formulating continuum mechanical models for granular systems, the spatial scale must be greater in comparison to the size of the grains. Physicists refer these theories to hydrodynamic and engineers to continuum mechanics when they apply to solids.

Generally, the density, momentum and energy obey general balance laws and constitutive equations are added to close the set of equations. Constitutive relations specify the properties of the material. For instance, the stress tensor of a Newtonian fluid is linear in the strain rate [45]. In an elastic body, the stress depends linearly on the elastic strain [46]. For natural composite plates, anisotropic relations are generally employed [47, 48]. There is in general no framework to rigorously derive constitutive equations. They can be obtained from experimental results, theoretical investigations or numerical simulations. Some other theories pay more attention to the respect of thermodynamic principles, which adds more constraints to the constitutive equations. Hydrodynamic theories have been successfully developed to model classical fluids, but and also (more recently) more complex systems like ferrofluids [49] or crystal liquids [50]. However, their applicability to granular systems is not trivial and often subject to debates. Some authors expressed some doubts on the validity of some granular hydrodynamic theory [28]. However, civil engineers have employed it successfully to predict the quasi-static properties of soils [13, 51] or design silos [18]. Additionally, kinetic models have been derived for 30 years to account for dilute granular flows, and can be seen as a relevant tool to simulate fluidized beds, granular jets or shear banding.

Generally, continuum mechanical problems require an approximation of the solution of some system of Partial Differential Equations (PDE's). The

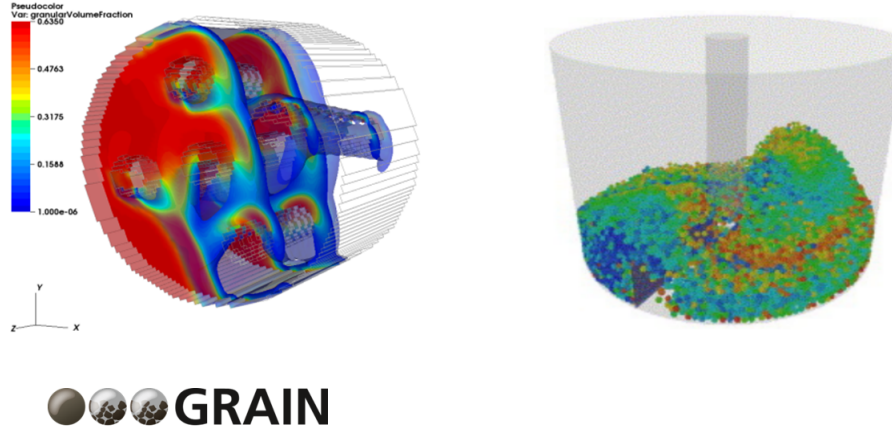


Figure 1.2: Two different approaches for the modeling of granular mixing processes. Left side: continuum simulation performed with the volume software CoRheoS (developed at Fraunhofer ITWM). Right side: discrete element simulation performed by Bertrand et al in [44].

equations are sometimes complex and it requires the application of advanced mathematical methods. Additionally, an important modeling effort is needed as well as the development of some calibration procedure to estimate the values of the material parameters. The calibration procedure is a long and expensive task which sometimes take several months [52]. Some models employ parameters which are not directly measurable. However, one can evaluate them a posteriori by analyzing their influence on the result of some simulations.

The computational cost of hydrodynamic models is low in comparison to the discrete element approach for which an equation of motion must be solved for each grain. Therefore, it is a relevant choice to simulate complex industrial processes. Both methods have been applied to simulate complex processes such as mixing, as it is illustrated on Figure 1.2.

Review of continuum models Granular systems are composed of many particles and the space between these particles is filled with a fluid like air or water. It is a multiphase medium. The interaction between particles and the interstitial fluid plays an important role in fluidized beds but can be neglected when particles are closely packed. This is the case in several applications, where the medium is generally treated as a single phase. A short and non-exhaustive review of these one-phase models is presented here.

Quasi-static behavior Civil and geophysical engineers have been employing soil mechanics for more than a hundred of years to model the slow plastic deformation of soils. This branch of solid mechanics is useful for the design of foundations. Several properties like Reynolds dilatancy, incremental non-linearity, stress-dependent stiffness and yield locus have been observed experimentally. Different models have been formulated to reproduce these effects [30, 51]. The material laws used for classical solids have been successfully adapted to soils. Quasi-elastic, plastic or viscoplastic constitutive relations can be found in the literature [7, 51, 53–55]. The observation of saturated remoulded clays during triaxial compression led to the critical state theory [56]. It describes the slow plastic motion of granular systems with flow rules, yield surfaces and plastic potentials.

Later, engineers have formulated constitutive relations based on rate-equations. Hypoelasticity is based on the formulation of a linear relation between the stress rate and the strain rate [57]. Hypoplastic laws consider non-linear rate-equations [58–60]. These laws have been inspired by rational mechanics, a theory which predicts the evolution of a mechanical system with rate-equations. Generally, they imply less parameters than elasto-plastic laws and can reproduce most of their properties. The development of all these constitutive laws have led to a very complex set of data [53]. Several yield surfaces and flow rules (associated, non associated) have been formulated. Generally they can correctly reproduce the effects they are constructed for. However they sometimes lead to complex mathematical formulations and there is no general agreement on what is the best model to employ. Nott explained that further studies are required to discuss the validity of associative flow rules [61]. Tardos underlined that constitutive laws for slow frictional powders are not very sensitive to the chosen yield surface and flow rule [2] what make their validation difficult. However, several work and conference have focused on very detailed comparison between these models [51].

Several authors proposed to include micro-mechanical effects in these models. Cosserat plasticity and viscoplasticity were developed to account for the rotations of the grains [61]. Micro-polar hypoplastic laws have been developed to model shear localization [62].

The general approach of soil mechanics is to solve the static momentum equation combined with a constitutive law and a kinematic relation. For numerical applications the applied load is discretized in small increments and the static part of the momentum is solved for each load increment. Solving the momentum equation allows the calculation of the new deformation field. A Lagrangian description is generally employed, i.e the position and physical properties of the system are described in terms of referential coordinates. In the numerical treatment, this can lead to some difficulties at larger defor-

mations because mesh distortion can occur. On the other hand, chemical engineers and fluid rheologists have written plastic constitutive laws to take into account that granular systems can behave like a solid or like a fluid. This interpretation of yield is somewhat different from that done by solid mechanics engineers for which it is linked to the apparition of irreversible deformations [63]. By combining some stress-strain rate constitutive law with the momentum and mass conservation, they obtain a Navier-Stokes like system of equations. The momentum equation is solved in term of velocity components. An Eulerian description is employed [2] and large deformations can be computed.

Granular flow More recently, physicists have concentrated their efforts on the theoretical study of granular flows. Bagnold's theoretical and experimental pioneering work about shear flows [64] is still a reference today. Later the granular gas kinetic theory has emerged as a powerful framework to describe dilute granular systems. Based on an analogy between a gas and a granular system in a dilute state, this theory is an extension of the granular gas kinetic theories to particles interacting through inelastic collisions. Remarkably, it allows the derivation of the macroscopic hydrodynamic equations as well as the constitutive relations [1, 29, 65, 66]. A key concept is the introduction of the granular temperature, defined as the mean of the square of velocity fluctuations. Kinetic theories have been applied to simulate fluidized beds [63] or pattern formation in granular gases [45]. Bocquet added high-density effects to describe shear bands [65, 67]. At larger dissipation, their validity become questionable since the basic assumptions of binary collisions and molecular chaos are not valid anymore. The quasi-static regime is actually governed by very different equations.

In the last decade, some experimental and theoretical studies have focused of the dense flow regime during which particles interact both by friction and collision. Pouliquen et al. [31, 68, 69] showed that a frictional viscoplastic law gives quantitative agreements with experiences and discrete element simulations. Several configurations like 2D shear bands, heap flow, rotating drums or flow in an inclined plane have been simulated with discrete elements and compared with this law. Although it fails to account for the transitions to the quasi-static and to gaseous regime, this rheological law has emerged as an unified first-order description of dense granular flows. Further investigations have been performed to extend its validity to the quasi-static regime. Non-local relations [61] have been formulated based on the idea that shear motion produces stress fluctuations.

Toward more general models The development of models covering several regimes is important for practical applications but a non-trivial task. A simple possibility is to directly combine a kinetic model with a critical state plastic one. The stress tensor is generally expressed as the sum of a rate-dependent part and a rate-independent solid-like contribution. These models are called kinetic-frictional and have been employed in diverse numerical simulations like flow down a vertical channel [70] or in the bubbling fluidized beds [71]. Alternatively, Savage started from a plastic critical state model and extended its validity to dilute flows by including strain fluctuations into the plastic flow rule. Then, he made its theory compatible with the results of the granular gas kinetic theory at low deformation rate [5]. This model was successfully applied to shear flows and flow in a vertical channel. In a recent work [3, 4], a simplified version was numerically integrated. Numerical simulations showed that it can predict some salient features of granular systems like the formation of sand piles with predictive slopes, flow in silos or in an inclined plane.

Another interesting approach has been proposed by Aranson and Tsimring [72, 73]. It is based on the theory of phase transition of Landau [74]. The main idea is to write the stress tensor as the sum of a solid and a fluid like part and to fix the relative importance of each part with an order parameter. This model is called continuum theory of partially fluidized granular flows. It correctly reproduces experimental observations on surface flows, where the depth of the flow is much smaller than its lateral dimensions and the hysteretic behavior of granular systems. In a more direct way, Leppert postulated a weight function and developed a numerical method based on a finite element space discretization [75]. It gives good agreements for flow in silos and avalanches phenomena.

Finally, Liu and Jiang proposed a hydrodynamic theory called Granular Solid Hydrodynamics to describe dry granular system at arbitrary shear rates [76–82]. The authors started from a hyperelastic law to describe the solid-like properties of soils [7, 83–86]. They have extended their theory by assuming the granular media to be transiently elastic, and have paid attention to the respect of thermodynamics principles. This theory covers wide range regimes and was employed to simulate shear bands, static stress distribution in sand piles or under point load.

Multiscale methods and homogenization Instead of postulating macroscopic constitutive relations, one can try to derive these laws from some information of the micro-scale. This is the purpose of multiscale methods which are used in several applications like flow in porous media, filtration

or micromechanics [87]. Some homogenization technique specifies how the macroscopic properties are determined from the micro-structure. Analytical and discrete modeling techniques can be employed [58]. The first method is applied when the microscopic quantities are continuous. The task is more difficult if the micro-scale is described in a discrete way because there is a difference of nature between both descriptions and averaging theorems must be used. In multiscale methods, the physical parameters employed are more easily identifiable and constitutive laws must not be postulated. In comparison to the discrete approach, it significantly reduces the computational cost. These promising methods are nowadays subject of intensive mathematical research. They are however more difficult to implement and to generalize [58]. Their applicability to granular system is not self-evident.

Numerical solution Continuum models are often written as a set of PDE's or integral equations. The majority of them cannot be analytically solved and discretization methods must be used to approximate the solution. The aim of the numerical approach is to transform a system of partial differential equations into algebraic ones from which the dependency of the variable in the entire domain can be reconstructed. Different discretization methods can be applied. The most employed are the finite element, finite volume and finite difference methods [88]. In the finite volume method, the computational domain is discretized into a number of control volumes, where unknowns are generally located at the volume centers. The equations are transformed into the integral form using the Gauss-Green theorem and discretized. One interesting advantage is that the calculated solution satisfies conservation laws. It is also relatively easy to formulate and compute on unstructured meshes. With finite elements, the unknowns are situated at the nodes of meshes and interpolation functions are employed. It can be linear functions or higher-order polynomials. The finite difference method is the easiest to implement and provides the simplest mathematical formalism. However, it suffers from a lack of flexibility to treat complicated geometries. Generally the finite element method is used to solve equations from solid mechanics and appears to be a relevant choice for complicated domains while the finite volume method is fully employed for fluid dynamics applications. Following this trend, many numerical applications concerning soil mechanics use the finite element discretization, like for instance to integrate elasto-plastic or hypoplastic laws [89]. Finite volume discretization have been successfully developed to simulate fluidized beds [14], or several processes including dilute and dense flows [4, 90].

1.2 About this work

1.2.1 Motivation and goals

In typical industrial operations, grains can be filled, sheared, compressed, mixed, pneumatically conveyed, etc. Developing some simulation tool which can model these phenomena is crucial to optimize industrial processes. Discrete element simulations can model a wide range of industrial processes but have a high computational cost. This is not the case if one employs a hydrodynamic model, where macroscopic relations are involved. Developing such a model and some numerical methods to approximate its solution have a great potential in the perspective of numerical simulations.

Some interesting progresses have been made in the last two decades. Several works of the last decade have underlined that granular hydrodynamic models have a great predictive power and can cover several flow regimes. Bocquet showed that a kinetic model with simple constitutive equations gives good quantitative agreements to describe shear bands [65,67]. The numerical simulations of Latz and Schmidt have revealed that a hydrodynamic model for dilute and dense flow can reproduce the formation of sand piles with predictive angle of repose but also shear bands or core and mass flows in silos [3,4]. Kamrin combined a hyperelastic model with a rate-dependent rheological law to build an unified elasto-plastic framework to model dense granular flows [91]. Liu and Jiang have developed a hydrodynamic framework to describe any granular system moving from the static equilibrium to rapid dilute flow [76]. Some of these theories consider both momentum and temperature equation and are based on relatively simple constitutive equations with a few parameters. They lead to several non-trivial results and a rich diversity of behaviors. However, a general hydrodynamic model covering the dilute, dense and quasi-static regimes and describing mechanisms for the transition between them is still lacking. Our goal is to formulate a hydrodynamic model which can be employed to model processes where dilute, dense flow and quasi-static regimes occur and to develop appropriate numerical methods to approach its solution. Although a general hydrodynamic model will probably not capture all the sophisticated phenomena observed in a granular systems, it may have a high predictive power, which would be very useful in the numerical simulation of complex industrial processes.

1.2.2 Structure of the thesis

In this work, we focus on the study of dry granular systems and treat them as a single-phase medium. This general approach let the possibility to extend

the proposed laws to more complicated materials like wet sand or to account for the interstitial fluid. Our strategy is to start from a hydrodynamic model valid for dilute flows and to extend its validity to dense flows and solid-like behavior.

In Section 2, we introduce some background of the continuum mechanical framework. We recall the Lagrangian and Eulerian description and how the balance equations are formulated in an Eulerian viewpoint.

In Section 3, we formulate a hydrodynamic model inspired from the work of Latz and Schmidt [3, 4]. We first introduce a kinetic model valid for dilute and intermediate granular flows and discuss its applicability to denser flows. Then, we extend the validity of the kinetic model to capture the dense flow behavior of granular systems. Further in this work, we call it EKM (Extended Kinetic Model).

In Section 4, we will show that the EKM covers several regimes previously observed in the literature. We first study the uniform dense shear flow regime. Then, we focus our attention on the high density limit of vanishing deformations. We show that in this regime the EKM reduces to a critical state plasticity model. To illustrate that, we run some numerical simulations with the finite volume software CoRheoS, developed at Fraunhofer ITWM [3, 4, 6]. We underline that critical states are reached in the simulations and that the EKM reproduces the formation of sand pile with predictive slope and a correct pressure distribution, with a local minimum in the middle of the pile.

In Section 5, we make investigations to extend the validity of the EKM to static states. Three different mechanisms are formulated, i.e transition to solid-rigid behavior, to a hyperelastic regime and to a hypoplastic one. For reasons that will be detailed, we prefer the third option, i.e to combine the EKM with a hypoplastic law. Following this approach, we formulate a general hydrodynamic model which can be employed to simulate a wide range of industrial processes where dilute, dense and solid-like behavior coexist.

In Section 6, we first discuss the numerical approach and underline that due to the high-complexity of the mathematical problem, it makes sense to first work on a one dimensional model. Thus we formulate a one dimensional version of the hydrodynamic model developed in Section 5. It includes the dilute, dense flow regime as well as the solid hypoplastic one. We develop an explicit numerical method based on a finite difference space discretization to solve the system of PDE's. The code is implemented into the computer algebra system *Mathematica 8.0*. We detail the algorithm and present three numerical examples, a kinetic flow, a filling simulation and the flow of a column of sand. To conclude, the main results and implications of this work are summarized and the perspectives are detailed.

2

Some basics of continuum mechanics

In this part, we introduce some basics of the continuum mechanical framework. In the continuum approach, the equations are formulated on volume elements which must be small in comparison to the size of the system and big enough to contain a great number of molecules. Several continuum quantities like velocity, pressure, density or temperature are defined to describe the spatial and temporal evolution of the fluid. Some of these quantities obey general laws which traduce some physical principle like mass or energy conservation. Generally the set of equations is completed by constitutive laws which specify the properties of the medium. The application of the principles of thermodynamics add some constraints on the choice of these laws.

In many applications, one can treat a granular system as a continuous medium. Thus, the concepts introduced in this chapter, will be employed further in this work, to develop our granular hydrodynamic model. In this chapter, we first recall the Lagrangian and Eulerian description of a fluid. Then, we shortly explain how mass conservation, momentum and energy equations are derived in an Eulerian viewpoint. Finally, we recall the definition of an ideal gas, a Newtonian fluid and of the Hooke law for an elastic body. For a detailed review of fluid dynamics, we refer to [45], and to [92] for solid mechanics.

2.1 Fluid kinematics

2.1.1 Lagrangian description

In the Lagrangian description, the motion of a given fluid particle is described at all times. If q is any property such as velocity v_i , density ρ or temperature T , etc., it will be expressed as

$$q = q(a_1, a_2, a_3, t) = q(a_i, t), \quad (2.1.1)$$

where a_i is the position of the tracked particle at time t . Physical laws like momentum balance or mass conservation directly apply to each fluid particle. This description is widely used in linear and non-linear solid mechanics. The Lagrangian viewpoint is less used in fluid dynamics, since it is not convenient to follow the high numbers of fluid particles moving on a fluid medium. In these cases, the Eulerian description is preferred.

2.1.2 Eulerian description

In the Eulerian description, the fluid properties (like velocity, pressure, etc.) are described as fields within a control volume. Each relevant variable of the problem is thus expressed as a function of the position of the fluid particle x_i and the time t

$$q = q(x_1, x_2, x_3, t) = q(x_i, t). \quad (2.1.2)$$

The rate of change of some physical quantity on a control volume moving in the space is called the material or total derivative and written $\frac{D}{Dt}(\cdot)$. It is expressed as the sum of the variation of the physical quantity at a fixed particle

$$\frac{\partial q}{\partial t}, \quad (2.1.3)$$

and of a second term which represents the changes of the quantity with respect to position at a given time

$$\frac{\partial q}{\partial x_1} \frac{\partial x_1}{\partial t} + \frac{\partial q}{\partial x_2} \frac{\partial x_2}{\partial t} + \frac{\partial q}{\partial x_3} \frac{\partial x_3}{\partial t}. \quad (2.1.4)$$

In this work, we call this term convective derivative. As the whole, the total derivative is given by

$$\frac{Dq}{Dt} = \frac{\partial q}{\partial t} + \frac{\partial q}{\partial x_1} \frac{\partial x_1}{\partial t} + \frac{\partial q}{\partial x_2} \frac{\partial x_2}{\partial t} + \frac{\partial q}{\partial x_3} \frac{\partial x_3}{\partial t}. \quad (2.1.5)$$

It can be expressed with the Einstein's summation convention (summation over the repeated index terms) as

$$\frac{Dq}{Dt} = \frac{\partial q}{\partial t} + v_i \frac{\partial q}{\partial x_i}. \quad (2.1.6)$$

2.2 Balance equations

2.2.1 Mass conservation

To derive the fundamental equation of mass conservation we consider a volume V bounded by a surface S that is fixed in space. The mass inside the volume is given by

$$\int_V \rho dV, \quad (2.2.1)$$

where ρ is the density and v_i the velocity. Thus, the local mass evolution is given by

$$\frac{\partial}{\partial t} \int_V \rho dV = \int_V \frac{\partial \rho}{\partial t} dV. \quad (2.2.2)$$

The rate of mass flux on the whole surface is given by

$$\int_S \rho n_i v_i dS, \quad (2.2.3)$$

where n_i is the outward normal of the surface V and v_i the velocity. Using the Gauss-Green theorem and writing that the mass evolution is equal to the mass flux entering on the whole surface, one gets

$$\int_V \left(\frac{\partial \rho}{\partial t} + \frac{\partial (\rho v_i)}{\partial x_i} \right) dV = 0. \quad (2.2.4)$$

This is valid for any volume V , so that

$$\frac{\partial \rho}{\partial t} + \frac{\partial (\rho v_i)}{\partial x_i} = 0. \quad (2.2.5)$$

This latter equation is the local form of the mass conservation.

2.2.2 Momentum balance

The momentum balance is derived by applying Newton's second law of motion to a volume element. The momentum in the volume element is given by

$$\int_{V(t)} \rho v_i dV. \quad (2.2.6)$$

The change of momentum can be expressed by applying Reynolds' transport theorem

$$\frac{d}{dt} \int_{V(t)} \rho v_i dV = \int_{V(t)} \left(\frac{\partial \rho v_i}{\partial t} \right) dV + \int_{S(t)} (n_j v_j \rho v_i) dS. \quad (2.2.7)$$

By applying the Gauss-Green theorem, one gets

$$\frac{d}{dt} \int_{V(t)} \rho v_i dV = \int_{V(t)} \left(\frac{\partial (\rho v_i)}{\partial t} + \frac{\partial (\rho v_i v_j)}{\partial x_j} \right) dV. \quad (2.2.8)$$

We can now write that the change of momentum in the volume is equal to the forces acting on the volume element

$$\int_{V(t)} \left(\frac{\partial (\rho v_i)}{\partial t} + \frac{\partial (\rho v_i v_j)}{\partial x_j} \right) dV = \int_{V(t)} \rho f_i^v dV + \int_{S(t)} f_i^s dS, \quad (2.2.9)$$

where f_i^v are the volume force acting on the body and f_i^s the surface force, which depends on the unit normal to the surface. The surface force is generally related to the Cauchy stress tensor σ_{ij}

$$f_i^s = \sigma_{ij} n_j, \quad (2.2.10)$$

where n_j is the unit normal surface vector. The Cauchy stress components on a volume element can be seen on Figure 2.1. Inserting (2.2.10) into the momentum balance gives

$$\int_{V(t)} \left(\frac{\partial (\rho v_i)}{\partial t} + \frac{\partial (\rho v_i v_j)}{\partial x_j} \right) dV = \int_{V(t)} \rho f_i^v dV + \int_{S(t)} \sigma_{ij} n_j dS. \quad (2.2.11)$$

By applying Gauss-Green theorem, one gets

$$\int_{V(t)} \left(\frac{\partial (\rho v_i)}{\partial t} + \frac{\partial (\rho v_i v_j)}{\partial x_j} \right) dV = \int_{V(t)} \left(\rho f_i^v + \frac{\partial \sigma_{ij}}{\partial x_j} \right) dV. \quad (2.2.12)$$

This equation is valid for any fluid elements V , and leads to

$$\frac{\partial (\rho v_i)}{\partial t} + \frac{\partial (\rho v_i v_j)}{\partial x_j} = \rho f_i^v + \frac{\partial \sigma_{ij}}{\partial x_j}. \quad (2.2.13)$$

It is the local form of the momentum balance equation. Note that the left hand side term can be transformed by making use of the mass conservation equation,

$$\frac{\partial (\rho v_i)}{\partial t} + \frac{\partial (\rho v_i v_j)}{\partial x_j} = \rho \left(\frac{\partial v_i}{\partial t} + v_j \frac{\partial v_i}{\partial x_j} \right) = \rho \frac{Dv_i}{Dt}. \quad (2.2.14)$$

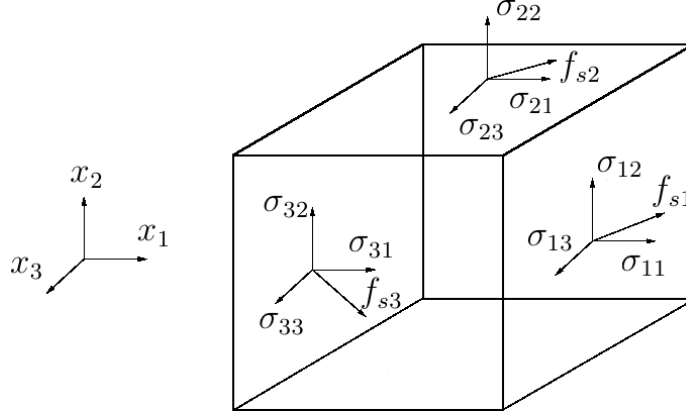


Figure 2.1: Volume element with stress components σ_{ij} .

It is actually equal to the product of the fluid particle acceleration with the density. In the static state, the momentum balance reduces to

$$\frac{\partial \sigma_{ij}}{\partial x_j} = \rho f_i^v. \quad (2.2.15)$$

This equation is generally employed in solid mechanics combined with some constitutive law. Additionally, one can show that the conservation of angular momentum requires the stress tensor to be symmetric

$$\sigma_{ij} = \sigma_{ji}. \quad (2.2.16)$$

In a classical continuum medium, the symmetry of the stress tensor ensures angular momentum conservation. However, in a granular system, external torques can act on the grains, and several authors proposed continuum theories based on non-symmetric stress tensor to fully account for this source of rotation [3, 61].

2.2.3 General heat transfer equation in a viscous fluid

Generally fluid dynamic theories consider an additional equation based on the application of the second law of thermodynamics. The energy per unit volume of fluid is given by

$$\frac{1}{2}\rho v^2 + \rho e, \quad (2.2.17)$$

where the first term is the kinetic energy and the second one the internal energy. For an ideal fluid, the law of conservation of energy is given by [45]

$$\frac{\partial}{\partial t} \left(\frac{1}{2}\rho v^2 + \rho e \right) = -\frac{\partial}{\partial x_i} \left(\rho v_i \left(\frac{1}{2}v^2 + w \right) \right), \quad (2.2.18)$$

where w is the fluid enthalpy per volume element. In a viscous fluid, the total energy remains conserved but additional energy flux are induced by friction and thermal conduction. These flux must be added in the right side of (2.2.18). The obtained equation can be transformed with the help of the equation of motion and thermodynamic relations [45] to give

$$\rho T \left(\frac{\partial s}{\partial t} + v_i \frac{\partial s}{\partial x_i} \right) = \tilde{\sigma}_{ij} \kappa_{ij} + \frac{\partial}{\partial x_i} \left(\lambda \frac{\partial T}{\partial x_i} \right), \quad (2.2.19)$$

where s is the fluid entropy per unit of mass and λ the conductivity. This is the general equation of heat transfer for a viscous fluid. The expression of the left side is the rate of change of entropy multiplied by ρT . The first term of the right hand side is the energy dissipated by viscous heating and the second one by conduction. If there is no viscous dissipation and no thermal conduction, it reduces to the energy conservation equation of a perfect fluid. This general equation takes a simplified form in some specific regimes. If the fluid velocity is small in comparison to the speed of sound, the temperature equation can be derived in a constant pressure ensemble [45]

$$\rho c_P \left(\frac{\partial T}{\partial t} + v_i \frac{\partial T}{\partial x_i} \right) = \tilde{\sigma}_{ij} \kappa_{ij} + \frac{\partial}{\partial x_i} \left(\lambda \frac{\partial T}{\partial x_i} \right), \quad (2.2.20)$$

where $c_p = T \left(\frac{\partial s}{\partial T} \right)_p$ is the specific heat at constant pressure. With the help of the mass conservation equation, and for a constant c_p , on can rewrite this law as

$$\frac{\partial (\rho c_p T)}{\partial t} + \frac{\partial (\rho c_p T v_i)}{\partial x_i} = \tilde{\sigma}_{ij} \kappa_{ij} + \frac{\partial}{\partial x_i} \left(\lambda \frac{\partial T}{\partial x_i} \right). \quad (2.2.21)$$

For granular systems, the thermal heat transfer doesn't play an important role and can be generally neglected. However, granular gas kinetic theories define the granular temperature as the mean of velocity fluctuations by analogy with a gas. In these theories, the granular temperature obeys a balance law which is similar to (2.2.21) (see Section 3).

2.3 Some classical constitutive relations

Constitutive relations specify the property of the medium, we recall here three classical constitutive laws that have been employed to model classical liquids, solid or gases. These laws cannot be directly applicable to describe the solid-like or flow-like behavior of a granular system but can be adapted to them (see Section 3.1.1). We recall that constitutive laws have to fulfill

several requirements [92] like determinism, objectivity (invariance of the law with respect to rigid body motion) and locality (no dependence in higher gradients). Additionally, other conditions may be applicable such as material invariance properties (like isotropy or anisotropy), and respect with the general principles like mass conservation and the second law of thermodynamics.

2.3.1 Ideal gas

An ideal gas is composed of perfectly spherical particles which collide elastically. This model has been widely used to describe the behavior of many gases. Ideal gases are known to follow the ideal gas law

$$P = \rho r T, \quad (2.3.1)$$

where r is the specific gas constant and P is the pressure. This law was first stated by Clapeyron but can also be derived from the gas kinetic theory [26]. In a dilute granular system, grains collisions are non-elastic and the kinetic theory must be adapted to account for this dissipative behavior (see Section 3.1.1).

2.3.2 Newtonian fluid

Classical fluids like water are called Newtonian in the sense that the viscous stresses are proportional to the local strain rate. Newtonian fluid obey a simple constitutive model which accounts for viscosity. To introduce it, it is convenient to split the stress tensor into a deviatoric and pressure part

$$\sigma_{ij} = -P\delta_{ij} + \sigma_{ij}^D, \quad (2.3.2)$$

where P is the pressure of the fluid and $\sigma_{ij}^D = \sigma_{ij} - \frac{\sigma_{kk}}{3}\delta_{ij}$ the deviatoric part of the stress tensor. In an isotropic Newtonian fluid, the deviatoric stress tensor is assumed to vary linearly with the strain rate

$$\sigma_{ij}^D = 2\eta\kappa_{ij}, \quad (2.3.3)$$

where $\kappa_{ij} = \frac{1}{2} \left(\frac{\partial v_i}{\partial x_j} + \frac{\partial v_j}{\partial x_i} \right)$ is the strain rate tensor and η the viscosity, which quantifies the shear resistance of the fluid. The mass conservation and momentum equation combined with the Newtonian constitutive law lead to the Navier-Stokes equations. Complex fluids exhibit a different behavior, the viscosity is generally a function of additional variables like the temperature or the shear rate. In this case, the fluid is called non-Newtonian. Later in this work, the granular medium in a fluid state will be treated as a non-Newtonian fluid.

2.3.3 Elastic solid

We shortly recall here some basics of the elasticity theory which has been widely used in solid mechanics to describe the reversible behavior of solids. Since solid mechanics applications focus on the deformation of initially static bodies submitted to external load, it is convenient to describe their motion with the help of a displacement field u_i . The stress tensor is generally expressed as a function of the strain tensor ε_{ij} , which is related to the medium deformation. For small deformations, i.e $|\frac{\partial u_i}{\partial x_j}| \ll 1$, the strain tensor is given by

$$\varepsilon_{ij} = \frac{1}{2} \left(\frac{\partial u_i}{\partial x_j} + \frac{\partial u_j}{\partial x_i} \right). \quad (2.3.4)$$

The stress tensor can be derived from the elastic strain energy function W

$$\sigma_{ij} = \frac{\partial W}{\partial \varepsilon_{ij}}, \quad (2.3.5)$$

and the generalized Hooke Law relates the stress tensor to the strain one

$$\sigma_{ij} = C_{ijkl} \varepsilon_{kl}, \quad (2.3.6)$$

where C_{ijkl} is the stiffness tensor, defined by

$$C_{ijkl} = \frac{\partial \sigma_{ij}}{\partial \varepsilon_{kl}}. \quad (2.3.7)$$

Combining this latter equation with (2.3.5) gives

$$C_{ijkl} = \frac{\partial^2 W}{\partial \varepsilon_{ij} \partial \varepsilon_{kl}}. \quad (2.3.8)$$

The symmetry of the stress and strain tensors, and the relation (2.3.8) imply symmetric properties on the stiffness which reduce to 21 its number of independent components

$$C_{ijkl} = C_{klij} = C_{jikl} = C_{ijlk}. \quad (2.3.9)$$

For an isotropic linear material, the stiffness tensor is given by

$$C_{ijkl} = 3K \delta_{ij} \delta_{kl} + 2G \varepsilon_{ij}^D, \quad (2.3.10)$$

where K and G are the bulk and shear modulus. Further in this work, more complex constitutive relations will be employed to describe the solid-like granular behavior. For instance, K and G cannot be considered to be constant anymore in a quasi-static granular medium (see Section 5).

3

Extended Kinetic Model (EKM)

Dilute granular flows have been the subject of intensive research in the last 40 years [1, 5, 29, 93–96]. They are present in many industrial applications, like for instance pneumatic conveying, fluidization or mixing [97]. In the last decades, the comprehension of their microscopic and macroscopic behavior has significantly improved. This progress is partially due to the application of new simulation and experimental tools as well as the use of statistical methods.

During dilute flow, grains interact essentially through instantaneous collisions. This regime is also called “rapid granular flow” or “granular gases” in the literature. The analogy with gases was used as a starting point for the theoretical description of dilute granular flows. The similarity between the random motion of granular grains and the thermal agitation of molecules led to the definition of the granular temperature, initially proposed by Ogawa [98]. It has become a key concept for describing the dynamics of dilute granular systems.

The main difference between a gas and a granular material in a gaseous state resides on the nature of the collisions. In gases, molecules interact elastically. Furthermore, the kinetic energy of two molecules is conserved after a collision. On the contrary, grains interact inelastically and their collisions lead to a dissipation of kinetic energy into heat. As a consequence, the granular gaseous state remains stable only if some energy is put into the system, for instance by agitating or shearing. This can be observed by filling some sand into a bottle and agitating it. If the agitation is stopped, kinetic energy dissipates into heat and grains loose their motion.

The granular gas kinetic theory provides a framework to derive the correct hydrodynamic equations from some extension of the Boltzmann equation [1]

and under the usual assumptions of instantaneous inelastic collisions and molecular chaos. To obtain a closed model, constitutive relations between the transport coefficients must be specified. In general, there is no way to derive these relations rigorously. Their exact form is often discussed in the literature [29, 96, 99, 100].

The validity of the kinetic approach becomes questionable for larger dissipation. This theory can be considered as some perturbation of the case of elastic gases and remains valid as long as dissipation is small [5]. However, several numerical studies showed quantitative agreements with experiments at large volume fractions. Bocquet et al. [65] showed that a simple kinetic model including high-density effects gives a pertinent representation of granular shear flows. It has also been employed to simulate fluidized beds [66] and its extension to multiphase flow reactors is particularly interesting for the chemical industry [101]. Although some aspects of the recent theoretical developments are still subject to intensive debates, it can be seen as a powerful framework to describe dilute granular flows at small and intermediate densities.

For all these reasons, we will choose to describe our granular system in a dilute state with a kinetic model which will be introduced in this part. We will formulate a simple version of the model of Bocquet [65].

3.1 Kinetic model

3.1.1 Balance equations

We start with the balance mass and the momentum balance on a spatial scale which is large in comparison to the size of the grains. In a Cartesian coordinate system, they are given by

$$\frac{\partial \rho}{\partial t} + \frac{\partial (\rho v_i)}{\partial x_i} = 0, \quad (3.1.1)$$

$$\frac{\partial (\rho v_i)}{\partial t} + \frac{\partial (\rho v_i v_j)}{\partial x_j} = \rho g_i - \frac{\partial P}{\partial x_i} + \frac{\partial \tilde{\sigma}_{ij}}{\partial x_j}, \quad (3.1.2)$$

where ρ is the density, v_i the mean velocity, $\tilde{\sigma}_{ij}$ is the dissipative, viscous stress tensor and g_i the gravitational force density. The derivation of these equations have been detailed in Section 2. The Cauchy stress tensor is given as the sum of the viscous stress and a pressure part,

$$\sigma_{ij} = -P\delta_{ij} + \tilde{\sigma}_{ij}, \quad (3.1.3)$$

where P is a pressure contribution. In the granular gas kinetic theory, the velocity is split into a mean and a fluctuating part c_i and the granular temperature T is defined as the local spatial average of the deviations from the mean velocity [1]

$$T = \langle c_i^2 \rangle, \quad (3.1.4)$$

where the brackets $\langle \rangle$ design the ensemble average. In gas kinetic theories, the granular temperature equation is derived from the Boltzmann equation in a constant volume ensemble. However, one may generally not neglect the effect of density variations on the granular temperature in an agitated granular system. Thus one should rather consider an equation for the temperature in a constant pressure ensemble. The granular temperature equation can be modified to be valid at constant pressure [90], it leads to the following equation

$$\frac{\partial(\rho T)}{\partial t} + \frac{\partial(\rho v_i T)}{\partial x_i} = \frac{2}{3} \left(\tilde{\sigma}_{ij} \kappa_{ij} - \frac{\partial q_i}{\partial x_i} \right) - \rho \epsilon T, \quad (3.1.5)$$

where $\kappa_{ij} = \frac{1}{2} \left(\frac{\partial v_i}{\partial x_j} + \frac{\partial v_j}{\partial x_i} \right)$ is the strain rate, ϵ the energy loss rate and q_i the heat flux. This equation has the usual form of the heat equation for a gas (see (2.2.21) in Section 2) for a constant specific heat. The only difference is the last term of the right hand side which accounts for the loss of energy due to inelastic collisions in a granular gas. This difference is however of crucial importance, since dissipative effects play a key role on the dynamical behavior of granular systems. The first term of the right-hand side is the work of viscous forces and the second one is the heat flux gradient.

3.1.2 Kinetic constitutive relations

To obtain a closed set of equations, constitutive relations must be specified. The viscous stress tensor $\tilde{\sigma}_{ij}$ and the heat flux q_i are, to lowest order, linear functions of the gradients of the macroscopic variables

$$\tilde{\sigma}_{ij} = 2\eta \kappa_{ij}^D + \zeta \kappa_{ll} \delta_{ij}, \quad (3.1.6)$$

$$q_i = -\lambda \frac{\partial T}{\partial x_i}, \quad (3.1.7)$$

where $\kappa_{ij}^D = \kappa_{ij} - \frac{1}{3} \kappa_{ll} \delta_{ij}$ is the deviatoric strain rate tensor, η and ζ stand respectively for the shear and bulk viscosity and λ denotes the thermal conductivity. As the whole, the stress tensor is given by combining (3.1.6) and (3.1.3)

$$\sigma_{ij} = -P \delta_{ij} + 2\eta \kappa_{ij}^D + \zeta \kappa_{ll} \delta_{ij}. \quad (3.1.8)$$

A first attempt to express a dependence of the stress tensor on the shear rate was proposed by Bagnold [90]. He experimentally studied wax spheres sheared in a coaxial cylinder rheometer. In the grain inertial regime, where the effects of the interstitial fluid are negligible, he found that the shear and normal stress on the shearing wall depend quadratically on the shear rate. This kind of dependence has been confirmed by a lot of experimental works and computer simulations and is a well accepted result about the rheology of granular flows. Constitutive relations can also be obtained from the granular gas kinetic theory. Their form can be improved with the help of discrete element simulations. Several relations proposed in the literature imply complicated analytical relations between the coefficient of restitution and the diameter of the grains [1, 99]. Bocquet et al. [65, 67] showed that simple kinetic relations, which include high density effects gives good agreements for shear granular flow. Inspired by this work, Latz and Schmidt proposed the following relations [3, 4]¹

$$P_K = T\rho g(\rho), \quad (3.1.9a)$$

$$\eta_K = \eta_0 \sqrt{T} g(\rho) \quad \varepsilon_K = \varepsilon_0 \sqrt{T} g(\rho), \quad (3.1.9b)$$

$$\zeta_K = \zeta_0 \sqrt{T} g(\rho) \quad \lambda_K = \lambda_0 \sqrt{T} g(\rho), \quad (3.1.9c)$$

where $g(\rho) = \left(1 - \frac{\rho}{\rho_{cp}}\right)^{-1}$ is the radial distribution function at contact, the parameters $\varepsilon_0, \lambda_0, \eta_0, \zeta_0$ are material constants and ρ_{cp} is the density at random close packing. The subscript K refers to the kinetic regime. More details about the definition of random packings can be found in Appendix A.1.

In the low density limit the pressure reduces to that of a gas $P_K = \rho T$. It diverges for $\rho \rightarrow \rho_{cp}$. This can be seen in Figure 3.1, where the variation of the kinetic pressure with the density is plotted for different values of the granular temperature. The bulk viscosity ζ which quantifies the influence of volume change on the shear stress is chosen to have a similar form as the shear viscosity η . Both are assumed to diverge at the close packing. It will be underlined in Section 4.2 that this kinetic model covers Bagnold's scaling, a well-known rheological law.

¹In their initial work, Latz and Schmidt added a dependence in ρ^2 on ε_K , i.e $\varepsilon_K = \varepsilon_0 \sqrt{T} \rho^2 g(\rho)$, and employed a non-symmetric stress tensor. This leads to some surface instabilities at low flow rates in the filling simulations performed with the internal software CoRheoS. These effects do not happen with the choice made in this work, and this motivates our choice. Further investigations should however focus on a quantitative analysis of the influence of this factor for several simulation tests. Notice also that the main results of this work remain valid also if other dependences on the density are postulated and can be easily extended to that case.

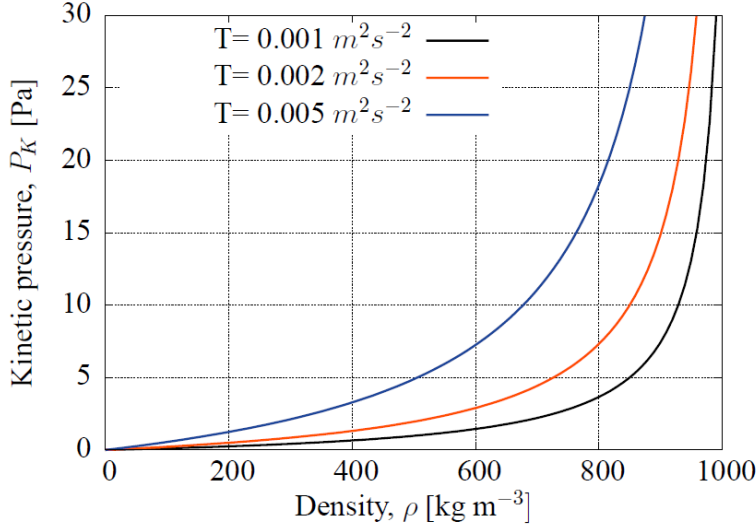


Figure 3.1: Variation of the kinetic pressure P_K with the density for different values of the granular temperature.

Shortcomings of the kinetic constitutive model As previously mentioned, the main difference between a perfect gas and a granular gas resides on the nature of the collisions. The kinetic approach has been developed as a perturbation of the case of a gas of elastic particles. This approach remains valid as long as “small” dissipation occurs. The structure of the granular temperature equation (3.1.5) suggests that the ratio of heat dissipation and viscous heating plays a key role on the granular temperature evolution. It is thus convenient to introduce the dimensionless ratio R of viscous heating and dissipation

$$R = \frac{\tilde{\sigma}_{ij}\kappa_{ij}}{\rho\epsilon T}. \quad (3.1.10)$$

Combining this latter relation with (3.1.6) gives

$$R = \frac{2\eta\dot{\gamma}^2 + \zeta\kappa_{ll}^2}{\rho\epsilon T}, \quad (3.1.11)$$

where $\dot{\gamma} = \sqrt{\kappa_{ij}^D\kappa_{ij}^D}$ is the shear rate. Applying the kinetic constitutive equations (3.1.9) gives

$$R = \frac{2\eta_0\dot{\gamma}^2 + \zeta_0\kappa_{ll}^2}{\rho\epsilon_0 T}. \quad (3.1.12)$$

Homogeneous cooling states In the homogeneous case, the granular temperature equation (3.1.5) is given by

$$\frac{\partial(\rho T)}{\partial t} = \frac{2}{3} \tilde{\sigma}_{ij} \kappa_{ij} - \rho \epsilon T. \quad (3.1.13)$$

The evolution of the granular temperature is controlled by the ratio R . If $R > 1$, viscous heating is dominating and produces granular temperature. In the contrary, for $R < 1$, heat dissipation is dominating and lead to a decrease of temperature. Starting from a state of high granular temperature, let say ($R \ll 1$), if no external source is applied so that viscous heating is negligible, the granular temperature will decay because of the dissipation implied by inelastic grains collisions. To analyze how states of zero granular temperature and high packing fractions are reached, we can study the states where viscous heating is negligible, as it has been done in [3]. The granular temperature equation reduces to

$$\frac{\partial(\rho T)}{\partial t} = -\rho \epsilon T. \quad (3.1.14)$$

Inserting the value of the energy loss rate (3.1.9), one gets

$$\frac{\partial(\rho T)}{\partial t} = -\rho \epsilon_0 g(\rho) T^{3/2}. \quad (3.1.15)$$

For states of high density, where ρ is close to ρ_{cp} , it gives

$$\frac{\partial T}{\partial t} = -\epsilon_0 g(\rho) T^{3/2}. \quad (3.1.16)$$

Solving this latter equation with Haff's law [1] gives

$$T(\rho, t) = \frac{T_i (1 - \rho/\rho_c)^2}{(1 - \rho/\rho_c + \epsilon_0 \sqrt{T_i} (t - t_i))^2}, \quad (3.1.17)$$

where $T_i = T(t = t_i)$ is the initial temperature. One can now insert this expression into (3.1.9a) to get

$$P_K = \frac{T_i (1 - \rho/\rho_c)^2 g(\rho) \rho}{(1 - \rho/\rho_c + \epsilon_0 \sqrt{T_i} (t - t_i))^2}. \quad (3.1.18)$$

This latter expression shows that the kinetic pressure vanishes for $\rho \rightarrow \rho_c$. Additionally the compressibility $\frac{\partial P}{\partial \rho}$, at large times is given by

$$\frac{\partial P_K}{\partial \rho} \approx \frac{1}{\epsilon_0^2 (t - t_i)^2} \left(1 - 2 \frac{\rho}{\rho_c}\right). \quad (3.1.19)$$

Thus, the compressibility would become negative for $\rho > \frac{\rho_{cp}}{2}$. Additionally, one can show that during an evolution at constant pressure, the system will reach states of zero granular temperature, where no mechanism can prevent the system to go beyond the maximum packing fraction for negative compressibility [3]. Although homogeneous cooling states are probably not reached during numerical simulations because of the existence of density or velocity spatial fluctuations, they reveal some shortcomings on the kinetic approach and motivate our choice to modify the constitutive relation to better account for the dense flow behavior.

3.2 Extension to dense flow

3.2.1 Combining dilute and dense flow

In the literature, different models have been employed to capture both dilute and dense granular regimes. Some of them directly combine a fluid model with a solid one. Other theories pay more attention the respect of thermodynamic principles or take into account microscopic aspects.

In an early work, Savage proposed to write the shear stress as the sum of a frictional term and a rate-dependent one to describe free-surface chute flow under gravitation [102]. Later, he formulated a model which combines a kinetic regime with a critical state plastic one [5]. By inserting Gaussian fluctuations into an associative plastic flow rule and relating them to the granular temperature, he derived macroscopic relations between the mean stress and the mean strain. For large strain fluctuations, he found a viscous-like relation. More recently, Kamrin and Bazant introduced random fluctuations into a Mohr-Coulomb plastic model [103] and applied their theory to Couette cells, flow in silos, heap flows and plate dragging experiments.

Kinetic-frictional models were also developed, based on a more direct combination of quasi-static stresses with rate-dependent ones. They have been successfully applied to model discharge of particles in a bin [104], granular flow in a rectangular spouted vessel [105] and gas-particle flow [106].

An alternative approach based on the theory of phase transition according to Landau [74], was proposed by Aranson and Tsiming [72, 73]. They write the stress tensor as the sum of a solid and a fluid-like part. The relative importance of the solid and liquid stress is fixed with an order parameter which obeys a Landau-type equation. This model can reproduce experimental observations of surface flows, where the depth of the flow is much smaller than its lateral dimensions. Its main interest is probably that it can predict the hysteretic character of granular flows. It was successfully applied to flows in rotating drums and shear cells. In [75], the expression for the order parameter was directly postulated. Additionally, a finite element numerical scheme was developed and simulations showed that the introduced model can well predict granular flows in silos and avalanches.

In this work, we will employ the results of Savage [5] to extend the kinetic constitutive equations defined in the previous section. The stress tensor will be written as the sum of the kinetic and yield term, both depending on the density and the granular temperature. This avoids negative energy dissipation and presents interesting properties which will be derived later in this work (see Section 4).

3.2.2 Extended kinetic model

At the microscopic scale, dilute flows are characterized by instantaneous collisions. In the contrary, long-term contacts occur during dense flows. This regime is governed by very different equations. The kinetic model introduced in Section 3.1.1 can be extended to account for dense flow. Inspired by the work of Savage [5], Latz and Schmidt [4] proposed to add a rate-independent pressure P_Y contribution above a cross-over volume fraction ρ_{co} . For simplicity, the yield pressure contribution was chosen to have the same form as the kinetic one

$$P = P_K + P_Y \quad \text{with} \quad \begin{cases} P_Y = 0, & \rho \leq \rho_{co}, \\ P_Y = T_0 (\rho - \rho_{co}) g(\rho), & \rho > \rho_{co}, \end{cases} \quad (3.2.1)$$

with T_0 being a positive constant which ensures that the total pressure doesn't vanish when the temperature goes to zero. From (3.2.1), one can express the equation of state for the density depending on pressure and granular temperature [4]

$$\rho(P, T) = \begin{cases} \rho_{cp} \frac{P}{\rho_{co} T + P}, & P \leq P_{co} \\ \rho_{cp} \frac{P + T_{co} \rho_{co}}{P + \rho_{cp}(T + T_{co})}, & P > P_{co}, \end{cases} \quad (3.2.2)$$

with

$$P_{co} = \rho_{co} T g(\rho_{co}). \quad (3.2.3)$$

This last relation shows that the density is continuous at P_{co} but not continuously differentiable. Viscosities, transport and dissipation coefficient are modified to account for dense flow, with the same dependence on the granular temperature as found by Savage [5]

$$\eta = \eta_K \left(1 + \frac{P_Y}{P_K} \right), \quad \zeta = \zeta_K \left(1 + \frac{P_Y}{P_K} \right), \quad (3.2.4a)$$

$$\epsilon = \epsilon_K \left(1 + \frac{P_Y}{P_K} \right), \quad \lambda_K = \lambda_K \left(1 + \frac{P_Y}{P_K} \right). \quad (3.2.4b)$$

The subscript Y stands for the yield regime. The viscosity can also be written as

$$\eta = \eta_K + \eta_Y = \eta_K + \frac{\eta_0 P_Y}{\rho \sqrt{T}}, \quad (3.2.5)$$

where $\eta_Y = \eta_0 P_Y / (\rho \sqrt{T})$ is the yield shear viscosity. One defines similarly the yield bulk viscosity ζ_Y , yield thermal conductivity λ_Y and the yield energy

loss rate ϵ_Y . The yield viscosities diverge for vanishing granular temperature and for density close to the maximum packing. In the dense regime, we treat the granular system as a high-viscous fluid. Additionally, no strict transition between the fluid-like and solid-like behavior is considered. The expression of the yield pressure (3.2.1) ensures a smooth transition from the kinetic to the yield regime. This can be justified by recent experimental studies which have focused on granular flow down a sand pile [31, 34, 107]. In this configuration, the velocity profile within the flowing layer was found to exhibit an exponential tail, with no clear transition to a solid-like state. Additionally, fluid rheologists employ viscoplastic law to capture the rheology of avalanches or debris flow [2, 21].

The high-density quasi-static limit of the EKM will be intensively underlined in Section 4.3. The EKM is given by:

Balance laws

$$\left\{ \begin{array}{l} \frac{\partial \rho}{\partial t} + \frac{\partial (\rho v_i)}{\partial x_i} = 0, \end{array} \right. \quad (3.2.6)$$

$$\left\{ \begin{array}{l} \frac{\partial (\rho v_i)}{\partial t} + \frac{\partial (\rho v_i v_j)}{\partial x_j} = \rho g_i - \frac{\partial P}{\partial x_i} + \frac{\partial \tilde{\sigma}_{ij}}{\partial x_j}, \end{array} \right. \quad (3.2.7)$$

$$\left\{ \begin{array}{l} \frac{\partial (\rho T)}{\partial t} + \frac{\partial (\rho v_i T)}{\partial x_i} = \frac{2}{3} \left(\tilde{\sigma}_{ij} \kappa_{ij} - \frac{\partial q_i}{\partial x_i} \right) - \rho \epsilon T \end{array} \right. \quad (3.2.8)$$

Constitutive relations

$$\tilde{\sigma}_{ij} = 2\eta \kappa_{ij}^D + \zeta \kappa_{ll} \delta_{ij}, \quad (3.2.9a)$$

$$q_i = -\lambda \frac{\partial T}{\partial x_i} \quad (3.2.9b)$$

with

$$P = P_K + P_Y \quad \text{with} \quad \left\{ \begin{array}{ll} P_Y = 0, & \rho \leq \rho_{co} \\ P_Y = T_0 (\rho - \rho_{co}) g(\rho), & \rho > \rho_{co} \end{array} \right. \quad (3.2.9c)$$

$$\eta = \eta_K \left(1 + \frac{P_Y}{P_K} \right), \quad \zeta = \zeta_K \left(1 + \frac{P_Y}{P_K} \right), \quad (3.2.9d)$$

$$\epsilon = \epsilon_K \left(1 + \frac{P_Y}{P_K} \right), \quad \lambda_K = \lambda_K \left(1 + \frac{P_Y}{P_K} \right), \quad (3.2.9e)$$

and

$$\eta_K = \eta_0 \sqrt{T} g(\rho), \quad \epsilon_K = \epsilon_0 \sqrt{T} g(\rho), \quad (3.2.9f)$$

$$\zeta_K = \zeta_0 \sqrt{T} g(\rho), \quad \lambda_K = \lambda_0 \sqrt{T} g(\rho), \quad P_K = T \rho g(\rho), \quad (3.2.9g)$$

with $g(\rho) = \left(1 - \frac{\rho}{\rho_{cp}} \right)^{-1}$.

4

Analysis of dense flow regimes

4.1 Flow regimes

The EKM is built to account for dilute and dense granular flows. It is given on page 31. It can be employed to simulate processes involving the evolution of some granular system from rapid collisional flow to quasi-static plastic motion. It considers simultaneously the momentum balance and temperature equation. We will show in this part that it covers some well-known regimes previously observed by physicists or engineers.

In the high-collisional dilute regime, shear rates are high (typically greater than 1s^{-1}) and grains mostly interact through inelastic collisions. In the EKM, this regime corresponds to densities smaller than the cross-over value ρ_{co} , where the kinetic constitutive relations apply. Under these assumptions, stationary uniform shear flows obey Bagnold's scaling [22], a well-known rheological law. This will be recalled in Section 4.2. These states remain stable only if a constant energy input is provided to the system, so that viscous heating avoids a decay of granular temperature ($R \ll 1$).

For denser flow ($\rho > \rho_{co}$), the stress tensor is composed of the sum of the kinetic term and the rate-independent one. Looking at the constitutive equations (3.2.9), it is obvious that, if a granular temperature is maintained into the system, so that $T \sim T_0$, both collisional and rate-independent contributions significantly affect the total stress. In Section 4.2, we will study the frictional properties of this regime and compare it with the rheological law of Pouliquen et al [31]. In the limiting state of high agitation ($\frac{T}{T_0} \gg 1$), Bagnold's regime is covered and in the limiting state of small deformations ($\frac{T}{T_0} \ll 1$) a rate-independent behavior is covered.

In the EKM, viscosities are the sum of a kinetic term and a yield contribution. Furthermore, yield viscosities depend on the granular temperature

in $1/\sqrt{T}$, as found by Savage. He derived this viscous-like relation by including strain-rate fluctuations into a critical state plastic model, averaging the stress and relating the strain-rate fluctuations to the granular temperature [5]. According to this result, the high-viscous regime of the EKM can be seen as a plastic dissipative regime undergoing strain-rate fluctuations.

In the high density quasi-static limit, the granular temperature varies with the square of the deformation rate, $T \sim \kappa_{ij}\kappa_{ij}$. We will show that in this regime the stress components describe an elliptic yield surface. This is a plastic regime which corresponds, in the model of Savage to vanishing strain-rate fluctuations.

A summary of this basic regime classification is presented in Table 4.1. Notice that since the EKM considers the full hydrodynamic equations without simplifications, other effects may happen like waves, as observed in the numerical simulations of Schmidt [4].

Volume fraction	Temperature	Covered regimes
Dilute Flow $\rho < \rho_{co}$	$T \gg T_0, R \ll 1$	Kinetic regime
	High collisional regime	Bagnold's scaling
	$T \sim T_0,$	High-viscous behavior
Dense Flow	Strain-rate fluctuations	Midi law for shear flows
$\rho > \rho_{co}$	$T \ll T_0, R \sim 1$	Quasi-static
	Small deformations	Plastic regime

Table 4.1: Identification of some regimes of the EKM.

4.2 Rapid dense shear flow

In the last two decades, a lot of theoretical and experimental studies have focused on dense granular flows [21,31,34,107]. In this regime, grains interact both with friction and collisions. It is an intermediate state between the solid state and kinetic regime. Note however that this distinction between collision and friction is quite artificial since both effects may appear at the same time. Dense flow can be found in a lot of industrial and geophysical applications like for instance rock avalanches. Viscoplastic laws have been developed to model dense granular flows [21] and more generally any material which exhibits both fluid-like and solid-like behavior.

In this section, the behavior of EKM in the rapid dense shear regime is investigated. By rapid we mean that the granular temperature is maintained around T_0 and by dense that the volume fraction is greater than its cross-over value $\rho > \rho_{co}$. In the pure shear regime ($\kappa_{ll} = 0$), the shear stress, defined by $\sigma_s = \sqrt{\sigma_{ij}^D \sigma_{ij}^D}$, can be calculated by $\sigma_s = 2\eta\dot{\gamma}$, where $\dot{\gamma} = \sqrt{\kappa_{ij}^D \kappa_{ij}^D}$ is the shear rate. We investigate the stationary uniform case, in which the granular temperature equation (3.2.8) reduces to the equilibrium between viscous heating and dissipation

$$2\eta\dot{\gamma}^2 = \frac{3}{2}\rho\epsilon T. \quad (4.2.1)$$

From the latter equation, one can calculate the granular temperature as

$$T = \frac{4\eta\dot{\gamma}^2}{3\rho\epsilon}. \quad (4.2.2)$$

According to the constitutive relations (3.2.9), the ratio of the viscosity coefficient with the dissipation one turns to a constant

$$\frac{\eta}{\epsilon} = \frac{\eta_K}{\epsilon_K} = \frac{\eta_0}{\epsilon_0}. \quad (4.2.3)$$

Inserting the latter equation into (4.2.2), the granular temperature depends on the square of the shear rate

$$T = \frac{4\eta_0\dot{\gamma}^2}{3\rho\epsilon_0}. \quad (4.2.4)$$

In the EKM, the stress tensor is the sum of the pressure and of the viscous term. Since $\kappa_{ll} = 0$, the stress strain-rate relation is given by

$$\sigma_{ij} = -(P_K + P_Y)\delta_{ij} + 2(\eta_K + \eta_Y)\kappa_{ij}^D. \quad (4.2.5)$$

We recall the dependence of the pressure on the density and temperature which was postulated in Section 3,

$$P = P_K + P_Y = T\rho g(\rho) + T_0(\rho - \rho_{co})g(\rho). \quad (4.2.6)$$

The viscosity is given by

$$\eta = \eta_K + \eta_Y = \eta_0\sqrt{T}g(\rho) + \frac{\eta_0 T_0(\rho - \rho_{co})g(\rho)}{\rho\sqrt{T}}. \quad (4.2.7)$$

The pressure can now be calculated by inserting the expression of the temperature (4.2.4) into (4.2.6) which gives

$$P = \frac{4\eta_0\dot{\gamma}^2}{3\epsilon_0}g(\rho) + T_0(\rho - \rho_{co})g(\rho). \quad (4.2.8)$$

Similarly, the shear stress $\sigma_s = 2(\eta_K + \eta_Y)\dot{\gamma}$ can be calculated as

$$\sigma_s = 2\eta_0\sqrt{T}\dot{\gamma}g(\rho) + \frac{2\eta_0T_0(\rho - \rho_{co})}{\rho\sqrt{T}}\dot{\gamma}g(\rho). \quad (4.2.9)$$

Substituting the expression of the temperature (4.2.4), one gets

$$\sigma_s = 4\eta_0\sqrt{\frac{\eta_0}{3\rho\epsilon_0}}\dot{\gamma}^2g(\rho) + T_0\sqrt{\frac{3\eta_0\epsilon_0}{\rho}}(\rho - \rho_{co})g(\rho). \quad (4.2.10)$$

According to (4.2.8) and (4.2.10), the pressure and shear stress are both composed of a static term and a dynamic contribution. The variation of the shear stress with the shear rate can be seen on Figure 4.1. The quadratic dependence of shear stress on the shear rate was already observed by Bagnold in a work which is still a reference nowadays [22]. In the dilute flow regime, i.e $\rho < \rho_{co}$, there is no yield contribution and Bagnold's regime is covered. The ratio of the shear stress with the pressure can now be calculated by combining (4.2.8) and (4.2.10)

$$\frac{\sigma_s}{P} = \frac{4\eta_0\sqrt{\frac{3\eta_0\epsilon_0}{\rho}}\dot{\gamma}^2 + 3\sqrt{\frac{3\eta_0\epsilon_0}{\rho}}T_0(\rho - \rho_{co})\epsilon_0}{4\eta_0\dot{\gamma}^2 + 3\epsilon_0T_0(\rho - \rho_{co})}, \quad (4.2.11)$$

which gives

$$\frac{\sigma_s}{P} = \sqrt{\frac{3\eta_0\epsilon_0}{\rho}} = \mu_s. \quad (4.2.12)$$

This latter expression shows that the dense shear flow regimes of the EKM is characterized by a static friction coefficient μ_s , which only depends on the density.

Comparison with the rheological law of Midi Starting from the study of granular flows on a simple sheared configuration, Pouliquen et al. proposed a viscoplastic law as a first-order description of dense granular flow [31]. A crucial observation is that dense granular flows are controlled by a non-dimensional number $I \sim \frac{\dot{\gamma}}{\sqrt{P}}$, called inertial number. The authors found the following relation for the effective friction coefficient

$$\frac{\sigma_s}{P} = \frac{\mu_1 + \mu_2 I}{1 + I}, \quad (4.2.13)$$

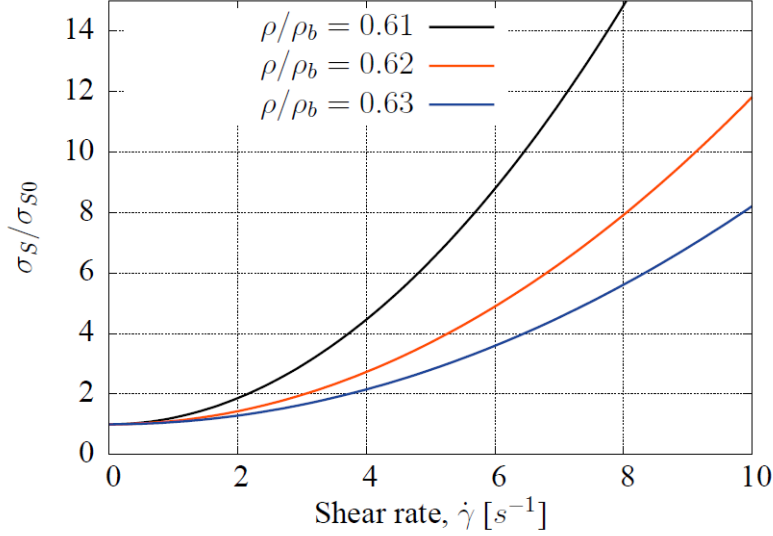


Figure 4.1: Variation of the shear stress (scaled with its static value $\sigma_{s0} = \sigma_s(\dot{\gamma} = 0) = \sqrt{\frac{3\eta_0\epsilon_0}{\rho}}P_Y$) with the shear rate for different values of density.

where μ_1 and μ_2 are two material parameters. The effective friction coefficient varies between the value μ_1 reached at vanishing shear rate and μ_2 reached for higher shear rate. This rheological law was tested by their authors on several simple geometries [31]. It can correctly predict the velocity profiles on a granular layer flowing down an inclined plane or near the free surface of a sand pile, the instabilities of Kapiza waves [108] and the transient flows during 3D granular collapse [100]. Additionally, a recent general hydrodynamic model, called Granular Solid Hydrodynamics provides good quantitative agreement with this rheological law [79]. This theory is more general and has been constructed by Jiang and Liu to model the evolution of granular systems from static elastic state to rapid flow.

According to (4.2.12), the friction coefficient in the rapid shear flow of the EKM remains constant in the dense and dilute regimes. However, we will see that the frictional behavior observed by Pouliquen et al. can be included by applying a small change into the constitutive equations. It requires to introduce a non-dimensional coefficient ν so that

$$\eta = \eta_K \left(1 + \nu \frac{P_Y}{P_K}\right) \quad \epsilon = \epsilon_K \left(1 + \nu \frac{P_Y}{P_K}\right). \quad (4.2.14)$$

With this modification, the ratios expressed in (4.2.3) remain constant and

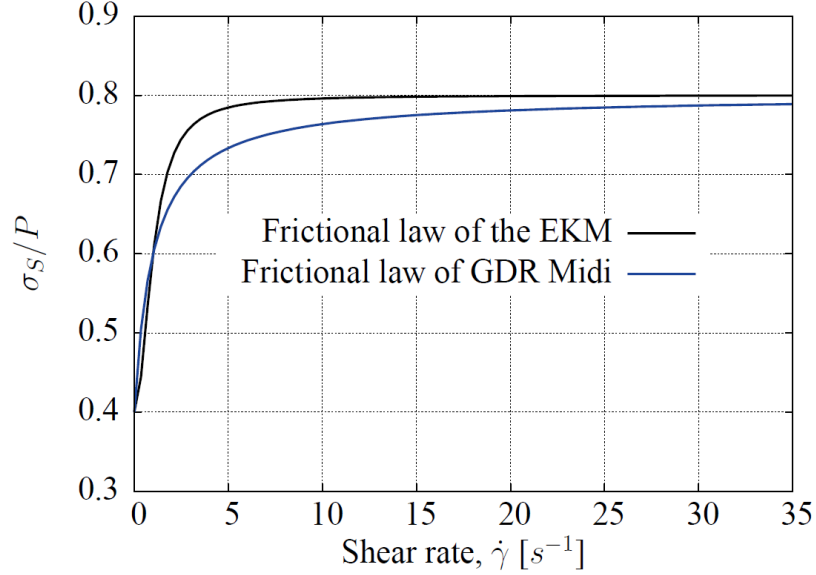


Figure 4.2: Comparison of the constitutive law of Midi with the relation derived from the EKM at constant density. Shear rate in s^{-1} .

the friction coefficient (4.2.11) becomes

$$\frac{\sigma_s}{P} = \sqrt{\frac{3\eta_0\epsilon_0}{\rho}} \frac{4\eta_0\dot{\gamma}^2 + 3\nu\epsilon_0T_0(\rho - \rho_{co})}{4\eta_0\dot{\gamma}^2 + 3\epsilon_0T_0(\rho - \rho_{co})}. \quad (4.2.15)$$

According to (4.2.15), the effective friction coefficient tends to $\nu\sqrt{\frac{3\eta_0\epsilon_0}{\rho}} = \nu\mu_s$ at vanishing shear rate and to $\sqrt{\frac{3\eta_0\epsilon_0}{\rho}} = \mu_s$ for higher shear rate. The two friction coefficients of the constitutive law of Midi can thus be identified, $\mu_1 = \nu\mu_s$ and $\mu_2 = \mu_s$. The coefficient ν is then simply expressed as the ratio between the two friction coefficients of the viscoplastic law of Midi. Notice that the relation (4.2.15) is similar to that derived by Jiang and Liu from the Granular Solid Hydrodynamics [109]. In this theory, the stress is also assumed to be the sum of a dynamic and a static part, but the static part is elastic. Elastic effects are not yet included in the EKM but investigations will be performed in Section 5 to take them into account. Figure 4.2 shows the good agreement between (4.2.15) and (4.2.13) at given density.

Like in [109], we can express the friction coefficient at constant pressure P_0 by

$$\frac{\sigma_s}{P_0} = \sqrt{\frac{3\eta_0\epsilon_0}{\rho}} \frac{(4\eta_0\dot{\gamma}^2 g(\rho) + 3\nu\epsilon_0T_0(\rho - \rho_{co})g(\rho))}{P_0}. \quad (4.2.16)$$

At higher shear rate, the friction coefficient varies like $\sqrt{\frac{3\eta_0\epsilon_0}{\rho}}4\eta_0\dot{\gamma}^2g(\rho)/P_0$ and doesn't necessary tend to a constant value, contrary to the law of Midi. However a similar dependence is found in the Granular Solid Hydrodynamics, and the authors have discussed the validity of the Midi relation for pressure controlled experiments [109].

In the work of Schmidt [4], it was argued that a different friction coefficient between kinetic and yield regime creates some numerical instabilities during filling simulation. However, taking a constant friction coefficient between the kinetic and the yield regime is in contradiction with the rheological law of Midi. It illustrates also that some minor changes in the constitutive relations significantly influence the frictional properties. The exact impact of the modification (4.2.14) on the numerical solution of a filling simulation has not been yet studied.

In the last two decades, the viscoplastic law of Midi has emerged as an unified first-order description of dense granular flows. Hence, it is an important result to know how this regime can be included into the EKM. Further investigations should focus on more detailed studies of the dense flow regime and the implication of the modification (4.2.14). In the following, for simplicity, we will take $\nu = 1$, and focus on the high density quasi-static regime. The results presented in the following parts remain however valid for $\nu \neq 1$ and can be easily extended to these cases.

4.3 Quasi-static behavior in the dense slow regime

In this part, the quasi-static behavior of the EKM at densities close to the maximal one and at small temperature ($T \ll T_0$) is studied. This latter condition implies that yield terms dominate ($\frac{P_Y}{P_K} \gg 1$) in the constitutive equations. In the quasi-static regime, the acceleration term in the momentum equation can be neglected. Thus the momentum balance (3.2.7) reduces to

$$\frac{\partial \tilde{\sigma}_{ij}}{\partial x_j} - \frac{\partial P}{\partial x_i} + \rho g_i = 0. \quad (4.3.1)$$

Similarly, by neglecting temperature gradients and time derivatives, the granular temperature equation (3.2.8) gives

$$\tilde{\sigma}_{ij} \kappa_{ij} - \frac{3}{2} \rho \epsilon T = 0. \quad (4.3.2)$$

By derivating the mass conservation equation (3.2.6), one gets

$$\frac{\partial \rho}{\partial t} + \frac{\partial(\rho v_i)}{\partial x_i} = \frac{\partial \rho}{\partial t} + \rho \frac{\partial v_i}{\partial x_i} + v_i \frac{\partial \rho}{\partial x_i} = 0. \quad (4.3.3)$$

In the high density regime and for vanishing velocities, we can assume the last term to be negligible to get

$$\frac{\partial \rho}{\partial t} = -\rho \frac{\partial v_i}{\partial x_i} = -\rho \kappa_{ll}. \quad (4.3.4)$$

Thus, in the high density quasi-static limit, the balance equations reduce to

$$\left\{ \begin{array}{l} \frac{\partial \tilde{\sigma}_{ij}}{\partial x_j} - \frac{\partial P}{\partial x_i} + \rho g_i = 0, \end{array} \right. \quad (4.3.5)$$

$$\left\{ \begin{array}{l} \tilde{\sigma}_{ij} \kappa_{ij} - \frac{3}{2} \rho \epsilon T = 0, \end{array} \right. \quad (4.3.6)$$

$$\left\{ \begin{array}{l} \frac{\partial \rho}{\partial t} + \rho \kappa_{ll} = 0. \end{array} \right. \quad (4.3.7)$$

Notice that since the yield pressure is given by $P_Y = T_0(\rho - \rho_{co})g(\rho)$, it is easy to check that $\frac{\partial P_Y}{\partial \rho} = T_0 g(\rho) + T_0(\rho - \rho_{co}) \left(1 - \frac{\rho}{\rho_{cp}}\right)^{-2} \geq 0$ diverges for $\rho \rightarrow \rho_{cp}$. It illustrates that density variations significantly influence the pressure distribution in this regime.

The temperature equation (4.3.6) reduces to the equilibrium between viscous heating and dissipation. One can combine it with the expression of the viscous stress (3.1.6) to get

$$2\eta\kappa_{ij}^D\kappa_{ij}^D + \zeta\kappa_{ll}^2 - \frac{3}{2}\rho\epsilon T = 0.$$

Since the shear rate was defined as $\dot{\gamma} = \sqrt{\kappa_{ij}^D\kappa_{ij}^D}$, this last equation gives

$$2\eta\dot{\gamma}^2 + \zeta\kappa_{ll}^2 - \frac{3}{2}\rho\epsilon T = 0,$$

so that the granular temperature is given by

$$T = \frac{4\eta\dot{\gamma}^2 + 2\zeta\kappa_{ll}^2}{3\rho\epsilon}. \quad (4.3.8)$$

According to the constitutive equations (3.2.9), the ratios η/ϵ and ζ/ϵ are constant and respectively equal to η_0/ϵ_0 and ζ_0/ϵ_0 . As a result, the temperature can be expressed as a linear combination of the square of the shear rate and of the compression rate

$$T = \frac{4\eta_0\dot{\gamma}^2 + 2\zeta_0\kappa_{ll}^2}{3\rho\epsilon_0}. \quad (4.3.9)$$

This latter equation shows how shear and compressional flow convert macroscopic kinetic energy into granular temperature. Since the granular temperature is explicitly given as a function of the strain rate and the density, this variable becomes redundant in the quasi-static regime. One can thus substitute its quasi-static value (4.3.9) into the stress-strain relations and formulate the equations exclusively in terms of density and velocities. This will allow us in the following to identify some salient properties of the EKM.

4.3.1 Stress-strain relation, yield surface and flow rule

Stress-strain relation In the EKM, the stress tensor is the sum of a kinetic and a yield part (the full model was summarized on page 31). When yield terms dominate ($\frac{P_Y}{P_K} \gg 1$), the stress tensor is approximately given by

$$\sigma_{ij} = -P_Y\delta_{ij} + \frac{2\eta_0 P_Y}{\rho\sqrt{T}} \kappa_{ij}^D + \frac{\zeta_0 P_Y}{\rho\sqrt{T}} \kappa_{ll}\delta_{ij}. \quad (4.3.10)$$

By substituting the expression of the granular temperature (4.3.9) into the expression of the stress tensor, one gets

$$\sigma_{ij} = -P_Y\delta_{ij} + \frac{2\eta_0\sqrt{3\rho\epsilon_0}P_Y}{\rho\sqrt{4\eta_0\dot{\gamma}^2 + 2\zeta_0\kappa_{ll}^2}}\kappa_{ij}^D + \frac{\zeta_0\sqrt{3\rho\epsilon_0}P_Y}{\rho\sqrt{4\eta_0\dot{\gamma}^2 + 2\zeta_0\kappa_{ll}^2}}\kappa_{ll}\delta_{ij}. \quad (4.3.11)$$

Constitutive laws for frictional granular systems	
Incompressible Coulomb powder [111]	$\sigma_{ij} = -P\delta_{ij} + \frac{\sqrt{2}P \sin(\phi) \kappa_{ij}}{\sqrt{\kappa_{ij}\kappa_{ij}}}$
Compressible powder (Pitman and Schaeffer [110])	$\sigma_{ij} = -P\delta_{ij} + \frac{\tau(P, \rho) \kappa_{ij}^D}{\sqrt{2}\dot{\gamma}}$

Table 4.2: Some constitutive laws for dense slow granular flow. ϕ is the angle of friction.

According to (4.3.11), the viscosities exhibit a dependence in $\sim 1/(\sqrt{\kappa_{ij}\kappa_{ij}})$. In the literature similar relations have been proposed to describe the flow of slow frictional granular systems [2, 31], as shown in Table 4.2. The incompressible Coulomb law provides a simple description based on the Mohr-Coulomb yield criteria. More sophisticated laws have been proposed, for example by Pitman and Schaeffer [110]. In this case, $\tau(P, \rho)$ specifies the properties of the material at yield. The model is generally completed by adding a normality condition to account for experimental observation. A quantitative comparison of these laws with (4.3.11) is a tricky issue, since, as emphasized by Tardos [2], stress distributions aren't strongly influenced by the choice of the yield criteria in these constitutive laws. At this stage, we restrict ourselves on underlining that the EKM exhibits a viscoplastic behavior in its high density quasi-static limit and derive its properties.

Flow direction For the following, it is first convenient to introduce the deviatoric stress $\sigma_{ij}^D = \sigma_{ij} - \frac{\sigma_{ll}}{3}\delta_{ij}$. From (4.3.11), we obtain

$$\sigma_{ij}^D = \frac{2\eta_0 P_Y \sqrt{3\rho\epsilon_0}}{\rho \sqrt{4\eta_0 \dot{\gamma}^2 + 2\zeta_0 \kappa_{ll}^2}} \kappa_{ij}^D. \quad (4.3.12)$$

From the stress-strain rate relationship (4.3.11), it is possible to calculate the values of the deviatoric and volumetric strain as a function of the stress tensor. One gets

$$\frac{\kappa_{ll}}{\sqrt{\dot{\gamma}^2 + \frac{\zeta_0}{2\eta_0} \kappa_{ll}^2}} = \frac{2}{\zeta_0} \sqrt{\frac{\rho\eta_0}{3\epsilon_0}} \frac{(\sigma_{ll} + 3P_Y)}{3P_Y}, \quad \frac{\kappa_{ij}^D}{\sqrt{\dot{\gamma}^2 + \frac{\zeta_0}{2\eta_0} \kappa_{ll}^2}} = \frac{\sqrt{\rho}\sigma_{ij}^D}{\sqrt{3\eta_0\epsilon_0}P_Y}. \quad (4.3.13)$$

Notice that the term $\sqrt{\dot{\gamma}^2 + \frac{\zeta_0}{2\eta_0} \kappa_{ll}^2}$ is similar to the norm of the strain rate. As a whole, by combining these two latter equations, the strain is calculated

as

$$\frac{\kappa_{ij}}{\sqrt{\dot{\gamma}^2 + \frac{\zeta_0}{2\eta_0}\kappa_{ll}^2}} = \frac{2}{9\zeta_0} \sqrt{\frac{\rho\eta_0}{3\epsilon_0}} \frac{(\sigma_{ll} + 3P_Y)}{P_Y} \delta_{ij} + \frac{\sigma_{ij}^D \sqrt{\rho}}{\sqrt{3\eta_0\epsilon_0}P_Y}. \quad (4.3.14)$$

This latter equation can be seen as a flow rule since it expresses the ratio of the normalized strain rate as a function of the stress tensor. Generally in plasticity theories, flow rules specify the evolution of the plastic strain (and not the total strain like in (4.3.14)). Here no decomposition of the strain into an elastic and a plastic part is applied. It is interesting to remark that a similar relation applies in the limit state of a hypoplastic law (see Section 5.3).

The rate of dilation β which controls plastic volume changes can be introduced as

$$\beta = -\frac{\kappa_{ll}}{\dot{\gamma}}. \quad (4.3.15)$$

This parameter is often employed in soil mechanics to describe the quasi-static behavior of soils but also of concrete and rock [112]. The evolution of the dilation angle θ , defined here by $\sin \theta = \beta$, can now be determined from the flow rules (4.3.13)

$$\theta = -\arcsin\left(\frac{2\eta_0(\sigma_{ll} + 3P_Y)}{3\zeta_0\sigma_s}\right), \quad (4.3.16)$$

where $\sigma_s = \sqrt{\sigma_{ij}^D \sigma_{ij}^D} = 2\eta\dot{\gamma}$ denotes the shear stress.

Yield surface By taking the square of the relations (4.3.13), one gets

$$\frac{\kappa_{ll}^2}{\dot{\gamma}^2 + \frac{\zeta_0}{2\eta_0}\kappa_{ll}^2} = \frac{4}{\zeta_0^2} \frac{\rho\eta_0}{27\epsilon_0} \frac{(\sigma_{ll} + 3P_Y)^2}{P_Y^2}, \quad \frac{\dot{\gamma}^2}{\dot{\gamma}^2 + \frac{\zeta_0}{2\eta_0}\kappa_{ll}^2} = \frac{\sigma_s^2 \rho}{3\eta_0\epsilon_0 P_Y^2}. \quad (4.3.17)$$

Combining the relation $\left(\dot{\gamma}^2 + \frac{\zeta_0}{2\eta_0}\kappa_{ll}^2\right) / \left(\dot{\gamma}^2 + \frac{\zeta_0}{2\eta_0}\kappa_{ll}^2\right) = 1$ with (4.3.17) imposes the following relation on the stress components

$$\frac{\rho\sigma_s^2}{3\eta_0\epsilon_0 P_Y^2} + \frac{2\rho(\sigma_{ll} + 3P_Y)^2}{27\zeta_0\epsilon_0 P_Y^2} = 1. \quad (4.3.18)$$

This latter expression can be written as

$$f_Y = 0 \quad (4.3.19)$$

with

$$f_Y = f_Y(\sigma_s, \sigma_{ll}, \rho) = (\sigma_{ll} + 3P_Y)^2 + \frac{9\zeta_0}{2\eta_0}\sigma_s^2 - \frac{27\zeta_0\epsilon_0}{2\rho}P_Y^2, \quad (4.3.20)$$

where f_Y is the expression of the yield surface. At given volume fraction and in the (σ_s, σ_{ll}) plane, it is an ellipse. The ellipticity e is given by $e = 9\zeta_0/2\eta_0$ and the center of the ellipse is situated at the coordinate $(-3P_Y, 0)$ in the (σ_s, σ_{ll}) plane. The yield surface at given volume fraction can be seen on Figure 4.4. In plasticity theories yield surfaces are often expressed as function of the stress invariants, in a similar way as (4.3.20). This ensures that the material response is isotropic. An elasto-plastic body initially at rest and loaded behaves elastically until plastic motion occurs. The yield criteria specifies when plastic flow occurs. Different yield criteria have been investigated in the literature. The Drucker-Prager [113] criterion has been often employed in soil mechanics and implemented in a lot of finite element codes. It is a smooth approximation of the Mohr-Coulomb yield surface. Elliptical yield envelopes have been employed in the modified Cam-Clay model [114] but also to model other materials like ice or foams. They ensure that no deviatoric plastic strain occurs at purely hydrostatic states of stress. More sophisticated models like the Matsuoka/Nakei [115] or the Ehlers [55] one have also been proposed for soils. However, the differences to the Mohr-Coulomb or Drucker-Prager criteria are not large and the introduction of more complicated yield surface is not necessary in many engineering applications [112].

Notice that in high density quasi-static limit of the EKM, the yield condition (4.3.20) always holds and the evolution of the total strain is given by (4.3.14) without any distinction between plastic and elastic deformation.

Associativity Classically in plasticity theories, plastic strain rates are derived from a plastic potential function g

$$\dot{\epsilon}_{ij}^p = \kappa_{ij}^p = \bar{\lambda} \frac{\partial g}{\partial \sigma_{ij}}, \quad (4.3.21)$$

with $\bar{\lambda}$ being a non-negative multiplier. If $g = f_Y$ the flow rule is called associated and the strain increment is in the direction of the normal of the yield surface. If this is satisfied and if the yield surface is convex, material stability is ensured by Drucker's stability postulate [92]. Constitutive laws are often derived to fulfill the principle of maximum plastic dissipation, which is a consequence of Drucker's stability postulate. It states that for all the possible stress states inside the yield surface or at yield, the one which effectively occur is that which leads to the maximum plastic dissipation. In perfect rate-independent plasticity, the value of $\bar{\lambda}$ is determined by writing the so-called consistency condition

$$\frac{\partial f}{\partial \sigma_{ij}} \dot{\sigma}_{ij} = 0, \quad (4.3.22)$$

which ensures that the material stays at yield during plastic flow. It allows to calculate $\bar{\lambda}$ by combining this relation with (4.3.21) and the elastic stress-strain relation

$$\sigma_{ij} = C_{ijkl} \varepsilon_{kl}^e, \quad (4.3.23)$$

where C_{ijkl} is the compliance matrix and ε_{kl}^e the elastic strain. In our present theory, the stress-strain relation has a rate-independent form (see equation 4.3.11) and its expression ensures that the yield criteria $f_Y = 0$ is fulfilled. Thus the system always stays at yield and the consistency condition is always fulfilled. However one can investigate the nature of the flow rule to check if it is associative. The flow rule associated to f_Y , given in (4.3.20), and applied to the total strain rate, can thus be calculated as

$$\kappa_{ij} = \bar{\lambda} \left(2(\sigma_{ll} + 3P_Y) \delta_{ij} + \frac{9\zeta_0}{\eta_0} \sigma_{ij}^D \right), \quad (4.3.24)$$

which leads to

$$\frac{\kappa_{ij}}{\sqrt{\dot{\gamma}^2 + \frac{\zeta_0}{2\eta_0} \kappa_{ll}^2}} = \frac{2(\sigma_{ll} + 3P_Y) \delta_{ij} + \frac{9\zeta_0}{\eta_0} \sigma_{ij}^D}{\sqrt{18 \frac{\zeta_0}{\eta_0} (3P_Y + \sigma_{ll})^2 + \frac{81\zeta_0^2}{\eta_0^2} \sigma_s^2}}, \quad (4.3.25)$$

and gives

$$\frac{\kappa_{ij}}{\sqrt{\dot{\gamma}^2 + \frac{\zeta_0}{2\eta_0} \kappa_{ll}^2}} = \frac{2(\sigma_{ll} + 3P_Y) \delta_{ij} + \frac{9\zeta_0}{\eta_0} \sigma_{ij}^D}{3\sqrt{\frac{2\zeta_0}{\eta_0} \left((\sigma_{ll} + 3P_Y)^2 + \frac{9\zeta_0}{2\eta_0} \sigma_s^2 \right)}}. \quad (4.3.26)$$

The condition $f_Y = 0$ can also be written as

$$(\sigma_{ll} + 3P_Y)^2 + \frac{9\zeta_0}{2\eta_0} \sigma_s^2 = \frac{27\zeta_0 \epsilon_0}{2\rho} P_Y^2,$$

and introduced into (4.3.26) to obtain

$$\frac{\kappa_{ij}}{\sqrt{\dot{\gamma}^2 + \frac{\zeta_0}{2\eta_0} \kappa_{ll}^2}} = \frac{2(\sigma_{ll} + 3P_Y) \delta_{ij} + \frac{9\zeta_0}{\eta_0} \sigma_{ij}^D}{9\zeta_0 \sqrt{\frac{3\epsilon_0}{\eta_0 \rho}} P_Y}. \quad (4.3.27)$$

It can finally be expressed as

$$\frac{\kappa_{ij}}{\sqrt{\dot{\gamma}^2 + \frac{\zeta_0}{2\eta_0} \kappa_{ll}^2}} = \frac{2}{9\zeta_0} \sqrt{\frac{\rho \eta_0}{3\epsilon_0}} \frac{(\sigma_{ll} + 3P_Y) \delta_{ij}}{P_Y} + \frac{\sigma_{ij}^D \sqrt{\rho}}{\sqrt{3\eta_0 \epsilon_0} P_Y}. \quad (4.3.28)$$

This expression is exactly the same as the flow rule derived from the EKM, see (4.3.14). It means that the flow relation which was derived from the EKM is compatible with an associative flow rule. Alternatively, by comparing (4.3.24) with (4.3.28), one can see the flow rule of the EKM as an associative flow rule where the multiplier is

$$\bar{\lambda} = \frac{\sqrt{\rho\eta_0}}{9\zeta_0\sqrt{3\epsilon_0}} \sqrt{\dot{\gamma}^2 + \frac{\zeta_0}{2\eta_0}\kappa_{ll}^2}.$$

The specification of $\bar{\lambda}$ is however not necessary in the present theory.

Plastic models based on associated flow rules give a pertinent representation of the quasi-static nature of soils and have been widely used in the literature. However some experimental observations have revealed that associative flow rules lead to excessive dilatant volume changes [33, 60]. Consequently, plasticity models based on non-associative flow rules have been developed to better account for dilatancy [112, 116–118]. The validity of associative flow rules is however still subject to discussions and requires further investigations [61].

Equations governing the quasi-static regime In the high-density quasi-static limit of the EKM, the system flows under critical conditions. The equations which characterize this state, and were established in this Section, can be summarized as

Mass conservation

$$\frac{\partial \rho}{\partial t} + \rho \kappa_{ll} = 0 \quad (4.3.29)$$

Momentum balance

$$\frac{\partial \tilde{\sigma}_{ij}}{\partial x_j} - \frac{\partial P}{\partial x_i} + \rho g_i = 0 \quad (4.3.30)$$

Granular temperature

$$T = \frac{4\eta_0\dot{\gamma}^2 + 2\zeta_0\kappa_{ll}^2}{3\rho\epsilon_0} \quad (4.3.31)$$

Stress-Strain relation

$$\sigma_{ij} = -P_Y \delta_{ij} + \frac{2\eta_0\sqrt{3\rho\epsilon_0}P_Y}{\rho\sqrt{4\eta_0\dot{\gamma}^2 + 2\zeta_0\kappa_{ll}^2}}\kappa_{ij}^D + \frac{\zeta_0\sqrt{3\rho\epsilon_0}P_Y}{\rho\sqrt{4\eta_0\dot{\gamma}^2 + 2\zeta_0\kappa_{ll}^2}}\kappa_{ll}\delta_{ij} \quad (4.3.32)$$

Yield condition

$$f_Y(\sigma_s, \sigma_{ll}, \rho) = (\sigma_{ll} + 3P_Y)^2 + \frac{9\zeta_0}{2\eta_0}\sigma_s^2 - \frac{27\zeta_0\epsilon_0}{2\rho}P_Y^2 = 0 \quad (4.3.33)$$

Flow rule

$$\frac{\kappa_{ij}}{\sqrt{\dot{\gamma}^2 + \frac{\zeta_0}{2\eta_0}\kappa_{ll}^2}} = \frac{2}{9\zeta_0}\sqrt{\frac{\rho\eta_0}{3\epsilon_0}}\frac{(\sigma_{ll} + 3P_Y)\delta_{ij}}{P_Y} + \frac{\sigma_{ij}^D\sqrt{\rho}}{\sqrt{3\eta_0\epsilon_0}P_Y} \quad (4.3.34)$$

In the following, we will analyze the properties implied by these equations.

4.3.2 Frictional properties

In this section, we study the frictional properties of the quasi-static regime of the EKM. In Section 4.2, we analyzed the rapid dense shear flow of the EKM and found that states of vanishing shear rate are characterized by a constant friction coefficient. We now investigate how the friction coefficient is influenced by the kinematic variables in the quasi-static limit, where compressive effects play an important role.

From the stress-strain relation (4.3.32), one can calculate the shear stress $\sigma_s = \sqrt{\sigma_{ij}^D\sigma_{ij}^D}$ as

$$\sigma_s = \frac{2\eta_0\sqrt{3\rho\epsilon_0}P_Y}{\rho\sqrt{4\eta_0\dot{\gamma}^2 + 2\zeta_0\kappa_{ll}^2}}\dot{\gamma}. \quad (4.3.35)$$

The viscous part of the normal stress $\tilde{P} = -\frac{\tilde{\sigma}_{ll}}{3}$ can be expressed as

$$\tilde{P} = -\frac{\zeta_0\sqrt{3\rho\epsilon_0}P_Y}{\rho\sqrt{4\eta_0\dot{\gamma}^2 + 2\zeta_0\kappa_{ll}^2}}\kappa_{ll}. \quad (4.3.36)$$

The ratio of the shear stress with the total pressure $P_t = -\frac{\sigma_{ll}}{3} = P_Y + \tilde{P}$ is given by

$$\frac{\sigma_s}{P_t} = \frac{2\eta_0\sqrt{3\epsilon_0}\dot{\gamma}}{\sqrt{4\rho\eta_0\dot{\gamma}^2 + 2\rho\zeta_0\kappa_{ll}^2} - \sqrt{3\epsilon_0}\zeta_0\kappa_{ll}}. \quad (4.3.37)$$

This latter expression can also be expressed as a function of the rate of dilation $\beta = -\kappa_{ll}/\dot{\gamma}$ by

$$\frac{\sigma_s}{P_t} = \frac{2\eta_0\sqrt{3\epsilon_0}}{\sqrt{4\rho\eta_0\left(1 + \frac{\zeta_0}{2\eta_0}\beta^2\right) + \sqrt{3\epsilon_0}\zeta_0\beta}}. \quad (4.3.38)$$

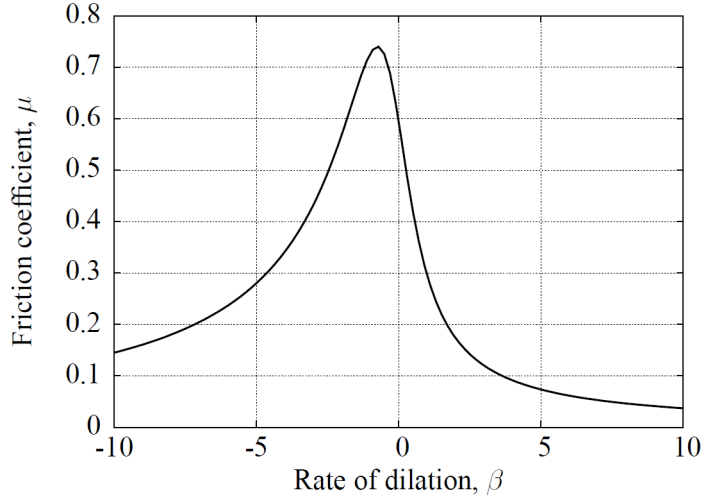


Figure 4.3: Plot of the variation of the friction coefficient with the rate of dilation β at constant density.

According to this last relation, the friction coefficient μ depends only on the rate of dilation and the density

$$\frac{\sigma_s}{P_t} = \mu(\beta, \rho). \quad (4.3.39)$$

As illustrated in Figure 4.3, the effective friction coefficient tends to $\mu_s = \sqrt{3\epsilon_0\eta_0/\rho}$ for $\beta = 0$ and to 0 for $\beta \rightarrow +\infty$. Notice that the value reached for $\beta \rightarrow 0$ is the static friction coefficient μ_s , previously introduced in Section 4.2. Additionally, the friction coefficient can reach values bigger than μ_s in extensive states, i.e for $\beta < 0$. This effect has been observed at the early stage of triaxial tests where dilatant volume increase can appear [114] and is qualitatively reproduced in our model. The dependence of the friction coefficient specifies the influence of dilatancy on the friction coefficient. The evolution of the friction coefficient along typical strain paths can be clearly identified

$$\begin{cases} \kappa_{ll} = \kappa_{ll}^c & \text{and} & \dot{\gamma} \rightarrow 0 & \Rightarrow & \mu \rightarrow 0, \\ \dot{\gamma} = \dot{\gamma}^c & \text{and} & \kappa_{ll} \rightarrow 0 & \Rightarrow & \mu \rightarrow \mu_s. \end{cases} \quad (4.3.40)$$

The rate of dilation is the parameter which determines the frictional properties of the quasi-static limit of the EKM. Depending on the strain path, the shear stress may vanish or be maintained at a constant value. In contrast, the pressure term never vanishes since the yield pressure does not. For an evolution at constant compression or extension and vanishing shear rate, the

pressure becomes constant and the shear stress vanishes, similarly to a fluid equilibrium. In this case, the system loses its resistance to shearing.

The EKM exhibits static frictional properties and the angle of friction can be defined as material parameter (see (4.3.43) in the next section). The numerical simulation of Latz and Schmidt showed that the formation of sand pile can be reproduced with the EKM [3, 119]. The angle of the pile varies from a few degree with the internal friction angle, defined as material parameter. Generally, a granular layer flowing on an inclined plane stops to flow when the angle of the plane becomes smaller than an angle, called dynamic angle of repose. This angle is generally different from the static friction angle [120]. This phenomena is not explicitly included into the EKM. However, we showed in Section 4.2 how a second friction coefficient can be introduced. Further investigations are required to quantitatively study the influence of these parameters in typical flow configurations such as heap flow or rotating drums.

4.3.3 Asymptotic behavior

Motivated by experimental observations, the concept of asymptotic behavior has been fully employed in soil mechanics. They can be defined as states of constant stress ratio reached after sufficiently long stretching with a constant strain rate direction [114]. The critical state is a particular asymptotic behavior observed during shearing at constant volume. More generally, the critical state soil mechanics has been built to account for both compression asymptotic states and isochoric critical states [56]. It includes the Cam-Clay model which gives a pertinent representation of normally consolidated clays with only a few parameters. More recently, critical states have been identified as a feature of hypoplastic laws [8, 59], see Section 5.3. Their existence was also confirmed by discrete element simulations. In this section, we identify the asymptotic behavior of the EKM.

Isochoric critical states If an initially static granular system is continuously and slowly sheared until it flows, it reaches a stationary state independent of the initial conditions, called critical state. The critical state is characterized by a constant stress and void ratio (more details are given in Appendix A.1). To study how the EKM models these states, we consider the case of shearing at constant volume $\kappa_{ll} = 0$, or equivalently $\rho = \rho_c$. According to (4.3.32), the pressure is given by

$$\sigma_{ll} = -3P_Y = -\frac{3T_0(\rho - \rho_{co})}{1 - \frac{\rho}{\rho_{cp}}}, \quad (4.3.41)$$

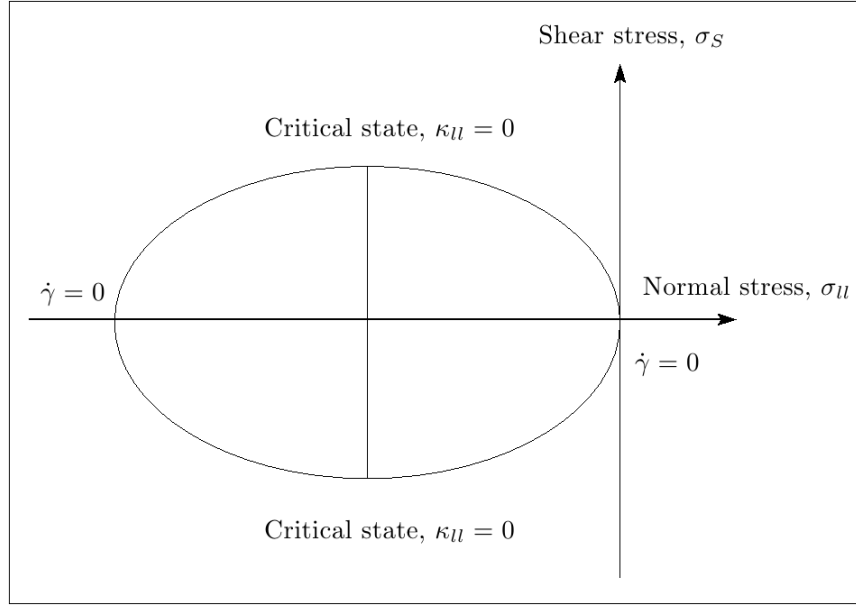


Figure 4.4: Representation of the yield surface in the (σ_s, σ_{ll}) plane at constant density.

and the yield condition (4.3.20), takes the form of a Drucker-Prager condition

$$\frac{\sigma_s}{P_Y} = \sqrt{\frac{3\eta_0\epsilon_0}{\rho_c}}. \quad (4.3.42)$$

In this state, the friction coefficient remains constant although distortion occurs ($\dot{\gamma} > 0$). This state is characterized by the following relations

$$T = \frac{4\eta_0\dot{\gamma}^2}{3\rho\epsilon_0}, \quad \dot{\gamma} = \dot{\gamma}_c, \quad \rho = \rho_c, \quad \sigma_{ll} = -3P_Y, \quad \sigma_s/P_Y = \sqrt{\frac{3\eta_0\epsilon_0}{\rho_c}}.$$

Assuming that the Drucker-Prager yield surface circumscribes the Mohr-Coulomb one, the angle of friction in the critical state ϕ is generally defined by [13]

$$\frac{\sigma_s}{P_Y} = \frac{2 \sin \phi}{\sqrt{3}(3 - \sin \phi)}. \quad (4.3.43)$$

Looking at the yield surface f_Y , plotted in Figure 4.4, it is easy to check that critical states are located at the two horizontal tangents of the ellipse.

Compression and extension asymptotic states Pure compression states are characterized by zero shear rate $\dot{\gamma} = 0$. Looking at the stress-strain relation (4.3.32), it is easy to check that the shear stress vanishes. Additionally, the pressure depends only on the density and the loading direction

$$\sigma_{ll} = -3P_Y + 3\sqrt{\frac{3\epsilon_0\zeta_0}{2\rho}} \frac{\kappa_{ll}}{|\kappa_{ll}|}. \quad (4.3.44)$$

Small density variations are governed by $\frac{\partial \rho}{\partial t} = -\rho\kappa_{ll}$. For compression states ($\kappa_{ll} < 0$) one gets

$$T = \frac{2\zeta_0\kappa_{ll}^2}{3\rho\epsilon_0}, \quad \dot{\gamma} = 0, \quad \frac{\partial \rho}{\partial t} = -\rho\kappa_{ll}, \quad \sigma_{ll} = -3P_Y \left(1 + \sqrt{\frac{3\epsilon_0\zeta_0}{2\rho}} \right).$$

These asymptotic states are generally called normal compression lines in soil mechanics [56]. The dependence of the pressure on the density in this state has been often discussed in the literature, but there is no general agreement about it [114]. In our model, it is given by

$$\sigma_{ll} = -3T_0 \frac{(\rho - \rho_{co})}{\left(1 - \frac{\rho}{\rho_{cp}}\right)} \left(1 + \sqrt{\frac{3\epsilon_0\zeta_0}{2\rho}} \right). \quad (4.3.45)$$

Extension asymptotic states ($\kappa_{ll} > 0$) are characterized by the set of equations

$$T = \frac{2\zeta_0\kappa_{ll}^2}{3\rho\epsilon_0}, \quad \dot{\gamma} = 0, \quad \frac{\partial \rho}{\partial t} = -\rho\kappa_{ll}, \quad \sigma_{ll} = -3P_Y \left(1 - \sqrt{\frac{3\epsilon_0\zeta_0}{2\rho}} \right).$$

Note that extension asymptotic states seem not to have been observed experimentally [114]. They are however predicted in critical state models. In the EKM, for both compression and extension states, the yield surface reduces to $f_Y = (\sigma_{ll} + 3P_Y)^2 - \frac{27\zeta_0\epsilon_0 P_Y^2}{2\rho}$.

Asymptotic dilative behavior We study here the asymptotic behavior observed at constant rate of dilation. Generally, the stress-strain curve obtained from a triaxial test approximatively displays a linear regime before that a constant stress ratio is reached. In this case, the rate of dilation is

constant [112]. We investigate here how these states are accounted for in the EKM.

According to (4.3.38), if the value of the rate of dilation $\beta = -\kappa_{ll}/\dot{\gamma}$ is constant and equal to β_c , the effective friction coefficient only depends on the density. This state can be summarized as follows

$$T = \frac{(4\eta_0\beta^2 + 2\zeta_0)\kappa_{ll}^2}{3\rho\epsilon_0}, \quad \beta = -\frac{\kappa_{ll}}{\dot{\gamma}}|_c, \quad \frac{\partial\rho}{\partial t} = -\rho\kappa_{ll}, \quad \frac{\sigma_s}{\sigma_{ll}} = \frac{\sigma_s}{\sigma_{ll}}|_c.$$

The stress-strain relation reduces to

$$\sigma_{ij} = -P_Y\delta_{ij} + \frac{2\eta_0 P_Y \sqrt{3\rho\epsilon_0}}{\rho\sqrt{4\eta_0 + 2\zeta_0\beta_c^2}} \frac{\kappa_{ij}^D}{\dot{\gamma}} + \frac{\zeta_0 P_Y \sqrt{3\rho\epsilon_0}}{\rho\sqrt{4\frac{\eta_0}{\beta_c^2} + 2\zeta_0}} \frac{\kappa_{ll}}{|\kappa_{ll}|} \delta_{ij}. \quad (4.3.46)$$

The shear stress and pressure are thus explicitly given by:

$$\begin{cases} \sigma_s = \frac{2\eta_0 P_Y \sqrt{3\rho\epsilon_0}}{\rho\sqrt{4\eta_0 + 2\zeta_0\beta_c^2}} & \text{and} & \sigma_{ll} = -3 \left(P_Y + \frac{\zeta_0 P_Y \sqrt{3\rho\epsilon_0}}{\rho\sqrt{4\frac{\eta_0}{\beta_c^2} + 2\zeta_0}} \right), & \kappa_{ll} < 0 \\ \sigma_s = \frac{2\eta_0 P_Y \sqrt{3\rho\epsilon_0}}{\rho\sqrt{4\eta_0 + 2\zeta_0\beta_c^2}} & \text{and} & \sigma_{ll} = -3 \left(P_Y - \frac{\zeta_0 P_Y \sqrt{3\rho\epsilon_0}}{\rho\sqrt{4\frac{\eta_0}{\beta_c^2} + 2\zeta_0}} \right), & \kappa_{ll} > 0. \end{cases}$$

At constant dilation, the shear stress and the pressure depends only on the density. If small density variation occurs, the friction coefficient is approximatively constant. This is thus compatible with what is observed during a triaxial test.

4.4 Limits of vanishing and increasing deformations

In this section, we study the two limiting states of the high-density quasi-static regime. For vanishing granular temperatures, the system tends to asymptotic static states. For increasing deformations, kinetic contributions must be accounted for and it modifies the shape of the yield surface.

4.4.1 Asymptotic static limits

We identify here the asymptotic static limits of EKM. Since viscosities and transport coefficients typically vary in $\frac{1}{\sqrt{T}}$, the EKM requires a non-vanishing

granular temperature. One can however study the asymptotic limits where $T \rightarrow 0$. In regions of very low granular temperature (see Section 4.6.1), the system should tend to these asymptotic limits, depending on the loading path. We show here the existence of asymptotic static states characterized by constant values for the shear and normal stress.

Vanishing shear rate at constant volume For an evolution at constant volume $\kappa_{ll} = 0$, i.e $\rho = \rho_c$, the total pressure and shear stress are given by

$$\sigma_{ll} = -3P_Y, \quad \sigma_s = \mu_s P_Y. \quad (4.4.1)$$

If the shear rate tends to zero, i.e $\dot{\gamma} \rightarrow 0$, the stress components remain constant and the relation (4.4.1) remains valid. This asymptotic static limit is characterized by the following relations

$$\sigma_{ll} = -3P_Y, \quad \sigma_s = \mu P_Y, \quad T \rightarrow 0, \quad \rho = \rho_c, \quad \eta \rightarrow +\infty.$$

This state can be seen as an isochoric critical state at zero shear rate. For simplicity, we wrote that the bulk viscosity tends to infinite. It is obvious that it is the case for all the transport coefficients. Additionally, we can express the value of ρ_c as a function of the total pressure $P_t = -\frac{\sigma_{ll}}{3}$

$$\rho_c = \rho_{cp} \frac{P_t + \rho_{co} T_0}{P_t + \rho_p T_0}. \quad (4.4.2)$$

Vanishing compression rate at zero dilation Consider the case of zero shearing $\dot{\gamma} = 0$. The shear stress and pressure are given by

$$\sigma_{ll} = -3P_Y + 3\sqrt{\frac{3\epsilon_0\zeta_0}{2\rho}} P_Y \frac{\kappa_{ll}}{|\kappa_{ll}|}, \quad \sigma_s = 0. \quad (4.4.3)$$

If the compression rate tends to zero, i.e $\kappa_{ll} \rightarrow 0$, the stress only depends on the density and will tend to constant. For negative compressive states $\kappa_{ll} < 0$, this asymptotic static limit is given by

$$\sigma_{ll} = -3(\mu_s + 1)P_Y, \quad \sigma_s = 0, \quad T \rightarrow 0, \quad \rho \rightarrow \rho_c, \quad \eta \rightarrow +\infty.$$

Evolution at constant rate of dilation We consider now the case where $\kappa_{ll} \rightarrow 0$ and $\dot{\gamma} \rightarrow 0$, and for which the dilation stays constant, i.e $\beta = \beta_c$. Since the compression rate tends to zero, the density will tend to a constant value, as well as the normal and shear stress.

$$\sigma_{ll} = -3 \left(P_Y + \frac{\zeta_0 P_Y \sqrt{3\rho\epsilon_0}}{\rho \sqrt{4\frac{\eta_0}{\beta_c^2} + 2\zeta_0}} \right), \quad \sigma_s = \frac{2\eta_0 P_Y \sqrt{3\rho\epsilon_0}}{\rho \sqrt{4\eta_0 + 2\zeta_0 \beta_c^2}},$$

$$T \rightarrow 0, \quad \rho \rightarrow \rho_c, \quad \eta \rightarrow +\infty.$$

In these static states, all the transport coefficients diverge, since they vary in $\frac{1}{\sqrt{T}}$.

4.4.2 Yield surface evolution for increasing deformations

In Section 4.3.1, we derived the yield criteria for states of small granular temperature $T \ll T_0$, for which the kinetic stress terms can be neglected. In the limit of increasing deformations, this is not valid anymore, let say around $T \sim T_0$. In the EKM, the normal stress is given by

$$\sigma_{ll} = -3(P_K + P_Y - \zeta_K \kappa_{ll} - \zeta_Y \kappa_{ll}), \quad (4.4.4)$$

and the deviatoric stress is given by,

$$\sigma_{ij}^D = 2(\eta_K + \eta_Y) \kappa_{ij}^D = 2 \left(\eta_0 \sqrt{T} g(\rho) + \frac{\eta_0 P_Y}{\rho \sqrt{T}} \right) \kappa_{ij}^D, \quad (4.4.5)$$

from which one can get the shear stress as

$$\sigma_s = 2(\eta_K + \eta_Y) \dot{\gamma} = 2 \left(\eta_0 \sqrt{T} g(\rho) + \frac{\eta_0 P_Y}{\rho \sqrt{T}} \right) \dot{\gamma}. \quad (4.4.6)$$

For the following, it is convenient to define the kinetic shear stress $\sigma_{s,K}$ as

$$\sigma_{s,K} = 2\eta_K \dot{\gamma} = 2\eta_0 \sqrt{T} g(\rho) \dot{\gamma}. \quad (4.4.7)$$

In the stationary uniform regime, the granular temperature is equal to

$$T = \frac{4\eta_0 \dot{\gamma}^2 + 2\zeta_0 \kappa_{ll}^2}{3\rho\epsilon_0}. \quad (4.4.8)$$

One can thus derive the flow rule and the yield surface in the same manner as in Section 4.3.1 by including the kinetic contributions. The extension can be easily obtained by inserting the kinetic terms into (4.3.14) and (4.3.20). The flow direction is now given by

$$\frac{\kappa_{ij}}{\sqrt{\dot{\gamma}^2 + \frac{\zeta_0}{2\eta_0}\kappa_{ll}^2}} = \frac{2}{9\zeta_0 P_Y} \sqrt{\frac{\rho\eta_0}{3\epsilon_0}} \left(\sigma_{ll} + 3P_Y + 3P_K - 3\zeta_K \kappa_{ll} \right) \delta_{ij} + \frac{\sqrt{\rho} (\sigma_{ij}^D - \sigma_{ij,K}^D)}{\sqrt{3\eta_0 \epsilon_0} P_Y},$$

and the yield surface can be calculated, in a similar way as in Section 4.3.1, by including the kinetic contributions

$$f_Y = (\sigma_{ll} + 3P_Y + 3P_K - 3\zeta_K \kappa_{ll})^2 + \frac{9\zeta_0}{2\eta_0} (\sigma_s - 2\eta_K \dot{\gamma})^2 - \frac{27\zeta_0 \epsilon_0}{2\rho} \nu^2 P_Y^2.$$

One can now insert the kinetic constitutive relations (3.1.9) into the expression of the yield surface to get

$$f_Y = \left(\sigma_{ll} + 3P_Y + 3Tg(\rho)\rho - 3\zeta_0 \sqrt{T}g(\rho)\kappa_{ll} \right)^2 + \frac{9\zeta_0}{2\eta_0} (\sigma_s - 2\eta_0 \sqrt{T}g(\rho)\dot{\gamma})^2 - \frac{27\zeta_0 \epsilon_0}{2\rho} \nu^2 P_Y^2.$$

By substituting the steady uniform value of the granular temperature (4.4.8), the yield surface is given by

$$f_Y = \left(\sigma_{ll} + 3P_Y + \frac{4\eta_0 \dot{\gamma}^2 + 2\zeta_0 \kappa_{ll}^2}{\epsilon_0} \rho g(\rho) - 3\zeta_0 g(\rho) \kappa_{ll} \sqrt{\frac{4\eta_0 \dot{\gamma}^2 + 2\zeta_0 \kappa_{ll}^2}{3\rho \epsilon_0}} \right)^2 + \frac{9\zeta_0}{2\eta_0} \left(\sigma_s - 2\eta_0 g(\rho) \dot{\gamma} \sqrt{\frac{4\eta_0 \dot{\gamma}^2 + 2\zeta_0 \kappa_{ll}^2}{3\rho \epsilon_0}} \right)^2 - \frac{27\zeta_0 \epsilon_0 \nu^2 P_Y^2}{2\rho}.$$

In the states of zero compression rate, i.e. $\kappa_{ll} = 0$, we find the regime previously studied in Section 4.2. In the case of pure compression rates ($\kappa_{ll} < 0$)

and $\dot{\gamma} = 0$), the pressure depends only on the density and the compression rate

$$\sigma_{ll} = 3 \left(\zeta_0 \sqrt{\frac{2\zeta_0}{3\rho\epsilon_0}} - \frac{2\zeta_0}{3\epsilon_0} \right) g(\rho) \kappa_{ll}^2 - 3P_Y \left(\sqrt{\frac{3\epsilon_0\zeta_0}{2\rho}} + 1 \right). \quad (4.4.9)$$

At constant deformation, the yield surface is an ellipse in the (σ_S, σ_{ll}) plane. For increasing deformations the size of the yield surface grows. In the case of vanishing of deformations, it reduces to the static yield surface found in Section 4.3.1.

The concept of dynamic yield surface has been employed in the plasticity and viscoplasticity theories [92]. Generally the rule which describes the evolution of the yield surface is called hardening rule. Isotropic hardening refers to an increase of the size of the yield surface with the deformation. Kinematic hardening refers to a translation of the yield surface in the stress space. In the high density quasi-static limit of the EKM, the yield surface translates and grows when increasing deformations. Thus, both isotropic and kinematic hardening appear.

Finally, we want to point out that this regime is found in states of stationary uniform granular temperatures and not only in the limit of small deformations. In this part, we identified some salient properties of the quasi-static regime, i.e yield surface, hardening rule and asymptotic behavior. It is remarkable to notice that these properties appear as a consequence of our (deliberately simple) choice of constitutive equations (see part 3) and have not been explicitly postulated. It emphasizes the high predictive power of the EKM. With only a few parameters and simple constitutive relations, a wide range of behavior are accounted for.

4.5 Shortcoming: discontinuous transition from loading to unloading

In the limit of small deformations, the system flows slowly at yield. We analyze here the influence of a change in the loading path. According to (4.3.46), the total pressure in the stationary limit of the EKM is given by

$$\sigma_{ll} = -3P_Y + 3 \frac{\zeta_0 P_Y \sqrt{3\rho\epsilon_0}}{\rho \sqrt{4\frac{\eta_0}{\beta^2} + 2\zeta_0}} \frac{\kappa_{ll}}{|\kappa_{ll}|}, \quad (4.5.1)$$

which can be rewritten as

$$\begin{cases} \sigma_{ll} = -3P_Y - 3 \frac{\zeta_0 P_Y \sqrt{3\rho\epsilon_0}}{\rho \sqrt{4\frac{\eta_0}{\beta^2} + 2\zeta_0}}, & \kappa_{ll} < 0 \\ \sigma_{ll} = -3P_Y + 3 \frac{\zeta_0 P_Y \sqrt{3\rho\epsilon_0}}{\rho \sqrt{4\frac{\eta_0}{\beta^2} + 2\zeta_0}}, & \kappa_{ll} > 0, \end{cases} \quad (4.5.2)$$

Consider a material having a negative compression rate, i.e $\kappa_{ll} < 0$. If κ_{ll} becomes positive because of the applied load, then according to (4.5.2), a pressure jump appears. According to (4.3.11), it is obvious, that not only the pressure but also all the stress components may vary discontinuously. This can be identified as a shortcoming of the EKM. Stress discontinuities appear during transition from loading to unloading. Since the system cannot reach states inside the yield surface, it must jump between different yield states. Further investigations should focus on a more precise study of the loading/unloading transitions in the EKM, and particularly investigate the formation of acceleration waves probably implied by stress discontinuities.

4.6 Some illustrative examples

We detail here some numerical examples to illustrate the notions of the previous sections. We first consider a simple one dimensional example. To study more sophisticated cases, it makes sense to run some simulations with the finite volume software CoRheoS, a finite volume solver for complex fluids [4,6]. The results of these numerical simulations are presented in the next sections.

4.6.1 1D-stationary extensional flow

Governing equations In this part, we consider a 1D pure extensional flow, i.e ($\dot{\gamma} = 0$), in a domain of length L . The material is assumed to slowly flow under gravity and a picture of the problem can be seen on Figure 4.5. According to (4.3.31), in the quasi-static limit, the granular temperature can be expressed as function of the square of the compression rate

$$T = \frac{2\zeta_0 \kappa_{ll}^2}{3\rho\epsilon_0}. \quad (4.6.1)$$

At small deformations, the volumetric stress tensor is approximately the sum of the yield pressure and the collisional term

$$\sigma_{ll} = -3P_Y + 3\zeta \kappa_{ll}. \quad (4.6.2)$$

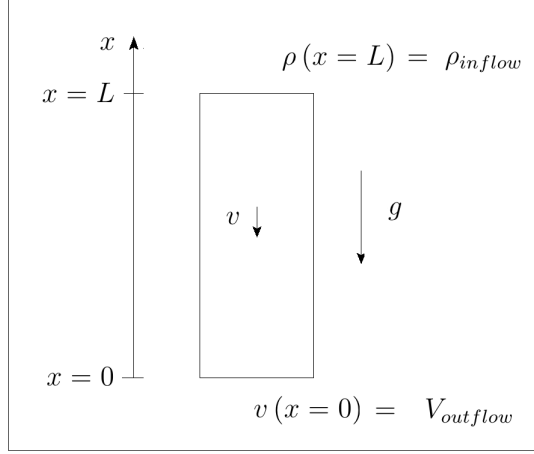


Figure 4.5: 1D extensional flow: picture of the numerical problem

Its value is explicitly given by substituting the expression of the bulk viscosity, expressed by (3.2.9)

$$\sigma_{ll} = -3P_Y + \frac{3\zeta_0 P_Y}{\rho\sqrt{T}} \kappa_{ll}. \quad (4.6.3)$$

Combining it with the expression of T given by (4.6.1) leads to

$$\sigma_{ll} = -3P_Y + 3\sqrt{\frac{3\epsilon_0\zeta_0}{2\rho}} P_Y \frac{\kappa_{ll}}{|\kappa_{ll}|}. \quad (4.6.4)$$

For a slow extensional flow, $\kappa_{ll} > 0$, the normal stress is finally given as

$$\sigma_{ll} = 3P_Y \left(\sqrt{\frac{3\epsilon_0\zeta_0}{2\rho}} - 1 \right). \quad (4.6.5)$$

By neglecting the convective term in the momentum equation, the pressure and the velocity obey

$$\begin{cases} v \frac{\partial \rho}{\partial x} + \rho \frac{\partial v}{\partial x} = 0, \\ \frac{\partial \sigma_{ll}}{\partial x} - \rho g = 0. \end{cases} \quad (4.6.6)$$

According to (4.6.5), the pressure depends only on the volume fraction, so that

$$\frac{\partial \sigma_{ll}}{\partial x} = \frac{\partial \sigma_{ll}}{\partial \rho} \frac{\partial \rho}{\partial x}. \quad (4.6.7)$$

The derivative of the pressure with the volume fraction can be obtained from (4.6.4)

$$\frac{\partial \sigma_{ll}}{\partial \rho} = 3 \frac{\partial P_Y}{\partial \rho} \left(\sqrt{\frac{3\zeta_0 \epsilon_0}{2\rho}} - 1 \right) - \frac{3P_Y}{2\rho} \sqrt{\frac{3\zeta_0 \epsilon_0}{2\rho}}. \quad (4.6.8)$$

Since $P_Y = T_0(\rho - \rho_{co})/(1 - \rho/\rho_{cp})$, one gets

$$\frac{\partial P_Y}{\partial \rho} = T_0 g(\rho) + \frac{P_Y}{\rho_{cp}} g(\rho). \quad (4.6.9)$$

Combining these two last equations, one gets

$$\frac{\partial \sigma_{ll}}{\partial \rho} = 3 \left(T_0 g(\rho) + \frac{P_Y g(\rho)}{\rho_{cp}} \right) \left(\sqrt{\frac{3\epsilon_0 \zeta_0}{2\rho}} - 1 \right) - \frac{3P_Y}{2\rho} \sqrt{\frac{3\epsilon_0 \zeta_0}{2\rho}}. \quad (4.6.10)$$

The force balance and mass conservation lead to a system of two equations for the unknowns v and ρ , which can be solved with appropriate boundary conditions. To mimic the condition of a granular layer flowing under critical conditions, we impose a pressure at the top ($x = L$) of the layer and a small velocity at the bottom ($x = 0$). According to (4.6.4), the specification of the density at the top of the layer, also fixes the value of the pressure. The boundary conditions are given by

$$v(x = 0) = v_{outflow}, \quad \rho(x = L) = \rho_{inflow}. \quad (4.6.11)$$

As the whole, the problem is formulated as

$$\left\{ \begin{array}{lcl} v \frac{\partial \rho}{\partial x} + \rho \frac{\partial v}{\partial x} & = & 0, \\ \left(3 \left(T_0 g(\rho) + \frac{P_Y g(\rho)}{\rho_{cp}} \right) (\bar{\mu} - 1) - \frac{3P_Y}{2\rho} \bar{\mu} \right) \frac{\partial \rho}{\partial x} & = & \rho g, \\ v(x = 0) & = & V_{outflow}, \\ \rho(x = L) & = & \rho_{inflow}. \end{array} \right. \quad (4.6.12)$$

with $\bar{\mu} = \bar{\mu}(\rho) = \sqrt{\frac{3\epsilon_0 \zeta_0}{2\rho}}$. If one postulates some dependence for the density or the velocity, one may be able to find a semi-analytical solution for the system (4.6.12). However, in this work, we integrate numerically the system of equations, so that we don't need to formulate additional assumptions.

Results The variation of the velocity, density and pressure obtained by solving numerically the system of equation with the Partial Differential Equation (PDE) solver of the computer algebra system *Mathematica 8.0*, can be seen in Figures 4.6 and 4.7. As expected, the stationary state is characterized by small velocity and density variations. A non-linear interpolation of these functions give $\rho/\rho_{cp} = 0.62x^{0.02}$ and $v/v_{out} = -0.98x^{0.02}$. Once the density is known, the pressure distribution can be calculated, its variation can be seen in Figure 4.7.

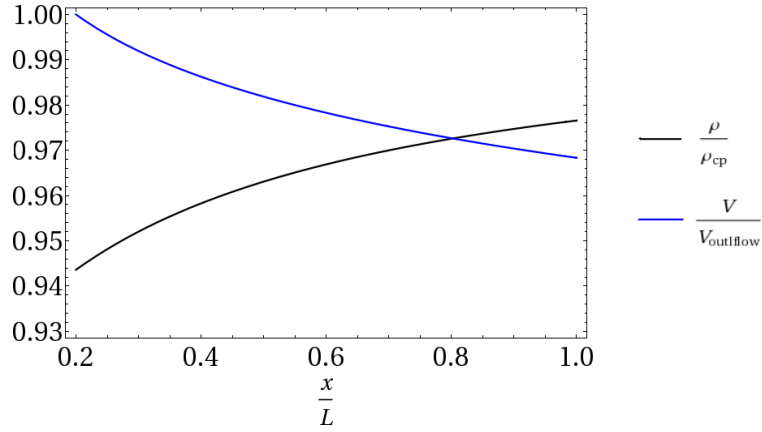


Figure 4.6: Variation of the volume fraction and the velocity scaled with $v_{outflow}$.

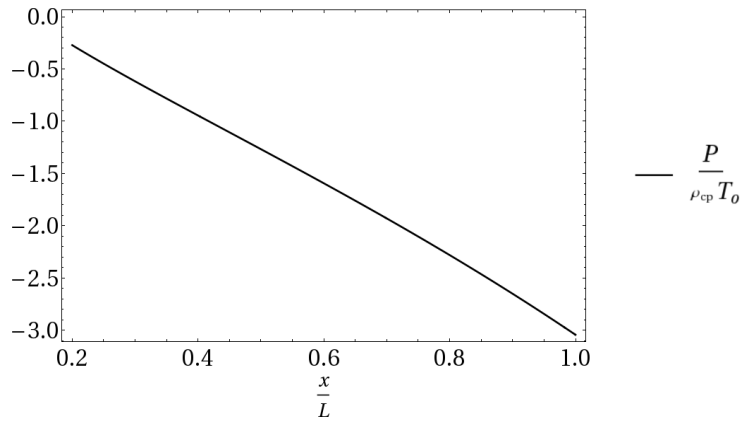


Figure 4.7: Variation of the pressure scaled with $\rho_{cp} T_0$.

4.6.2 Filling on a tube

Consider the filling of grains into a box. After a certain time, grains accumulate inside the box and a solid equilibrium is reached characterized by high density, zero velocity and zero granular temperature. The EKM is built to account for the evolution of a granular system from the dilute flow to the dense flow regime. Fully static states (characterized by $T = 0$) cannot be reached since they imply a divergence of the transport coefficients. However, we showed in Section 4.3 that in the quasi-static limit of high densities, the EKM exhibits a plastic behavior.

To get a more concrete representation of these states, we simulate a filling experiment with the finite volume solver CoRheoS. The numerical method implemented in this software has been detailed in [3, 6]¹. We consider a 2D problem here. The length of the box is 0.14 m and its width is 0.7 m. The computational domain contains 18×60 rectangular grids. The inflow velocity is set to -0.05 m s^{-1} . The values of the material parameters are taken as

$$\begin{aligned} \rho_{co}/\rho_b &= 0.6, \quad \zeta_0/\rho_b = 0.0001 \text{ m}^2 \text{ s}^{-1}, \quad \eta_0/\rho_b = 0.000355 \text{ m}^2 \text{ s}^{-1}, \\ T_0/\rho_b &= 1.5 \text{ m}^2 \text{ s}^{-1}, \quad \phi = 30^\circ, \quad \rho_b = 1600 \text{ kg m}^{-3}, \quad \rho_{cp}/\rho_b = 0.64, \\ \lambda/\rho_b &= 0.00034 \text{ m}^2 \text{ s}^{-1}. \end{aligned}$$

The evolution of the density at different steps of the filling process can be seen on Figure 4.8. Grains are first filled into the box. Consequently, the density inside the box increases, until the filling is stopped, at $t = 2.55 \text{ s}$. Figure 4.9 shows the evolution of the shear rate, compression rate, velocity and granular temperature on a fixed point, situated at the middle of the box ($x = 0.04 \text{ m}$, $y = 0.05 \text{ m}$). The evolution of the yield pressure, shear stress and collisional pressure at the same point can be seen on Figure 4.10. The plots begin at $t = 1.8 \text{ s}$, time at which density becomes greater than the cross-over value ρ_{co} . One can see that the end of the filling process (at $t = 2.55 \text{ s}$), implies a jump in the velocity and granular temperature and on the pressure.

Looking at Figure 4.9, we identify three steps on the evolution of the granular temperature:

- a decrease during the filling from $T = 0.001 \text{ m}^2 \text{ s}^{-2}$ to $T = 10^{-15} \text{ m}^2 \text{ s}^{-2}$,
- a peak corresponding to the end of the filling,

¹The time integration employed here has been detailed in [6]. It is combined with a finite volume space discretization which was explained in [3]. Note that, contrary to [3], our model imply a symmetric stress tensor which ensures angular momentum conservation.

- a constant evolution around $T=10^{-15}\text{m}^2 \text{ s}^{-2}$. During this step, the granular value is equal to its quasi-static value $\frac{(4\eta_0\dot{\gamma}^2+2\zeta\kappa_{II}^2)}{\rho\epsilon_0}$. This can be verified by at looking Figure 4.11.

Figure 4.9 shows that the velocity, shear rate and compression rate have a similar evolution to the temperature since they significantly diminish until a stationary value is reached. At the end of the simulation, the shear rate and compressional rate are at the order of 10^{-6}s^{-1} and the velocity reaches very low values (around 10^{-5} m s^{-1}). Looking at Figure 4.10, we see that the yield pressure term dominates. At the end of the filling process, the friction coefficient is around $\sigma_S/P \sim 1/7$. The pressure, density, velocity and temperature distributions at the end of the process can be seen on Figure 4.12. The pressure is maximal at the bottom center of the box, and decreases with the depth of box, as it can be intuitively expected.

4.6.3 Sand pile formation and pressure dip

Similarly, we present the result of a 2D numerical experiment of sand pile formation. It was previously shown in the work of Schmidt [3]² that a hydrodynamic model similar to this introduced in this work can predict the formation of sand piles. It was also outlined that the slope of the sand pile varies a few degree from the angle of friction [3], which can be defined as material parameter of the EKM through (4.3.43).

We complete here the analysis of this numerical experiment by studying the density and pressure distribution inside the sand pile. To do that, we run a 2D numerical simulation with the same values of the material and process parameters as previously. We first notice that in the early steps of filling, before that the first grains arrive at the bottom, only kinetic flows happen during which shear and compression rates are high (greater than 1s^{-1}). Once the first grains arrive at the bottom, they quickly lose their velocity and accumulate to form a pile. They move from the kinetic regime to the slow plastic one where shear and compressive rates are very low (below than 10^{-3}s^{-1}) as well as the granular temperature which is vanishing (values of $T= 10^{-14}\text{m}^2 \text{ s}^{-2}$ are reached at the end of the simulation). The volume fraction profiles are plotted on Figures 4.13-4.19 at different times. To better visualize the density profile inside the heap, we plot the volume fraction on two different scales. In all these figures, both dilute flow (in the filling jet, outside the pile) and the critical state regime (inside the pile) occur.

²As already mentioned in the previous footnote, in this reference a non-symmetric stress tensor was considered.

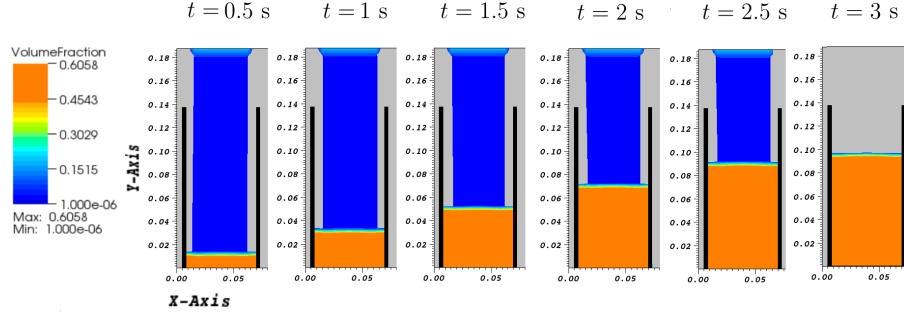


Figure 4.8: Volume fraction at the different steps of the filling process.

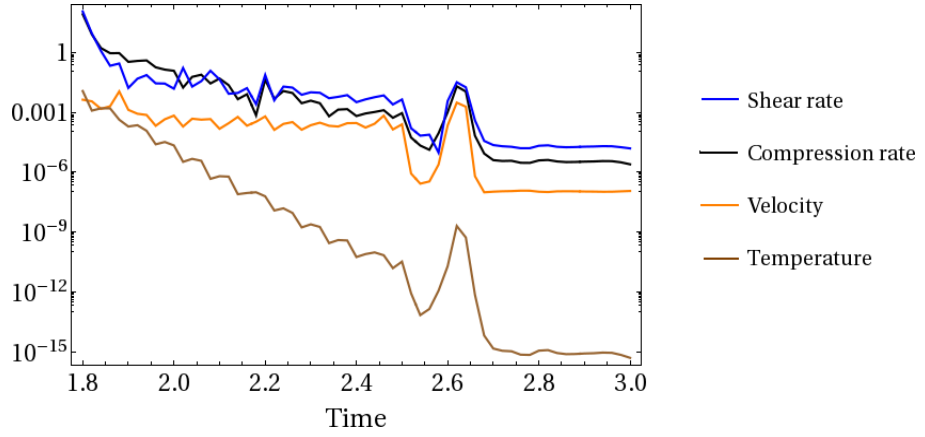


Figure 4.9: Plot of the evolution of relevant variables on a logarithmic scale. Unity: shear rate $\dot{\gamma}$ and compression rate κ_{ll} in s^{-1} , velocity in $m s^{-1}$, temperature in $m^2 s^{-2}$ and time in s .

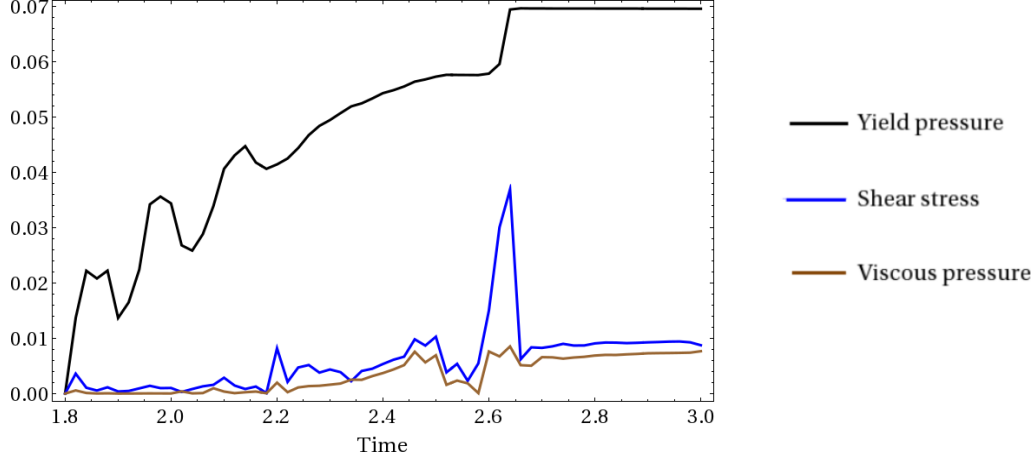


Figure 4.10: Plot of the evolution of the yield pressure P_Y , shear stress σ_s and viscous pressure $\tilde{P} = -\zeta\kappa_{II}$. The values are scaled with the bulk density and given in $\text{Pa}/(\text{kg m}^{-3})$. Time is in s.

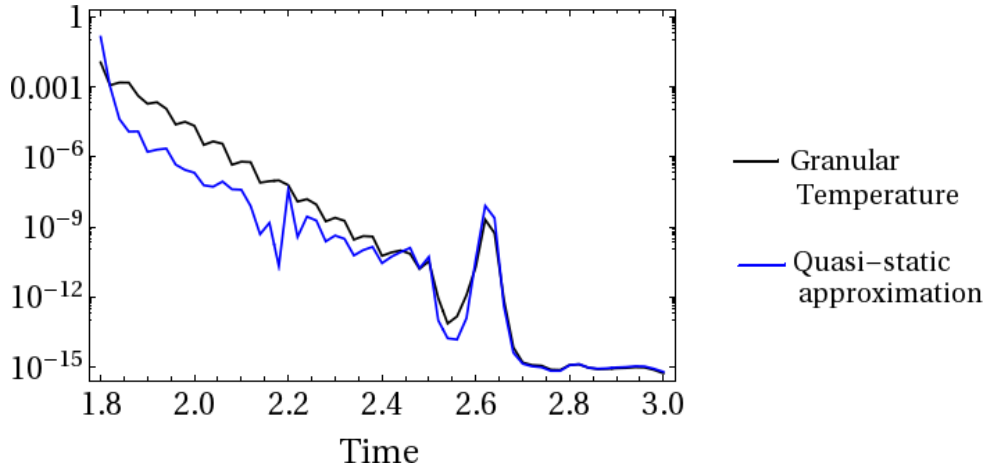


Figure 4.11: Plot of the evolution of the granular temperature ($\text{m}^2 \text{s}^{-2}$) and its value found in the high density quasi-static limit $T = \frac{4\eta_0\dot{\gamma}^2 + 2\zeta_0\kappa_{II}^2}{\rho\epsilon_0}$, found in part 4.3. Time is in s.

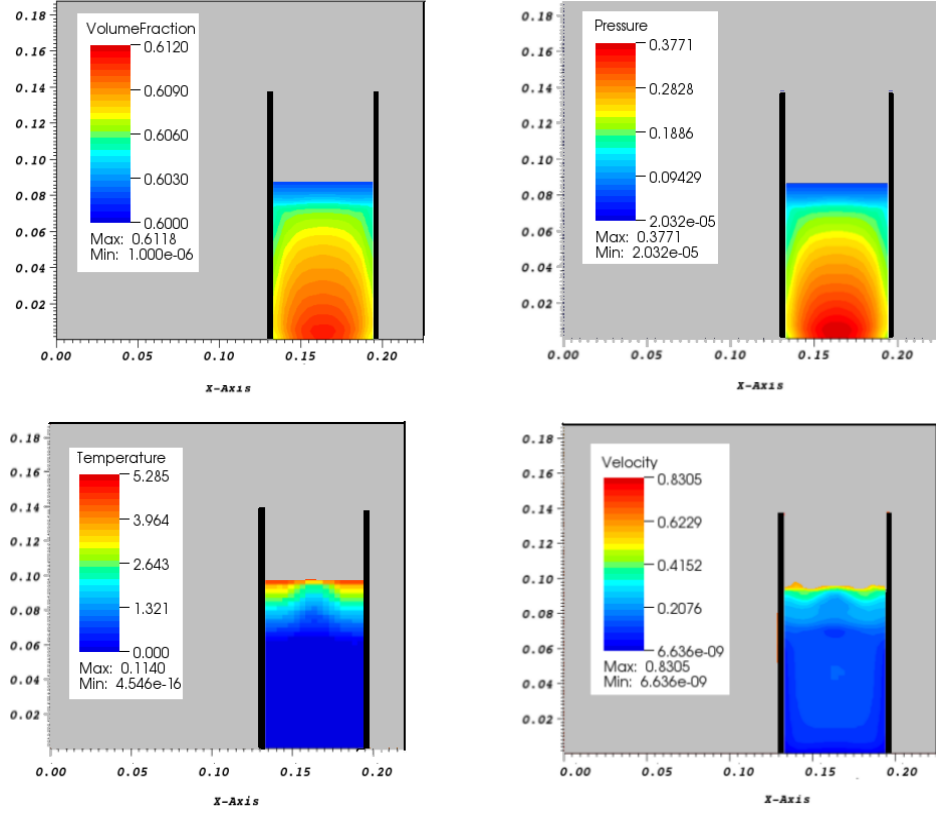


Figure 4.12: Plots of the volume fraction, velocity (m s^{-1}), temperature ($\text{m}^2 \text{s}^{-2}$) and pressure (scaled with bulk viscosity, in $\text{Pa}/(\text{kg m}^{-3})$) distributions at the end of the filling process.

The small volume fraction variations inside the heap can be seen on the bottom pictures. It can be observed that the density is not homogeneous inside the sand pile and that it is smaller at the middle of the pile. Figure 4.17 shows the pressure distribution at $t=3.5$ s. Remarkably, a pressure minimum appears at the bottom of the pile. It exhibits a similar profile than the density distribution. This is because the pressure is directly related to the density in this regime. Thus, the pressure dip is implied by the inhomogeneous density distributions produced by the filling of the grains. Additionally, this simulation shows that the pressure dip appears very early during the filling procedure. It is interesting to remark that this has also been observed in discrete element simulations [121].

In the literature, a lot of theoretical, numerical and experimental studies focus on the pressure distribution in sand piles. A pressure dip in the pile

has been experimentally observed (see Appendix A.1) and its origin has been intensively discussed. It was also observed that the stress distribution in sand piles depends on how grains were filled into the system. Vanel et al [122] showed that filling sand with a sieve leads to a maximum of pressure at the centre. When a hopper is used, a local minimum appears. Additionally, the presence of a base deflection has been identified as an important factor for producing a pressure dip. An intensive experimental study of the pressure dip and the influence of the parameters on the pressure distribution can be found in [121].

A lot of models have been proposed in the literature to explain this surprising phenomena. Some authors argued that density variations are the cause of the pressure dip [84]. One can postulate the existence of a inhomogeneous density distribution inside the pile and employ some quasi-elastic model involving some density-dependent shear and bulk modulus [84] to reproduce the pressure dip. As illustration, we show in Appendix B that the hyperelastic Jiang-Liu model [7] (at constant density) predicts a maximum of pressure at the bottom of the pile. If one assumes a non-homogeneous density distribution (in a similar form as this from Figure 4.19) and add some density dependence on the stiffness parameters, a pressure dip will be found in the pile [84]. Alternatively anisotropic elastic constitutive laws have been employed to model the pressure dip. Physicists proposed also a new class of models which suppose the existence of some relations between the components of the stress tensor [13, 123–125]. The simplest one is the incipient failure everywhere theory [13] which assumes a static granular system to be at slip failure everywhere. A more sophisticated one was proposed by Bouchaud et al. [123] who postulated a proportional relation between the horizontal and vertical principal stresses. Additionally, the pressure dip has been reproduced and studied with discrete element simulations [121]. Several engineers have also combined a elastoplastic model with a construction scheme to mimic the filling procedure. The pile must be decomposed into several layers which are progressively activated during the simulation. Thus, this model imposes some strong hypothesis about the filling process since it doesn't account for important dynamic processes such as avalanching or flowing [121]. However, it was shown that under these assumptions, a simple isotropic elastoplastic model can reproduce the pressure dip. Thus, in this case, material stiffness anisotropy must not be postulated [121].

In our numerical simulation, we are able to fully reproduce the filling process and the pile formation with the correct pressure distribution. To the best knowledge of the author, it is the first time that this phenomena is reproduced with a hydrodynamic model by fully accounting for the filling procedure. The spatial density variations occurring during the filling process

creates the minimum of pressure inside the pile. It validates the hypothesis that the pressure dip is implied by the inhomogeneous density distributions. It demonstrates also that a granular hydrodynamic model with relative simple constitutive equations can reproduce this phenomenon. The density is here the macroscopic variable which accounts for the history dependence of the grains. It is thus not necessary to introduce other macroscopic variables or apply some anisotropic stress-strain relation. In this respect, the development of complex mathematical methods which focus on the full hydrodynamic equations and the corresponding software CoRheoS [3,6] is a strong contribution. It provides us some key information on the behavior of granular systems. We note that the use of our internal code allows to study the influence of the filling process on stress distribution in quasi-static granular assemblies. Additional numerical investigations performed during this work showed that process parameters like the pouring rate, the size of the source, the number of the sources and their height influence the form of the pressure distribution. For example, we can show on Figure 4.20 that the pressure field exhibits a different profile if one fill the pile with two sources. Further investigations should focus on a quantitative comparison of the predictions of the EKM with recent experimental studies, like [121].

These numerical simulations give informations (like density distributions) which are sometimes difficult to measure. This is a crucial information for a lot of applications, like for instance bulk handling or civil engineering.

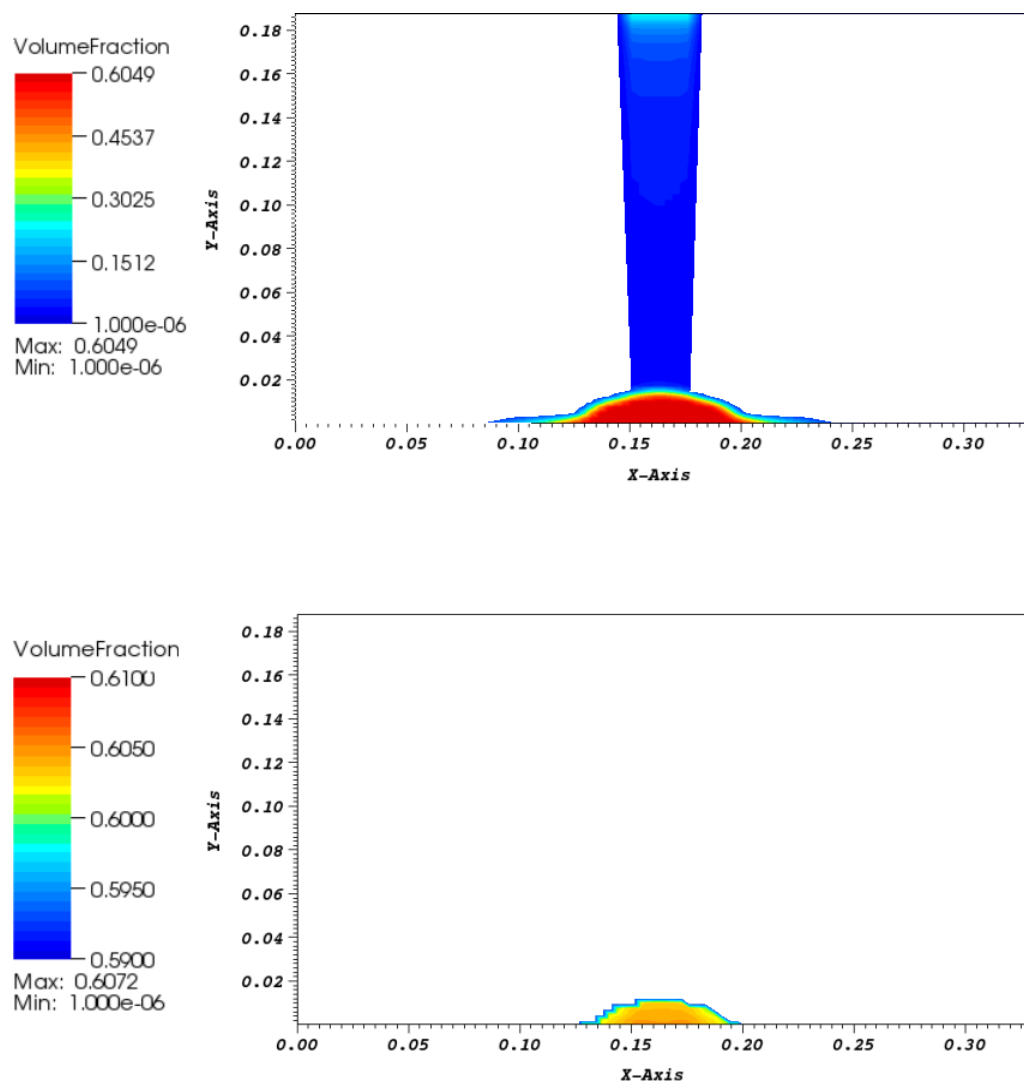


Figure 4.13: Plot of the volume fraction at the time $t = 0.5$ s. Top picture: scale varying from 0 to 0.6049. Bottom picture: scale varying from 0.59 to 0.61.

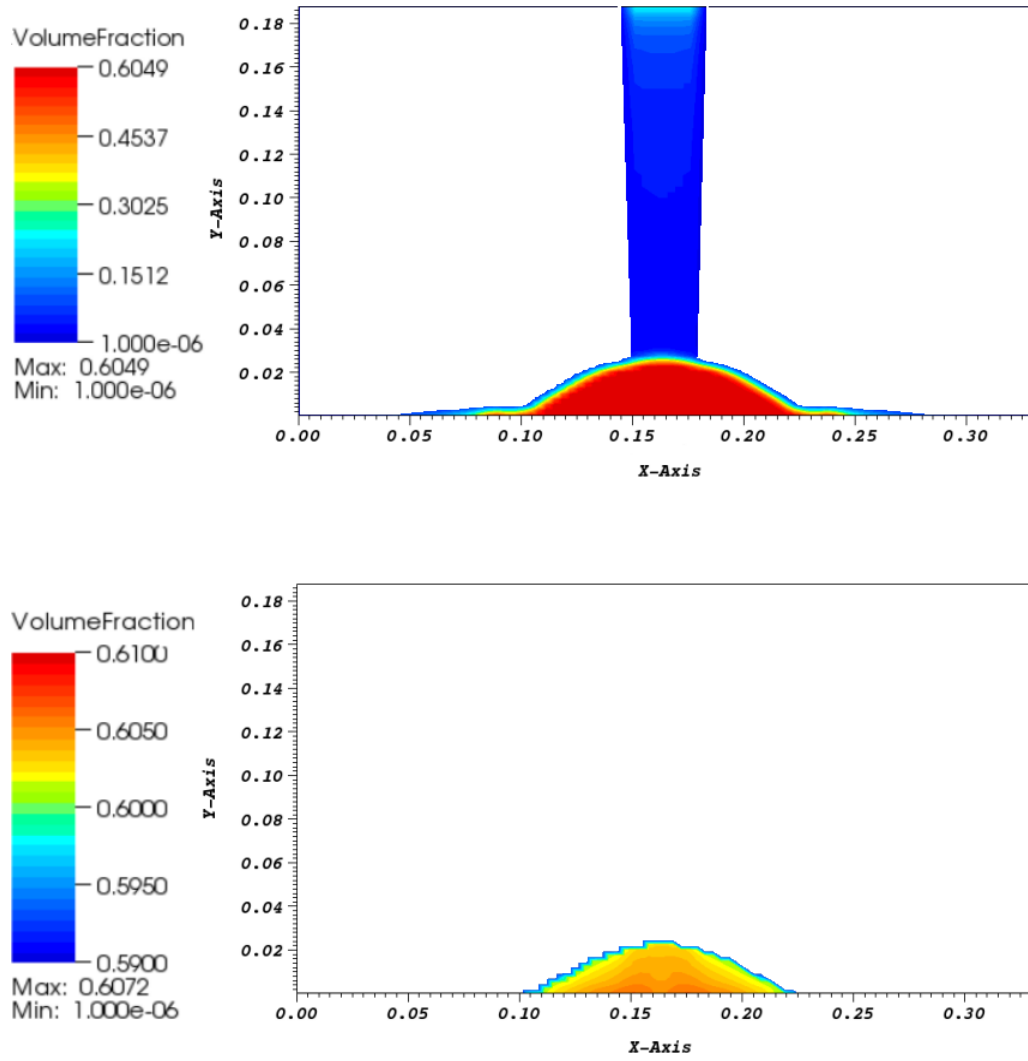


Figure 4.14: Plot of the volume fraction at the time $t = 1$ s. Top picture: scale varying from 0 to 0.6049. Bottom picture: scale varying from 0.59 to 0.61.

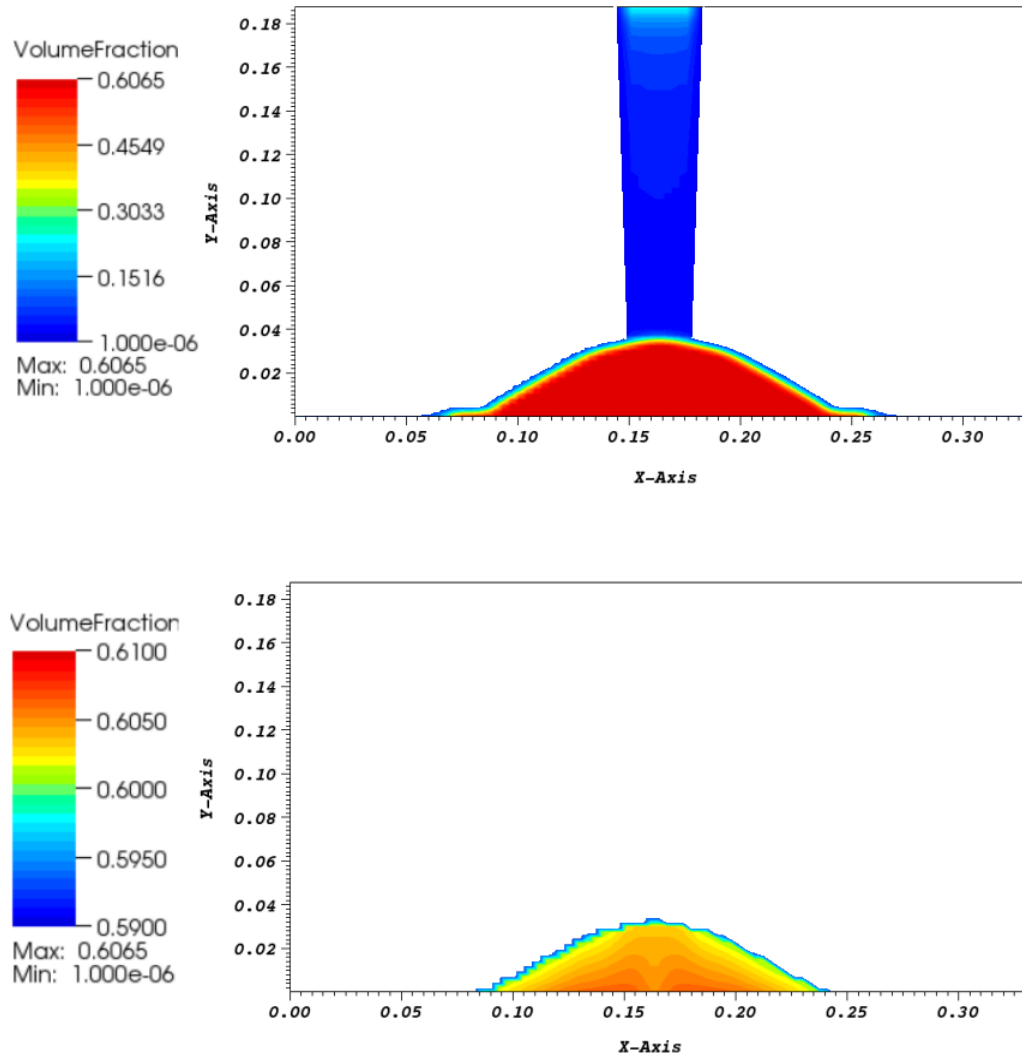


Figure 4.15: Plot of the volume fraction at the time $t = 1.5$ s. Top picture: scale varying from 0 to 0.6065. Bottom picture: scale varying from 0.59 to 0.61.

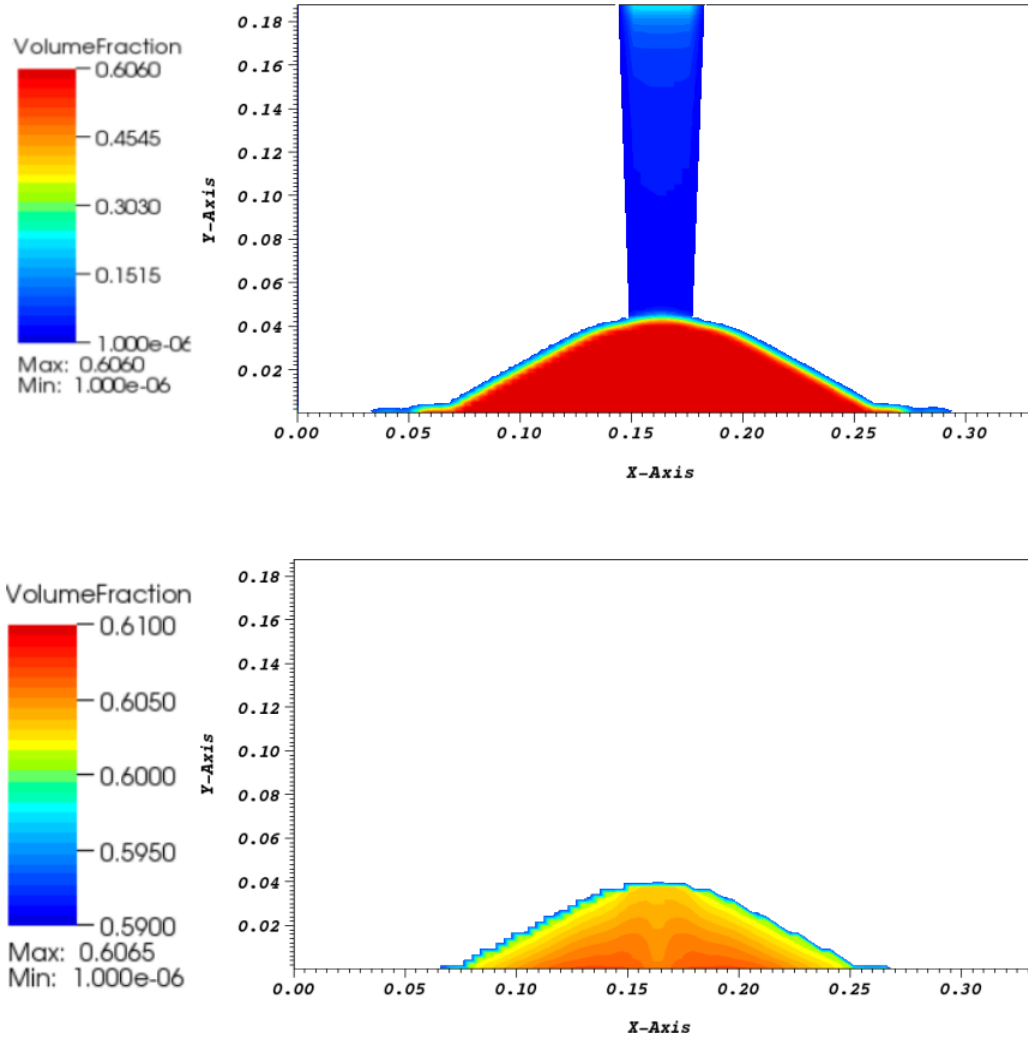


Figure 4.16: Plot of the volume fraction at the time $t = 2$ s. Top picture: scale varying from 0 to 0.6060. Bottom picture: scale varying from 0.59 to 0.61.

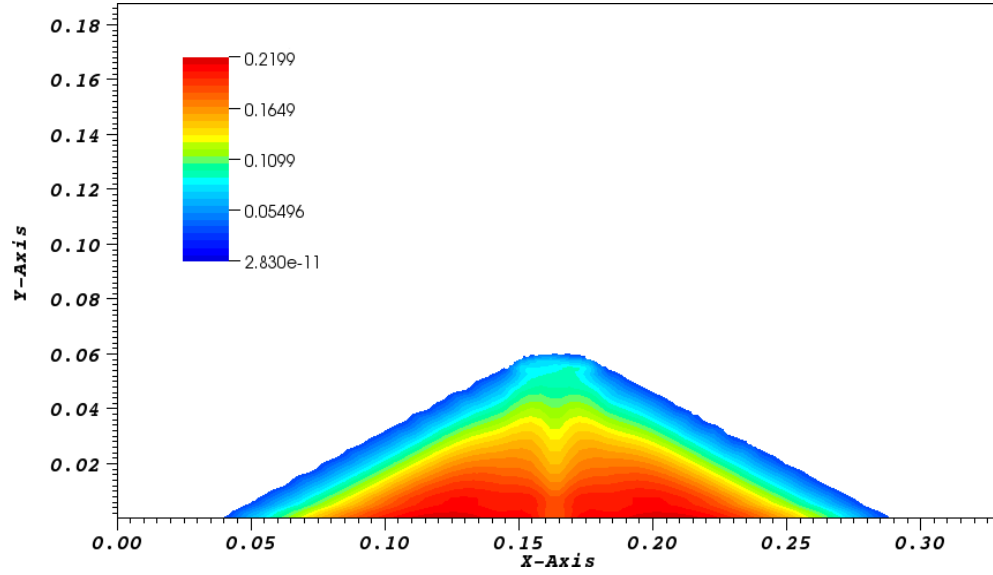


Figure 4.17: Plot of the pressure scaled with the bulk density at $t = 3.5$ s. Unity: $\text{Pa}/(\text{kg m}^{-3})$.

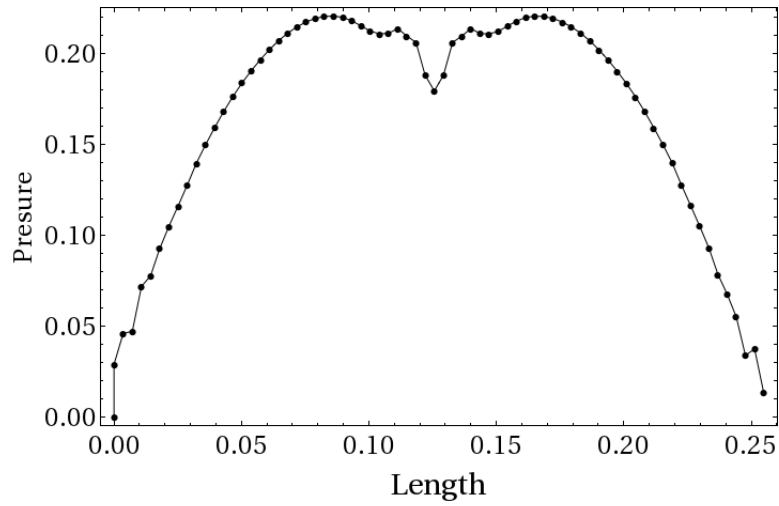


Figure 4.18: Plot of the pressure profile at the bottom of the sand pile from Figure 4.17 scaled with the bulk density at 3.5s. Unity: Scaled pressure $\text{Pa}/(\text{kg m}^{-3})$, length in m.

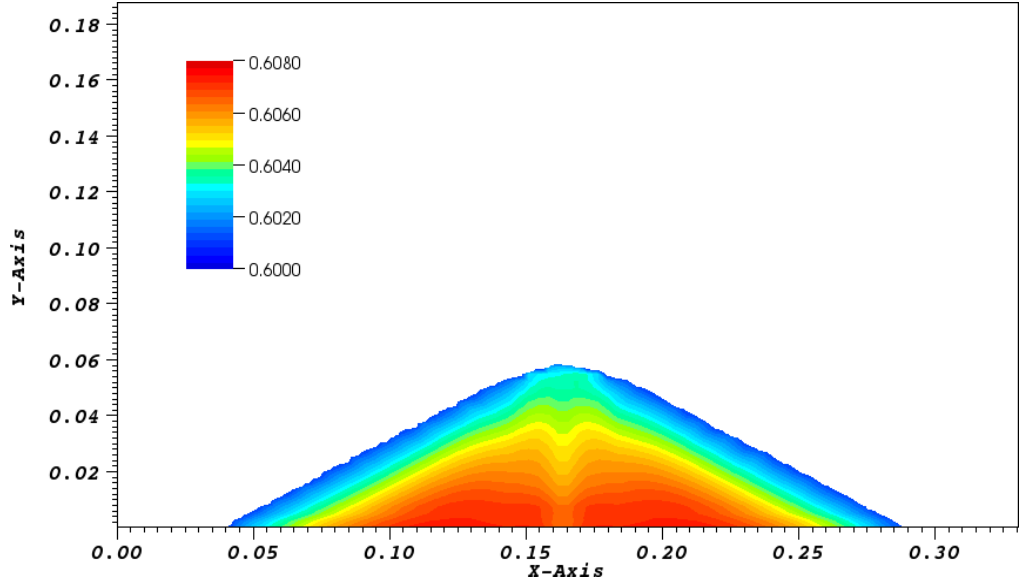


Figure 4.19: Plot of the volume fraction at $t = 3.5$ s. Length in m.

4.7 Conclusion and discussion

The hydrodynamic model introduced in this part provides a simple approach to model dry granular systems at both dilute and dense regime. We called it Extended Kinetic Model (EKM). In the limit of dilute rapid flow regime, it reduces to a kinetic model. In the high density quasi-static limit, it reduces to a critical state plasticity model. Contrary to more practical approaches where constitutive laws are formulated from the results of discrete numerical simulation or experiments without any thermodynamic consideration, the EKM considers both momentum and energy equation. It is interesting to remark that it covers some well-known behavior observed in granular systems.

In the pure shear regime, the granular temperature is proportional to the square of the shear rate and Bagnold's scaling is covered. For larger densities, viscosities and transport coefficients are the sum of kinetic term and a yield one, which depends on the inverse of the square root of the temperature, as found by Savage [5]. We explained how the constitutive equations can be modified to be consistent with the frictional law proposed by Pouliquen et al. [31] to describe dense shear flows.

In the quasi-static limit of small granular temperature, yield terms dominate and viscosities reach large values. The dependence of the viscosity on the granular temperature in $1/\sqrt{T}$ constrains the system to flow slowly at yield. In this regime, the stress components describe a yield surface. Small

density variations occur. The isochoric critical state was found as part of the solution and we explained how the internal friction angle can be defined as material parameter.

Remarkably, the development and implementation of efficient mathematical methods into the finite volume software CoRheoS by Niedzela [6] and Schmidt [3], have allowed to use granular hydrodynamic models to simulate a wide range of processes, including core and mass flow in silos, sand pile formation and powder mixing. We employed this code to better analyze and characterize the quasi-static state reached in the EKM when grains are filled in a plate or on a box. Quasi-static zones remain numerically stable, also at very small granular temperatures $\sim 10^{-16} \text{ m}^2 \text{ s}^{-2}$, i.e for huge viscosities $\sim 10^5 \text{ kg}^{-1} \text{ s}^{-1}$. By performing a filling experiment, we showed that, the density distribution inside the sand heap is not homogeneous and is smaller in the center of the pile. Looking at the pressure distribution, a pressure dip is established inside the heap. It is crucial to remark that this effect is reproduced with a model which involves relative simple constitutive equations.

The introduced model provides a pertinent way to simulate processes, where the transition from rapid collisional flow to slow motion appears. Notice however that the case of a bloc of sand initially at rest and flowing is more tricky. It is a priori not clear how to calculate initial conditions. However, we showed in this section how a stationary solution can be calculated in a one dimensional case.

We analyzed the quasi-static regime at slow temperature. We found that a transition from loading to unloading creates a discontinuous variation of stress. Additionally, no elastic effects are accounted for. In the quasi-static regime, the yield condition $f_Y = 0$ always applies and the constitutive laws do not allow the system to reach states inside the yield surface, except for infinite transport coefficients. Another important practical issue is that numerical instabilities may appear in quasi-static zones where viscosities become too large, let say greater than $10^7 \text{ kg}^{-1} \text{ s}^{-1}$. Static equilibrium, where $T = 0$ cannot be reached in the simulations since it implies a divergence of the viscosities and of the transport coefficients.

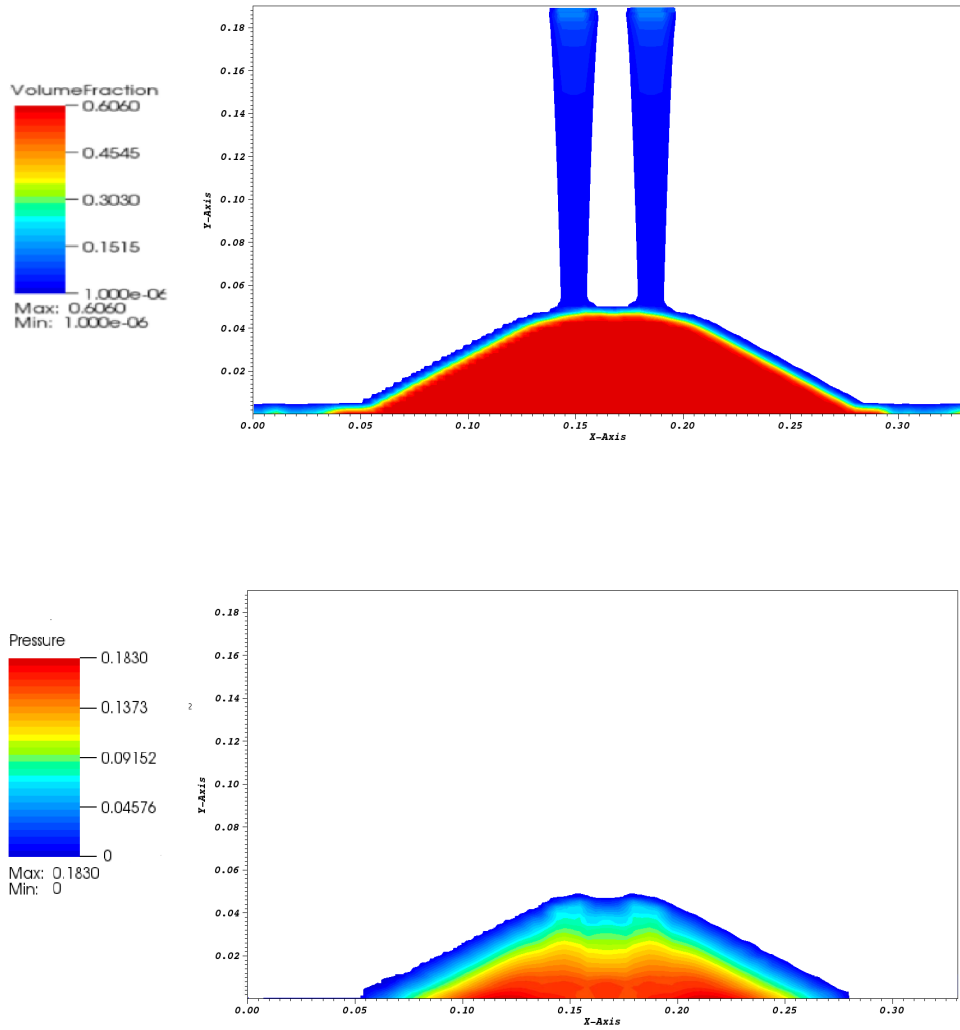


Figure 4.20: Top picture: plot of the volume fraction at $t=3.5s$ for a filling with two sources. Bottom picture: plot of the pressure scaled with the bulk density at $t= 3.5s$

5

From slow critical flow to static state

In Section 3, we introduced a hydrodynamic model valid for dilute and dense granular flow, called Extend Kinetic Model (EKM). It combines the results of the granular gas kinetic theory and critical state plasticity. In the quasi-static limit of small deformations, it reduces to a critical state model. Although quasi-static states can be reached (strain rates of 10^{-6} s^{-1} were found in the simulations of the previous part), the system still flows and cannot reach static states ($T = 0$). Additionally the transition from static states to critical states is not accounted for.

Generally soil mechanics models describe the evolution of initially static granular systems which are loaded. In the critical state plasticity theory, the material is sometimes assumed to be perfectly rigid-plastic [61]. It means that it behaves like a rigid body inside the yield surface.

In the elasto-plastic description, the material deforms elastically inside the yield surface and flows irreversibly at yield [92].

Alternatively, the quasi-static behavior can be modeled with hypoplastic laws [8]. It is based on the formulation of rate-equations and does not employ concepts like yield surface, or decomposition of strain into an elastic and a plastic part. In the hypoplastic theory, an irreversible behavior is assumed above the limit state as it was observed in experiments.

It is tempting to extend the validity of the EKM to states of vanishing granular temperature by combining it with some soil mechanics model. Before doing that, it is first convenient to recall the results of Section 4.3. We found that in the high density quasi-static limit of the EKM, the stress-strain

relation is viscoplastic and given by

$$\sigma_{ij} = -P_Y \delta_{ij} + \frac{2\eta_0 \sqrt{3\rho\epsilon_0} P_Y}{\rho \sqrt{4\eta_0 \dot{\gamma}^2 + 2\zeta_0 \kappa_{ll}^2}} \kappa_{ij}^D + \frac{\zeta_0 \sqrt{3\rho\epsilon_0} P_Y}{\rho \sqrt{4\eta_0 \dot{\gamma}^2 + 2\zeta_0 \kappa_{ll}^2}} \kappa_{ll} \delta_{ij}. \quad (5.0.1)$$

The flow rule was found by inverting the above relation

$$\frac{\kappa_{ij}}{\sqrt{\dot{\gamma}^2 + \frac{\zeta_0}{2\eta_0} \kappa_{ll}^2}} = \frac{2}{9\zeta_0} \sqrt{\frac{\rho\eta_0}{3\epsilon_0}} \frac{(\sigma_{ll} + 3P_Y) \delta_{ij}}{P_Y} + \frac{\sigma_{ij}^D \sqrt{\rho}}{\sqrt{3\eta_0 \epsilon_0} P_Y}. \quad (5.0.2)$$

Under these conditions, the stress components describe a yield surface, given by

$$f_Y = (\sigma_{ll} + 3P_Y)^2 + \frac{9\zeta_0}{2\eta_0} \sigma_s^2 - \frac{27\zeta_0 \epsilon_0}{2\rho} P_Y^2 = 0. \quad (5.0.3)$$

The relation (5.0.3), applies during a critical quasi-static flow of the medium ($T > 0$). The system is constrained to flow at yield and there is actually no mechanism which allows to reach states inside the yield surface $f_Y < 0$, except for infinite viscosities. We need to fully account for the solid-like behavior of granular systems. In the following, three possible extensions will be investigated. We will consider the cases of including a rigid solid behavior, a quasi-elastic regime and a hypoplastic one. In the literature, several studies have focused on developing some mathematical models involving a spatial coupling between a viscous flow regime and a core undergoing deformations [126]. In this part, we will formulate models which can be applied to the evolution of a granular system from the dense critical flow to static state. For reasons that will be detailed, we will prefer the third option, i.e to combine the EKM with an hypoplastic regime. This will allow us to formulate a general hydrodynamic model.

5.1 Transition to rigid solid behavior

The simplest scenario is discussed here. It consists on including a rigid solid behavior. In the critical state plasticity [56] or in the Bingham fluid model [60], the system undergoes deformation at yield and behaves like a rigid solid when the yield criteria is not satisfied. Specially in the case of the Bingham fluid [60], it gives, in the simple one dimensional case

$$\begin{cases} \sigma_{12} = \sigma_Y + \eta \dot{\gamma}, & \sigma_{12} > \sigma_Y, \\ \dot{\gamma} = 0, & \sigma_{12} < \sigma_Y, \end{cases} \quad (5.1.1)$$

where σ_{12} is the shear stress.

In parallel, in the critical state plastic theory [56], plastic deformation occurs at yield. Inside the yield surface, a rigid solid behavior can be assumed

$$\begin{cases} \dot{\epsilon}_{ij}^p \neq 0 & f_Y = 0, \\ \dot{\epsilon}_{ij}^p = 0 & f_Y < 0. \end{cases} \quad (5.1.2)$$

We propose here to incorporate a rigid solid behavior inside the EKM. In Section 4.3, we showed that in the high density quasi-static limit of the EKM, the following viscoplastic stress-strain relation applies

$$\begin{cases} \sigma_{ij} = -P_Y \delta_{ij} + \frac{2\eta_0 P_Y}{\rho \sqrt{T}} \kappa_{ij}^D + \frac{\zeta_0 P_Y}{\rho \sqrt{T}} \kappa_{ll} \delta_{ij}, \\ T = \frac{4\eta_0 \dot{\gamma}^2 + 2\zeta_0 \kappa_{ll}^2}{3\rho \epsilon_0}, \end{cases} \quad (5.1.3)$$

which requires the system to be at yield, i.e $f_Y = 0$. The extension to rigid solid-behavior can thus be written as

$$\begin{cases} \sigma_{ij} = -P_Y \delta_{ij} + \frac{2\eta_0 P_Y}{\rho \sqrt{T}} \kappa_{ij}^D + \frac{\zeta_0 P_Y}{\rho \sqrt{T}} \kappa_{ll} \delta_{ij}, & f_Y = 0 \\ T = 0, & f_Y < 0. \end{cases} \quad (5.1.4)$$

Consider the evolution of a granular system from the rapid flow regime to the dense flow, modeled with the EKM. If the quasi-static regime is reached, the yield condition $f_Y = 0$ applies and there is *a priori* no mechanism which allows the system to reach a state inside the yield surface, i.e $f_Y < 0$. A convenient way to explicitly include a rigid solid behavior, is to introduce a temperature of rigid transition $T_{rt} \ll T_0$ under which the rigid solid behavior applies. In these zones, the stress is unknown and the granular temperature and velocities are set to zero.

Another interesting consideration, made by Liu [79], is that a instability should occur when the density becomes too high to sustain shear flow, reminiscent of the jamming transition. In physics, jamming designs the process during which granular materials become rigid because of an increasing density. It can be modeled by assuming a drop of the shear rate at constant shear stress, if

$$\rho > \rho_j, \quad \frac{\partial \sigma_s}{\partial t} = 0 \quad \text{and} \quad \dot{\gamma} = 0, \quad (5.1.5)$$

where ρ_j is the density at the jamming transition. In the present theory, the value of ρ_j must be postulated.

The application of the model extensions proposed in this section are convenient for numerical applications since they should avoid diverging viscosities and can be easily implemented. However in this basic picture, no stress is computed in solid rigid zones. There is thus no way to define some criterium which specifies when the transition from rigid solid behavior to flow should happen. In reality, the granular solid may be rather treated as a deformable body.

5.2 Transition to quasi-elastic regime

In this part, investigations are performed to add a quasi-elastic regime into the EKM. Reversible deformations are observed in granular systems for strains smaller than 10^{-4} [38]. Although they are small in comparison to plastic deformations, they probably influence quasi-static stress distributions.

Elasto-plastic theories have been employed to model the behavior of permanent changes in metals and can be applied to soils [13, 51, 112, 117, 118]. In plasticity theories, a yield criteria specifies the occurrence of irreversible deformations. They are generally applied to an initially static situation which is loaded.

The arrest of a flowing granular system has been less studied and is investigated here. In this section we make investigations to include a transition from the plastic critical state of the EKM to a quasi-elastic regime. To do that, we will first compare the quasi-static limit of the EKM (see Section 4.3) with the yield state in elasto-plastic theories. Then, we will show how an elasto-plastic model can be formulated which combines the non-linear elastic model of Jiang and Liu [83] with the quasi-static dense flow regime of the EKM. We will thus show how an initial elastic strain can be calculated which ensures a continuous transition from the plastic flow to the quasi-elastic behavior. Finally an illustrative example is proposed.

5.2.1 Quasi-static limit of the EKM vs. yield in elasto-plasticity theories

In the quasi-static regime of the EKM and at low temperatures, the system slowly flows under critical conditions. The properties of this state are recalled on the left side of Table 5.1. In parallel, a plastic body flows when a yield criteria is satisfied and a flow rule specifies the evolution of the plastic strain. The stress tensor is expressed as a function of the elastic strain. Contrary to elasto-plastic theories, the EKM does not make any distinction between elastic and plastic strains. An important difference between these two states is that the flow rule of the EKM applies to the total strain rate and not only to the plastic one.

5.2.2 Jiang-Liu hyperelastic law

We first need to specify a stress-strain relation to account for elastic effects. Linear elastic laws are not appropriate for granular systems because they cannot account for stiffness-dependence on stress, yield, incremental non-linearity and Reynolds dilatancy. A more detailed explanation of incremental

EKM, quasi-static behavior for $T \ll T_0$	Elastoplastic law at yield
Yield condition $f_Y = 0$	Yield condition $f_Y = 0$
Stress-strain rate relation $\sigma_{ij} = -P_Y \delta_{ij} \frac{2\eta_0 P_Y \sqrt{3\rho\epsilon_0}}{\rho \sqrt{4\eta_0 \dot{\gamma}^2 + 2\zeta_0 \kappa_{ll}^2}} \kappa_{ij}^D$ $+ \frac{\zeta_0 P_Y \sqrt{3\rho\epsilon_0}}{\rho \sqrt{4\eta_0 \dot{\gamma}^2 + 2\zeta_0 \kappa_{ll}^2}} \kappa_{ll} \delta_{ij}.$	Stress-strain relation $\sigma_{ij} = f(\epsilon_{ij}^e)$
Flow rule $\frac{\kappa_{ij}}{\sqrt{\dot{\gamma}^2 + \frac{\zeta_0}{2\eta_0} \kappa_{ll}^2}} = \frac{2}{9\zeta_0} \sqrt{\frac{\rho\eta_0}{3\epsilon_0}} \frac{(\sigma_{ll} + 3P_Y) \delta_{ij}}{P_Y} + \frac{\sigma_{ij}^D \sqrt{\rho}}{\sqrt{3\eta_0 \epsilon_0} P_Y}.$	Flow rule $\dot{\epsilon}_{ij}^p = g(\sigma_{ij})$
Strain decomposition No distinction	Strain decomposition $\epsilon_{ij} = \epsilon_{ij}^e + \epsilon_{ij}^p$

Table 5.1: Yield state of the EKM and in the elasto-plastic framework

non-linearity and Reynolds dilatancy can be found in Appendix A.1. As a result, several non-linear elastic models have been proposed in the literature. First attempts to express non-linear stress-strain relations can be found in the early work of Boussinesq [54] who formulated stress-dependent bulk and shear moduli. In an early work, Goddard proposed to start from a nonlinear strain energy functional [127]. We will employ here the constitutive law of Liu et al. [7, 83–86], which was shown to have an interesting predictive power.

Assuming small deformations and rotations ($\left| \frac{\partial u_i}{\partial x_j} \right| \ll 1$), the elastic strain is given by

$$\varepsilon_{ij}^e = \frac{1}{2} \left(\frac{\partial u_i}{\partial x_j} + \frac{\partial u_j}{\partial x_i} \right), \quad (5.2.1)$$

where u_i is the displacement field. If the stress-strain relation is derived from an energy density W , the stress-strain relation is called hyperelastic. In this case, the stress tensor is given by

$$\sigma_{ij}(\varepsilon_{kl}^e) = \frac{\partial W}{\partial \varepsilon_{ij}^e}. \quad (5.2.2)$$

Liu et al. take the following expression for the energy density

$$\begin{cases} W(\Delta, \varepsilon_s^e) = \sqrt{\Delta} \left(\frac{2}{5} B \Delta^2 + A(\varepsilon_s^e)^2 \right) = B\sqrt{\Delta} \left(\frac{2}{5} \Delta^2 + \frac{(\varepsilon_s^e)^2}{\xi} \right), & \Delta \geq 0 \\ W(\Delta, \varepsilon_s^e) = 0, & \Delta < 0, \end{cases} \quad (5.2.3)$$

with $\Delta = -\varepsilon_{ll}^e$, $\varepsilon_s^e = \sqrt{\varepsilon_{ij}^{e,D} \varepsilon_{ij}^{e,D}}$, $\xi = B/A$ and A, B are two material parameters.

This energy density W is only defined for compaction states ($\Delta \geq 0$) and its expression makes it consistent with the results of the Hertz theory (see Appendix A.1). Remarkably, Jiang and Liu [7] demonstrated that W remains convex if the following criteria is fulfilled

$$\varepsilon_s^e / \Delta \leq \sqrt{2\xi}, \quad \text{or, equivalently,} \quad \sigma_s / P \leq \sqrt{2/\xi}. \quad (5.2.4)$$

This latter relation is actually the Drucker-Prager yield criterium [113]. The yield surface is thus fixed by the parameter $\xi = B/A$. The elastic energy is plotted on Figure 5.2.2 for different values of the elastic shear strain.

Once the expression of the energy density is specified, the stress-strain relation can be derived

$$\sigma_{ij}(\varepsilon_{kl}^e) = \frac{\partial W}{\partial \varepsilon_{ij}^e} = -B\Delta^{3/2} \delta_{ij} - \frac{A(\varepsilon_s^e)^2 \delta_{ij}}{2\sqrt{\Delta}} + 2A\sqrt{\Delta} \varepsilon_{ij}^{e,D}. \quad (5.2.5)$$

Note that compressive stress are taken negative into the EKM, and more generally in fluid dynamics. This is why we employ the opposite as in [128] for the stress-strain relation (5.2.5). According to this latter equation, the shear stress and pressure are given by

$$\sigma_s = 2A\sqrt{\Delta} \varepsilon_s^e, \quad P = \frac{\sigma_{ll}}{3} = -B\Delta^{3/2} - \frac{A(\varepsilon_s^e)^2}{2\sqrt{\Delta}}. \quad (5.2.6)$$

The dependence on B to the void volume fraction was chosen to be

$$B = B_0 \left(\frac{\rho - \rho_{co}}{\rho_{cp} - \rho} \right)^{0.15}. \quad (5.2.7)$$

With this dependence, the elastic energy density diverges at ρ_{cp} and remains convex between ρ_{co} and ρ_{cp} . This model was shown to correctly reproduce static stress distributions in silos, under point loads and on a sand pile. Additionally, the stiffness tensor was found to give good quantitative agreements with the experimental data of Kuwano and Jardine [38]. Other numerical investigations demonstrated its ability to predict the instability of the solid state [129]. It was also employed by Kamrin to develop a non-linear elastoplastic model which combines a hyperelastic response with the dense flow regime of Mids [130].

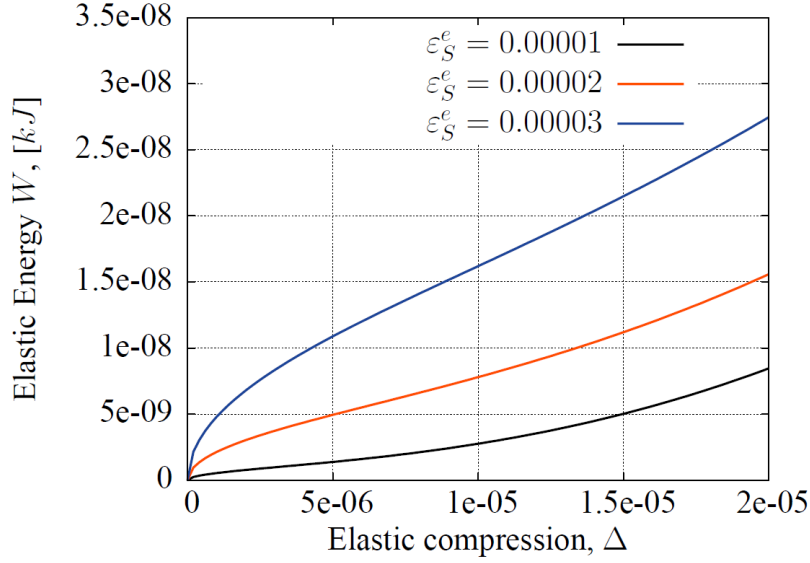


Figure 5.1: Plot of the elastic energy W as function of Δ for different values of ε_s^e .

5.2.3 Combining the plastic response of the EKM with the Jiang-Liu model

The purpose now is to include the Jiang-liu hyperelastic regime into the EKM. In the elastoplasticity theory, the total strain is decomposed into an elastic and a plastic part

$$\varepsilon_{ij} = \varepsilon_{ij}^e + \varepsilon_{ij}^p. \quad (5.2.8)$$

The stress tensor is expressed as a function of the elastic strain. In the last section, we propose to use the Jiang-Liu hyperelastic law

$$\sigma_{ij} = -B\Delta^{3/2}\delta_{ij} - \frac{A(\varepsilon_s^e)^2\delta_{ij}}{2\sqrt{\Delta}} + 2A\sqrt{\Delta}\varepsilon_{ij}^{e,D}. \quad (5.2.9)$$

The evolution of the plastic strain rate at yield (i.e $f_Y = 0$) must be specified by a flow rule. It is possible to formulate an elastoplastic law which combines the quasi-elastic response (5.2.9) with the plastic regime of the EKM. To do

that, one needs to set

$$\left\{ \begin{array}{l} \dot{\varepsilon}_{ij}^p = 0, \quad f_Y < 0 \\ \dot{\varepsilon}_{ij}^p = 0, \quad f_Y = 0 \quad \text{and} \quad \dot{f}_Y d\sigma_{ij} < 0 \\ \frac{\dot{\varepsilon}_{ij}^p}{\sqrt{(\dot{\varepsilon}_s^p)^2 + \frac{\zeta_0}{2\eta_0} (\dot{\varepsilon}_l^p)^2}} = \frac{2}{9\zeta_0} \sqrt{\frac{\rho\eta_0}{3\epsilon_0}} \frac{(\sigma_{ll} + 3P_Y)}{P_Y} \delta_{ij} + \frac{\sigma_{ij}^D \sqrt{\rho}}{\sqrt{3\eta_0\epsilon_0} P_Y}, \\ f_Y = 0 \quad \text{and} \quad \dot{f}_Y d\sigma_{ij} > 0, \end{array} \right. \quad (5.2.10)$$

where $f_Y = f_Y(\sigma_s, \sigma_{ll}, \rho) = (\sigma_{ll} + 3P_Y)^2 + \frac{9\zeta_0}{2\eta_0} \sigma_s^2 - \frac{27\zeta_0\epsilon_0}{2\rho} P_Y^2$ is the yield surface of the EKM, found in Section 4.3. According to this latter equation, the material behaves quasi-elastically inside the yield surface. The second relation ensures an elastic unloading. The third one imposes that the plastic strain obeys the same flow relation as this found in the EKM (see Table 5.1). However, according to (5.2.8), the total strain rate is given as the sum of the elastic and plastic one. In the EKM, the flow rule is expressed for the total strain rate and not only the plastic one. Thus, if one wants to exactly reproduce the flow rule of the EKM, one needs to additionally impose a vanishing elastic strain rate at yield

$$\dot{\varepsilon}_{ij}^e = 0, \quad f_Y = 0. \quad (5.2.11)$$

With this model, we explicitly make the distinction between loading and unloading and incorporate a quasi-elastic behavior inside the yield surface.

Rate equation The formulation of the elasto-plastic model in a rate form is not necessary in the present theory but is interesting since it will allow us to make the link to hypoplasticity (5.2.10) (see below). It is first convenient to differentiate the strain (5.2.8)

$$\dot{\varepsilon}_{ij} = \dot{\varepsilon}_{ij}^e + \dot{\varepsilon}_{ij}^p. \quad (5.2.12)$$

At constant stiffness, the rate of the stress is given by

$$\dot{\sigma}_{ij} = C_{ijkl} \dot{\varepsilon}_{kl}^e, \quad (5.2.13)$$

where $C_{ijkl} = \frac{\partial \sigma_{ij}}{\partial \varepsilon_{kl}^e}$ denotes the stiffness tensor. From (5.2.9), it is calculated as

$$\begin{aligned} C_{ijkl} = & -A\sqrt{\Delta} \left(\left(\frac{\varepsilon_s^2}{4\Delta^2} - \frac{3B}{2A} + \frac{2}{3} \right) \delta_{ij}\delta_{kl} - \delta_{ik}\delta_{jl} - \delta_{il}\delta_{jk} + \frac{1}{\Delta} (\delta_{kl}\varepsilon_{ij}^D + \delta_{ij}\varepsilon_{kl}^D) \right). \end{aligned} \quad (5.2.14)$$

One can combine (5.2.12) and (5.2.13) to get

$$\dot{\sigma}_{ij} = C_{ijkl} (\dot{\epsilon}_{kl} - \dot{\epsilon}_{kl}^p). \quad (5.2.15)$$

Inserting the flow rule given by (5.2.10) into 5.2.15 gives

$$\begin{aligned} \dot{\sigma}_{ij} = C_{ijkl} \dot{\epsilon}_{kl} - \\ C_{ijkl} \left(\frac{2}{9\zeta_0} \sqrt{\frac{\rho\eta_0}{3\epsilon_0}} \frac{(\sigma_{ll} + 3P_Y)}{P_Y} \delta_{kl} + \frac{\sigma_{kl}^D \sqrt{\rho}}{\sqrt{3\eta_0\epsilon_0}} P_Y \right) \sqrt{(\dot{\epsilon}_s^p)^2 + \frac{\zeta_0}{2\eta_0} (\dot{\epsilon}_{ll}^p)^2}. \end{aligned} \quad (5.2.16)$$

To simplify the formalism, let us introduce the tensor \tilde{N}_{ij} defined as

$$\tilde{N}_{ij} = \frac{2}{9\zeta_0} \sqrt{\frac{\rho\eta_0}{3\epsilon_0}} \frac{\sigma_{ll} + 3P_Y}{P_Y} \delta_{ij} + \frac{\sigma_{ij}^D \sqrt{\rho}}{\sqrt{\eta_0\epsilon_0}} P_Y. \quad (5.2.17)$$

With this definition, the relation (5.2.16) reads

$$\sigma_{ij} = C_{ijkl} \dot{\epsilon}_{kl} - C_{ijkl} \tilde{N}_{kl} \sqrt{(\dot{\epsilon}_s^p)^2 + \frac{\zeta_0}{2\eta_0} (\dot{\epsilon}_{ll}^p)^2}. \quad (5.2.18)$$

This equation can be written in a similar form as the hypoplastic relations (see part 5.3.1)

$$\frac{\partial \sigma_{ij}}{\partial t} = C_{ijkl} \dot{\epsilon}_{kl} - C_{ijkl} \tilde{N}_{kl} \chi \sqrt{\dot{\epsilon}_s^2 + \dot{\epsilon}_{ll}^2} \quad \text{with} \quad \chi = \frac{\sqrt{(\dot{\epsilon}_s^p)^2 + \frac{\zeta_0}{2\eta_0} (\dot{\epsilon}_{ll}^p)^2}}{\sqrt{\dot{\epsilon}_s^2 + \dot{\epsilon}_{ll}^2}}. \quad (5.2.19)$$

To finalize the formulation of the elastoplastic law, one needs to specify the value of χ . In comparison to (5.2.19), a hypoplasticity law (see part 5.3.1) imposes the condition $\chi = 1$. It is thus tempting to specify the evolution of χ as following:

$$\begin{cases} \chi = 0, & f_Y < 0 \\ \chi = 0, & f_Y = 0 \quad \text{and} \quad \dot{f}_Y d\sigma_{ij} < 0 \\ \chi = 1, & f_Y = 0 \quad \text{and} \quad \dot{f}_Y d\sigma_{ij} > 0. \end{cases} \quad (5.2.20)$$

This formulation ensures an elastic unloading and sets the equality between the plastic strain and the total strain at yield. This is consistent, with the additional condition imposed in (5.2.11). Note that this similarity between an elasto-plastic in a rate form and a hypoplastic law have been underlined by several authors [76, 131]. However we want to point out that

although both equations appear in the same form, a major difference is that hypoplastic models do not require to explicitly distinguish between loading and unloading. Summarizing, the non-linear elastic model is given by equations (5.2.8), (5.2.9) and (5.2.10). It must be completed with appropriate initial conditions.

5.2.4 Initial conditions

To calculate the initial conditions of the quasi-elastic regime previously introduced, one may distinguish two cases. For a system initially at rest, the initial deformation is elastic and one can solve the force balance equation combined with the non-linear elastic material law (5.2.9) to get the initial stress or strain distribution. This is the method generally employed in soil mechanics.

But one should also consider the case of a granular medium moving from a rapid collisional flow to a steady-like state where the elasto-plastic description should apply. In Section 4.3, we showed that a plastic regime is included into the EKM. Its properties are summarized on Table 5.1. The stress tensor in these states is given by

$$\sigma_{ij} = -P_Y \delta_{ij} + 2\eta_Y \kappa_{ij}^D + \zeta_Y \kappa_{ll} \delta_{ij}.$$

In the quasi-elastic regime, the stress tensor is expressed as a function of the elastic strain by (5.2.10),

$$\sigma_{ij}(\varepsilon_{kl}) = -B\Delta^{\frac{3}{2}} \delta_{ij} - \frac{A\varepsilon_s^2 \delta_{ij}}{2\sqrt{\Delta}} + 2A\sqrt{\Delta} \varepsilon_{ij}^D.$$

Notice that in order to simplify the notations, we will omit the superscript e on the elastic strain in this section. To calculate the initial values of the elastic strain, one can write the condition that the transition from the critical state of the EKM to the elasto-plastic regime does not imply any stress discontinuity. The initial values of the elastic strain ε_{ij} can thus be calculated as

$$\begin{cases} B\Delta^{3/2} + A\frac{\varepsilon_s^2}{2\sqrt{\Delta}} = P_Y - \zeta_Y \kappa_{ll}, \\ 2A\sqrt{\Delta} \varepsilon_{ij}^D = 2\eta_Y \kappa_{ij}^D. \end{cases} \quad (5.2.21)$$

$$(5.2.22)$$

The last expression allows to calculate ε_{ij}^D as

$$\varepsilon_{ij}^D = \frac{\eta_Y \kappa_{ij}^D}{A\sqrt{\Delta}}, \quad (5.2.23)$$

from which it is easy to get

$$\varepsilon_s^2 = \frac{\eta_Y^2 \dot{\gamma}^2}{A^2 \Delta}. \quad (5.2.24)$$

This expression can be incorporated into (5.2.21), to get

$$B \Delta^{3/2} + \frac{\eta_Y^2 \dot{\gamma}^2}{2A \Delta \sqrt{\Delta}} = P_Y - \zeta_Y \kappa_{ll}, \quad (5.2.25)$$

which can be written as a second order polynomial in $\Delta^{3/2}$

$$B (\Delta^{3/2})^2 + (\zeta_Y \kappa_{ll} - P_Y) \Delta^{3/2} + \frac{\eta_Y^2 \dot{\gamma}^2}{2A} = 0. \quad (5.2.26)$$

Solutions for $\Delta^{3/2}$, exist only if

$$\Theta = (\zeta_Y \kappa_{ll} - P_Y)^2 - \frac{2B \eta_Y^2 \dot{\gamma}^2}{A} \geq 0. \quad (5.2.27)$$

We recall the definition of the yield shear viscosity, initially defined in Section 3.2.2

$$\eta_Y = \frac{\eta_0 P_Y}{\rho \sqrt{T}}. \quad (5.2.28)$$

In the quasi-static limit of low temperatures, the temperature is given by (see part 4.3)

$$T = \frac{4\eta_0 \dot{\gamma}^2 + 2\zeta_0 \kappa_{ll}^2}{3\rho \epsilon_0}. \quad (5.2.29)$$

Inserting the expression of the temperature (5.2.29) into the expression of the shear viscosity (5.2.28) gives

$$\eta_Y = \frac{\eta_0 P_Y \sqrt{3\rho \epsilon_0}}{\rho \sqrt{4\eta_0 \dot{\gamma}^2 + 2\zeta_0 \kappa_{ll}^2}}. \quad (5.2.30)$$

Similarly one gets the following expression for the bulk viscosity

$$\zeta_Y = \frac{\zeta_0 P_Y \sqrt{3\rho \epsilon_0}}{\rho \sqrt{4\eta_0 \dot{\gamma}^2 + 2\zeta_0 \kappa_{ll}^2}}. \quad (5.2.31)$$

By inserting (5.2.30) and (5.2.31) into (5.2.27), Θ can be expressed as a function of the shear rate and the compression rate

$$\Theta = P_Y^2 \left[\left(\frac{\zeta_0 \sqrt{3\epsilon_0}}{\sqrt{\rho (4\eta_0 \dot{\gamma}^2 + 2\zeta_0 \kappa_{ll}^2)}} \kappa_{ll} - 1 \right)^2 - \frac{6\epsilon_0 B \eta_0^2 \dot{\gamma}^2}{\rho A (4\eta_0 \dot{\gamma}^2 + 2\zeta_0 \kappa_{ll}^2)} \right].$$

This latter relation can be expressed as function the rate of dilation β , which was introduced in Section (4.2) as $\beta = -\frac{\kappa_{ll}}{\dot{\gamma}}$

$$\Theta = \Theta(\beta, \rho) = P_Y^2 \left[\left(\frac{\sqrt{3\zeta_0\epsilon_0}}{\sqrt{2\rho \left(1 + \frac{2\eta_0}{\zeta_0\beta^2}\right)}} \frac{\kappa_{ll}}{|\kappa_{ll}|} - 1 \right)^2 - \frac{3\epsilon_0 B \eta_0}{2\rho A \left(1 + \frac{\zeta_0\beta^2}{2\eta_0}\right)} \right].$$

For compressional states $\kappa_{ll} < 0$, it gives

$$\Theta = \Theta(\beta, \rho) = P_Y^2 \left[\left(\frac{\sqrt{3\zeta_0\epsilon_0}}{\sqrt{2\rho \left(1 + \frac{2\eta_0}{\zeta_0\beta^2}\right)}} + 1 \right)^2 - \frac{3\epsilon_0 B \eta_0}{2\rho A \left(1 + \frac{\zeta_0\beta^2}{2\eta_0}\right)} \right].$$

A plot of the function Θ is shown in Figure 5.2. The limit of Θ for vanishing β gives

$$\lim_{\beta \rightarrow 0} \Theta(\beta, \rho) = \left(1 - \frac{3\epsilon_0\eta_0\xi}{2\rho} \right) P_Y^2 \quad (5.2.32)$$

It is obvious that the following condition ensures the positivity of Θ , i.e the existence of the elastic strain

$$\xi \leq \frac{2\rho}{3\epsilon_0\eta_0}. \quad (5.2.33)$$

If one sets $\xi = \frac{2\rho}{3\epsilon_0\eta_0}$, $\Theta = 0$ and a unique solution is found. We show in Section 5.2.2, that the static friction coefficient of the Jiang-Liu hyperelastic law is given by

$$\frac{\sigma_s}{P} = \sqrt{\frac{2}{\xi}}. \quad (5.2.34)$$

Substituting the maximal value of ξ given by (5.2.33), one gets

$$\frac{\sigma_s}{P} = \sqrt{\frac{3\epsilon_0\eta_0}{\rho}} = \mu_s. \quad (5.2.35)$$

By fixing the value of ξ to $2\rho/(3\epsilon_0\eta_0)$, one can define an initial elastic strain which ensures a continuous transition between both descriptions. Thus, the condition of existence of the initial strain is linked with the equality of the friction coefficient of the flow and hyperelastic model.

If the condition (5.2.33) applies, two elastic fields satisfy the positivity of Θ . In the case of an equality, i.e $\xi = \frac{2\rho}{3\epsilon_0\eta_0}$, the initial elastic strain is given

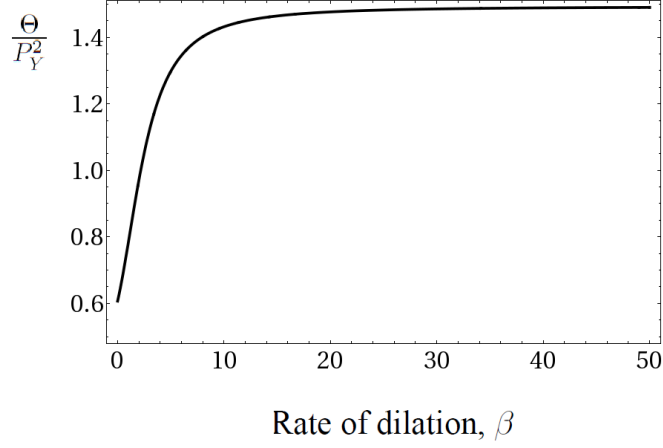


Figure 5.2: Plot of the function Θ at constant density $\rho = 0.61\rho_b$ (with ρ_b being the bulk density) scaled with P_Y^2 and standard values of parameters are taken from Latz and Schmidt in [3]).

by

$$\left\{ \begin{array}{l} \Delta = \left(\frac{P_Y - \zeta_Y \kappa_{ll}}{2B} \right)^{2/3} \\ \varepsilon_{ij}^D = \frac{\eta_Y \kappa_{ij}^D}{A\sqrt{\Delta}}. \end{array} \right. \quad (5.2.36)$$

$$(5.2.37)$$

5.2.5 Illustrative example

Critical state of the EKM Consider a 2D granular layer which is uniformly sheared, as illustrated on Figure 5.3. The study of the stationary limit of the EKM for densities close to the maximum ones and vanishing deformations was done in Section 4.3. We recall the properties of this state here. At constant volume ($\kappa_{ll} = 0$), the pressure is given by

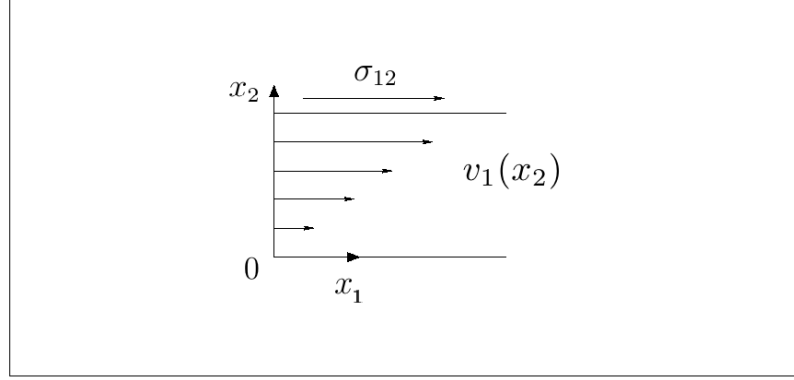
$$\sigma_{ll} = -3P_Y = -3T_0 (\rho - \rho_{co}) g(\rho). \quad (5.2.38)$$

The granular temperature is given by

$$T = \frac{4\eta_0}{3\rho\epsilon_0} \left(\frac{\partial v_1}{\partial x_2} \right)^2, \quad (5.2.39)$$

and the shear stress is written as

$$\sigma_{12} = \frac{\mu_s P_Y}{\left| \frac{\partial v_1}{\partial x_2} \right|} \frac{\partial v_1}{\partial x_2}. \quad (5.2.40)$$

**Figure 5.3:** Shear flow problem.

with $\mu_s = \sqrt{\frac{3\eta_0\epsilon_0}{\rho}}$ is the static friction coefficient of the EKM. It is explicitly given by

$$\begin{cases} \sigma_{12} = \mu_s P_Y, & \frac{\partial v_1}{\partial x_2} > 0 \\ \sigma_{12} = -\mu_s P_Y, & \frac{\partial v_1}{\partial x_2} < 0. \end{cases} \quad (5.2.41)$$

For the following, we consider a system initially loaded ($\frac{\partial v_1}{\partial x_2} > 0$). In this case, the yield criteria reduces to Coulomb friction

$$\frac{\sigma_{12}}{P} = \mu_s. \quad (5.2.42)$$

Transition to quasi-elasticity The initial values of the elastic strain can be obtained by using (5.2.37). By taking $\xi = \frac{3\rho\epsilon_0\eta_0}{2}$, one gets

$$\Delta_0 = \left(\frac{P_Y}{2B} \right)^{2/3} \quad (5.2.43)$$

and

$$\epsilon_{12,0} = \frac{\sigma_{12}}{2A\sqrt{\Delta_0}} = \frac{\mu_s P_Y}{2A\sqrt{\Delta_0}}, \quad (5.2.44)$$

where the subscript 0 denotes the initial value. By inserting (5.2.43), one gets

$$\epsilon_{12,0} = \frac{\mu P_Y^{2/3} (2B)^{1/3}}{2A}. \quad (5.2.45)$$

This specifies the calculation of the initial elastic strain. The value of the shear stress is now given by

$$\sigma_{12} = 2A\sqrt{\Delta}\varepsilon_{12}^e, \quad (5.2.46)$$

Elastic unloading Starting from a critical state, the further evolution of the system depends on the loading conditions. If the system is still loaded, then plastic flow happens and the system stays at yield. During elastic unloading, $\dot{\varepsilon}_{12}^p=0$, so that

$$\dot{\varepsilon}_{12} = \dot{\varepsilon}_{12}^e \quad (5.2.47)$$

and the evolution of the shear stress now governed by

$$\dot{\sigma}_{12} = 2A\sqrt{\Delta}\dot{\varepsilon}_{12}^e. \quad (5.2.48)$$

Depending on the loading condition, static states can be reached, where $|\sigma_{12}/P| < \mu_s$. Inside the yield surface, i.e for $\sigma_{12}/P < \mu_s$, the behavior is quasi-elastic.

5.2.6 Summary and discussion

In this part, investigations were made to include a quasi-elastic behavior into the EKM. The full model is summarized on page 93. It includes the dilute collisional regime, slow plastic motion and quasi-elastic behavior.

We paid particular attention to the question of the initial conditions of the quasi-elastic regime. Consider a granular system initially at rest, one can assume that all the deformation is elastic and calculate the initial stress distribution, like it is generally done in the solid mechanics (see also Appendix B). Note that the transition from solid-like to fluid-like behavior happens when the yield condition is fulfilled.

The case of the arrest of a slow flowing granular system, i.e the transition from the fluid-like to solid-like behavior has been investigated. We showed, that one can calculate an initial elastic strain which ensures the continuity from the critical state plastic regime to the quasi-elastic behavior.

For numerical applications, it must be underlined that the stress-strain relation (5.2.9) can lead to some difficulties, since it avoids negative Δ . We need also to add an additional variable, the elastic strain. It is also important to recall that the Jiang-Liu hyperelastic model possesses a thermodynamically unstable zone, bounded by a Drucker-Prager yield criteria. In the actual model formulation, there is nothing which guarantees that the elastic states stay in the convex stable domain. A possible solution to overcome this difficulty is to modify the non-linear elastic law, so that its convexity transition

coincides with the yield surface of the EKM, i.e $f_Y = 0$. It requires to add a third strain invariant $(\varepsilon_t^e)^3 = \varepsilon_{ij}^{e,D} \varepsilon_{jk}^{e,D} \varepsilon_{ki}^{e,D}$, in the elastic energy density [132]

$$W = B\sqrt{\Delta} \left(\frac{2}{5}\Delta^2 + \frac{(\varepsilon_s^e)^2}{\xi} - \frac{C(\varepsilon_t^e)^3}{B} \right), \quad (5.2.49)$$

where C is an additional material parameter. The value of C must be calculated so that the convex domain is bounded by the yield surface of EKM. This includes additional efforts (see [132], where several yield surfaces are derived from (5.2.49)) and to investigate again the case of the initial conditions. It is *a priori* not clear if one can calculate an initial elastic strain in a similar way as in Section 5.2.4. At this stage, we restrict ourselves to noting that these difficulties do not happen by combining the EKM, with a hypoplastic law (see below).

Balance equations

$$\begin{cases} \frac{\partial \rho}{\partial t} + \frac{\partial (\rho v_i)}{\partial x_i} = 0, \end{cases} \quad (5.2.50)$$

$$\begin{cases} \frac{\partial \rho v_i}{\partial t} + \frac{\partial (\rho v_i v_j)}{\partial x_j} = \rho g_i - \frac{\partial P}{\partial x_i} + \frac{\partial \tilde{\sigma}_{ij}}{\partial x_j}, \end{cases} \quad (5.2.51)$$

Kinetic and yield regime

$$\frac{\partial \rho T}{\partial t} + \frac{\partial \rho v_i T}{\partial x_i} = \frac{2}{3} \left(\tilde{\sigma}_{ij} \kappa_{ij} - \frac{\partial}{\partial x_i} \left(-\lambda \frac{\partial T}{\partial x_i} \right) \right) - \rho \epsilon T,$$

$$\tilde{\sigma}_{ij} = 2\eta \kappa_{ij}^D + \zeta \kappa_{ll} \delta_{ij} \quad (5.2.52a)$$

with

$$P = P_K + P_Y \quad \text{with} \quad \begin{cases} P_Y = 0, & \rho \leq \rho_{co} \\ P_Y = T_0 (\rho - \rho_{co}) g(\rho), & \rho > \rho_{co} \end{cases} \quad (5.2.52b)$$

$$\eta = \eta_K \left(1 + \frac{P_Y}{P_K} \right), \quad \zeta = \zeta_K \left(1 + \frac{P_Y}{P_K} \right), \quad (5.2.52c)$$

$$\epsilon = \epsilon_K \left(1 + \frac{P_Y}{P_K} \right), \quad \lambda = \lambda_K \left(1 + \frac{P_Y}{P_K} \right) \quad (5.2.52d)$$

and

$$\eta_K = \eta_0 \sqrt{T} g(\rho), \quad \epsilon_K = \epsilon_0 \sqrt{T} g(\rho), \quad (5.2.52e)$$

$$\zeta_K = \zeta_0 \sqrt{T} g(\rho), \quad \lambda_K = \lambda_0 \sqrt{T} g(\rho), \quad P_K = T \rho g(\rho), \quad (5.2.52f)$$

with $g(\rho) = \left(1 - \frac{\rho}{\rho_{cp}} \right)^{-1}$,

Quasi-elastic regime, $f_Y < 0$

$$f_Y = (\sigma_{ll} + 3P_Y)^2 + \frac{9\zeta_0}{2\eta_0} \sigma_s^2 - \frac{27\zeta_0 \epsilon_0}{2\rho} P_Y^2 \quad (5.2.53)$$

$$\sigma_{ij}(\varepsilon_{kl}) = -B \Delta^{3/2} \delta_{ij} - \frac{A(\varepsilon_s^e)^2 \delta_{ij}}{2\sqrt{\Delta}} + 2A\sqrt{\Delta} \epsilon_{ij}^{e,D}. \quad (5.2.54)$$

5.3 Transition to hypoplastic regime

In the previous part, we made investigations to include a quasi-elastic regime into the EKM. We assumed the total strain to be the sum of an elastic and a plastic contribution. The decomposition of the strain into a plastic and an elastic part is not a theoretical result but a phenomenological way to account for reversible effects. Generally, the development of elasto-plastic laws requires the formulation of two constitutive laws (elastic law inside the yield surface and a flow rule), a yield surface and a hardening rule. The existing models (applied to soils) involve many material parameters and can lead to complex mathematical formulations [8, 133]. This was one of the motivations for the development of alternative models based on the formulation of rate-equations. A second reason is that no clear separation between elastic and plastic behavior is observed in granular systems. As a result, yield surfaces are difficult to identify. Thus, the hypothesis of a pure elastic behavior inside yield, sometimes made by formulating elasto-plastic models is not realistic for soils [8]. In this part, we will perform investigations to include a hypoplastic regime in the EKM. Like for the transition to elasto-plasticity (see part 5.2), we will ensure a continuous transition from the fluid to solid-like behavior.

5.3.1 Hypoplastic constitutive laws

Alternative approaches to elasto-plasticity have been proposed to model typical effects in soils like incremental non-linearity or dilatancy. Truesdell formulated linear rate equations, called hypoelastic which are able to predict nonlinear stress-strain relations and failure [57]. Some works showed that failure criteria can be derived from these relations [134]. It is an interesting advantage in comparison to plasticity theories where it must be postulated. However these models exhibit a discontinuous response for certain loading conditions [60]. Later, a class of models based on non-linear rate equations has been developed by two different schools. Kolymbas and its coworkers from the university of Karlsruhe have developed the so-called K-hypoplasticity [59, 133] whereas Chambon and its coworkers from Grenoble have worked on the so-called CloE models [135]. The term “hypo” means that no potential is used in opposition to “hyper”. In this work, we will focus on the first class of laws. Kolymbas proposed a hypoplastic law based on a simple formalism with a few parameters [8]. However, it reproduces the salient properties of the granular solid. According to their authors [133], a hypoplastic constitutive relation is defined as

$$\frac{\partial \sigma_{ij}}{\partial t} = h(\sigma_{ij}, \dot{\epsilon}_{ij}, e), \quad (5.3.1)$$

where $e = \rho_g/\rho - 1$ is the void ratio and h a function which obeys several properties. The modeling effort consists in choosing an appropriate function h . This provides a more simple formalism than in classical elasto-plastic laws. In the hypoplasticity theory, one assumes that the history dependence can be kept by the value of the instantaneous stress.

To ensure the property of incremental non-linearity, the function h must be non-differentiable at $\dot{\varepsilon}_{ij} = 0$. Add to this, Wu has identified three important restrictions [133] :

- Positive homogeneity at the first order in $\dot{\varepsilon}_{ij}$,
 $h(\sigma_{ij}, \lambda \dot{\varepsilon}_{kl}, e) = \lambda h(\sigma_{ij}, \dot{\varepsilon}_{kl}, e)$, (this ensures the property of rate independence, in the sense that the stiffness $\frac{\partial \sigma_{ij}}{\partial \varepsilon_{kl}}$ is not dependent on the strain rate),
- Objectivity, $h(Q_{ik}\sigma_{kl}Q_{jl}, Q_{mk}\sigma_{kl}Q_{nl}) = Q_{ik}h(\varepsilon_{ij}, \dot{\varepsilon}_{mn})Q_{jl}$ where Q_{ij} is an orthogonal tensor,
- Homogeneity on σ_{ij} ,
 $h(\lambda \sigma_{ij}, \dot{\varepsilon}_{kl}) = \lambda^n h(\sigma_{ij}, \dot{\varepsilon}_{kl})$. This property ensures that the stiffness is proportional to the n power of stress, as generally observed in soil mechanics experiments.

Generally, the stress rate is expressed as the sum of a linear part in the strain rate and a non-linear one

$$\frac{\partial \sigma_{ij}}{\partial t} = L_{ijkl}\dot{\varepsilon}_{kl} - N_{ij}\sqrt{\dot{\varepsilon}_{mn}\dot{\varepsilon}_{mn}}, \quad (5.3.2)$$

where L_{ijkl} is a 4th-order tensor and N_{ij} a 2nd-order one. The tensors L_{ijkl} and N_{ij} depend on the stress and the void ratio e , whose evolution is given by

$$\frac{\partial e}{\partial t} = (1 + e)\dot{\varepsilon}_{ll}. \quad (5.3.3)$$

Note that by combining this latter equation with the definition of the void ratio, one gets

$$\frac{\partial \rho}{\partial t} = -\rho \kappa_{ll}, \quad (5.3.4)$$

what is the same with the mass conservation equation (4.3.7) in the quasi-static limit.

5.3.2 Quasi-static limit of the EKM vs. hypoplastic law at yield

In the hypoplastic theory, a material is said to be at failure, if there exists a non-vanishing strain rate for a given stress so that

$$\frac{\partial \sigma_{ij}}{\partial t} = 0. \quad (5.3.5)$$

This latter condition combined with (5.3.2) gives

$$L_{ijkl}\dot{\epsilon}_{kl} - N_{ij}\sqrt{\dot{\epsilon}_{mn}\dot{\epsilon}_{mn}} = 0. \quad (5.3.6)$$

From this last equation, one can get the value of the strain rate

$$\frac{\dot{\epsilon}_{kl}}{\sqrt{\dot{\epsilon}_{mn}\dot{\epsilon}_{mn}}} = (L^{-1})_{ijkl} N_{ij}. \quad (5.3.7)$$

This equation is generally called flow rule since it specifies the evolution of the strain rate in the limit state. Combining it with $\sqrt{\dot{\epsilon}_{kl}\dot{\epsilon}_{kl}}/\sqrt{\dot{\epsilon}_{mn}\dot{\epsilon}_{mn}} = 1$, one gets the equation of the limit surface

$$f_Y = (L^{-1})_{ijmn} N_{ij} (L^{-1})_{klmn} N_{kl} - 1 = 0. \quad (5.3.8)$$

Although hypoplastic laws don't require the explicit formulation of limit surfaces and flow rule, these properties are implicitly contained. They have been derived from the rate-equation. The isochoric critical state is also included into the failure state and given by

$$\kappa_{ll} = 0 \quad i.e. \quad (e = e_c), \quad \frac{\partial \sigma_{ij}}{\partial t} = 0. \quad (5.3.9)$$

The properties of the EKM in the quasi-static behavior and of the failure state in the hypoplastic model are summarized in Table 5.2. The quasi-static regime of the EKM was studied in Section 4.3. In both descriptions, a plastic limit state is implicitly defined and characterized by a limit surface and a flow direction. No strain decomposition into elastic and plastic is formulated. However, the hypoplastic law requires additionally a constant stress condition $\frac{\partial \sigma_{ij}}{\partial t} = 0$. These states are also found in the EKM for an evolution at constant deformation rate.

In the following, efforts are made to define a hypoplastic law that can be combined with the EKM. We will specify L_{ijkl} and N_{ij} so that the yield surface of the hypoplastic law coincides with this of the EKM. This ensures a continuous transition between the fluid-like and solid-like behavior.

EKM, quasi-static behavior, $T \ll T_0$	Hypoplastic law at yield
Yield criteria $f_Y = (\sigma_{ll} + 3P_Y)^2 + \frac{9\zeta_0}{2\eta_0}\sigma_s^2 - \frac{27\zeta_0\epsilon_0}{2\rho}P_Y^2 = 0$	Yield criteria $f_Y = (L^{-1})_{ijmn} N_{ij} (L^{-1})_{klmn} N_{kl} - 1 = 0$
Flow rule $\frac{\kappa_{ij}}{\sqrt{\dot{\gamma}^2 + \frac{\zeta_0}{2\eta_0}\kappa_{ll}^2}} = \frac{2}{9\zeta_0} \sqrt{\frac{\rho\eta_0}{3\epsilon_0}} \frac{(\sigma_{ll} + 3P_Y) \delta_{ij}}{P_Y} + \frac{\sigma_{ij}^D \sqrt{\rho}}{\sqrt{3\eta_0\epsilon_0} P_Y}$	Flow rule $\frac{\dot{\epsilon}_{kl}}{\sqrt{\dot{\epsilon}_{mn}\dot{\epsilon}_{mn}}} = (L^{-1})_{ijkl} N_{ij}$

Table 5.2: Yield state of the EKM and in the hypoplasticity framework.

5.3.3 Hypoplastic law

Due to the expression of the flow rule of the EKM (see Table 5.2), it is convenient to start from a hypoplastic law of the form

$$\frac{\partial \sigma_{ij}}{\partial t} = f \left(L_{ijkl} \dot{\epsilon}_{kl} - N_{ij} \sqrt{\dot{\epsilon}_s^2 + \frac{\zeta_0}{2\eta_0} \dot{\epsilon}_{ll}^2} \right) \quad (5.3.10)$$

with f being a material parameter which will be below specified. At failure i.e. $\frac{\partial \sigma_{ij}}{\partial t} = 0$, the flow rule of this hypoplastic law is

$$\frac{\dot{\epsilon}_{kl}}{\sqrt{\dot{\epsilon}_s^2 + \frac{\zeta_0}{2\eta_0} \dot{\epsilon}_{ll}^2}} = (L^{-1})_{ijkl} N_{ij}. \quad (5.3.11)$$

The flow rule of the EKM is

$$\frac{\kappa_{ij}}{\sqrt{\dot{\gamma}^2 + \frac{\zeta_0}{2\eta_0} \kappa_{ll}^2}} = \frac{2}{9\zeta_0} \sqrt{\frac{\rho\eta_0}{3\epsilon_0}} \frac{(\sigma_{ll} + 3P_Y) \delta_{ij}}{P_Y} + \frac{\sigma_{ij}^D \sqrt{\rho}}{\sqrt{3\eta_0\epsilon_0} P_Y}. \quad (5.3.12)$$

The purpose now is to formulate a hypoplastic law which exhibits at failure the same properties of the EKM in its limit of small deformations. To ensure that, the flow rule (5.3.11) of the hypoplastic law is chosen to be the same

as this derived from the EKM, expressed by (5.3.12). We can assume L_{ijkl} to take the isotropic form

$$L_{ijkl} = A_h \delta_{ij} \delta_{kl} + B_h (\delta_{ik} \delta_{jl} + \delta_{il} \delta_{jk}), \quad (5.3.13)$$

where A_h and B_h are two material parameters. The subscript h refers to hypoplastic. From this latter relation, $(L^{-1})_{ijkl}$ can be calculated as

$$(L^{-1})_{ijkl} = A'_h \delta_{ij} \delta_{kl} + B'_h (\delta_{ik} \delta_{jl} + \delta_{il} \delta_{jk}), \quad (5.3.14)$$

with

$$A'_h = -\frac{A_h}{2B_h(3A_h + 2B_h)}, \quad B'_h = \frac{1}{B_h}. \quad (5.3.15)$$

Now the flow rule (5.3.11) can be calculated as

$$\frac{\dot{\epsilon}_{kl}}{\sqrt{\dot{\epsilon}_s^2 + \frac{\zeta_0}{2\eta_0} \dot{\epsilon}_{ll}^2}} = (L^{-1})_{ijkl} N_{ij} = 3A'_h \delta_{kl} N_{ii} + 2B'_h N_{kl}, \quad (5.3.16)$$

and can be decomposed into a deviatoric and volumetric part

$$\frac{\dot{\epsilon}_{kl}}{\sqrt{\dot{\epsilon}_s^2 + \frac{\zeta_0}{2\eta_0} \dot{\epsilon}_{ll}^2}} = \left(3A'_h + \frac{2}{3}B'_h\right) N_{ii} \delta_{kl} + 2B'_h N_{kl}^D. \quad (5.3.17)$$

By identifying this latter expression with (5.3.12), the volumetric and deviatoric part of N_{ij} can be identified ¹

$$N_{ll} = \frac{2}{9\zeta_0(3A'_h + \frac{2}{3}B'_h)} \sqrt{\frac{\rho\eta_0}{3\epsilon_0}} \frac{(\sigma_{ll} + 3P_Y)}{P_Y} \quad N_{ij}^D = \frac{\sigma_{ij}^D \sqrt{\rho}}{2B'_h \sqrt{3\epsilon_0} \eta_0 P_Y}. \quad (5.3.18)$$

Combining these two latter equations, the expression of N_{ij} is fully given by

$$N_{ij} = \frac{\sqrt{\rho} \sigma_{ij}^D}{2B'_h \sqrt{3\epsilon_0} \eta_0 P_Y} + \frac{2}{27\zeta_0(3A'_h + \frac{2}{3}B'_h)} \sqrt{\frac{\rho\eta_0}{3\epsilon_0}} \frac{(\sigma_{ll} + 3P_Y)}{P_Y} \delta_{ij}. \quad (5.3.19)$$

Since the yield pressure is given by $P_Y = T_0 (\rho - \rho_{co}) / (1 - \rho/\rho_{cp})$, the stress components in (5.3.19) are preceded by a pre-factor which depends on the density in $\frac{(1-\rho/\rho_{cp})\sqrt{\rho}}{T_0(\rho-\rho_{co})}$. To finish the formulation of the hypoplastic law, one must specify the expression of f . Since the stiffness increases with the density, it is pertinent to take

$$f = \left(\frac{\rho - \rho_{co}}{\rho_{cp} - \rho} \right)^\alpha, \quad (5.3.20)$$

¹We recall that in the regime where the hypoplastic law applies small deformations occur, so that $\dot{\epsilon}_{kl} \approx \kappa_{kl}$.

with $\alpha < 1$ a material constant. To account for the proportional dependence of tangential stiffness to the n -th power of the stress level generally observed in experiments [133], it makes sense to scale the material coefficients A'_h and B'_h with the pressure

$$A' = A'_0 |\sigma_u|, \quad B' = B'_0 |\sigma_u|. \quad (5.3.21)$$

This completes the formulation of the hypoplastic law. It is then fully given by the relations (5.3.4), (5.3.13), (5.3.18), (5.4.8).

Hypoplastic law The formulated hypoplastic law can now be summarized as follows

$$\begin{aligned} \frac{\partial \sigma_{ij}}{\partial t} &= f \left(L_{ijkl} \dot{\varepsilon}_{kl} - N_{ij} \sqrt{\dot{\varepsilon}_s^2 + \frac{\zeta_0}{2\eta_0} \dot{\varepsilon}_u^2} \right), \\ L_{ijkl} &= A_h \delta_{ij} \delta_{kl} + B_h (\delta_{ik} \delta_{jl} + \delta_{il} \delta_{jk}), \\ N_{ij} &= \frac{\sqrt{\rho} \sigma_{ij}^D}{2B'_h \sqrt{3\varepsilon_0 \eta_0} P_Y} + \frac{2}{27\zeta_0 (A'_h + \frac{2}{3}B'_h)} \sqrt{\frac{\rho \eta_0}{3\varepsilon_0}} \frac{(\sigma_u + 3P_Y)}{P_Y} \delta_{ij}, \\ f &= \left(\frac{\rho - \rho_{co}}{\rho_{cp} - \rho} \right)^\alpha, \\ A'_h &= A'_0 |\sigma_u|, \quad B'_h = B'_0 |\sigma_u| \quad A'_h = -\frac{A_h}{2B_h (3A_h + 2B_h)}, \quad B'_h = \frac{1}{B_h}. \end{aligned}$$

5.3.4 Comparison with Wolffersdoff's law

The hypoplastic law of Wolffersdoff can be considered as the summary of 20 years of research and has been fully employed in soil mechanics [59]. A complete calibration procedure has been developed to evaluate material parameters. Its expression is recalled in Appendix A.2. A simple comparison with the hypoplastic law of the previous section reveals that N_{ij} has a similar form. For $\rho > \rho_{co}$, the non-linear contribution dominates but vanishes at the maximum packing $\rho = \rho_{cp}$. In the limit of maximum packings, the hypoplastic law reduces thus to

$$\frac{\partial \sigma_{ij}}{\partial t} = f L_{ijkl} \dot{\varepsilon}_{kl},$$

and exhibits an elastic behavior. These elastic states are also present in the law of Wolffersdorff. They have been called cryptoplastic and are experimentally observed during cycling deformations.

However, in Wolffersdorff law's, the 4th-order tensor L_{ijkl} has an additional term varying in σ_{ll} , which influences the yield surface and the flow rule. Actually, this law has been formulated to include a Matsuoka/Nakai limit surface. Thus, it exhibits a flowing behavior which is different from this of the EKM, where an elliptical limit surface is present. As a result, it cannot be directly combined with the EKM, in a way which ensures a continuous transition from flow to solid-like behavior. A possible solution to do that, would be to modify the flow model so that it reproduces a Matsuoka/Nakai yield condition in its quasi-static limit.

5.3.5 Initial conditions

The hypoplastic law must be employed with appropriate initial conditions. There is however no way to calculate initial conditions inside the hypoplastic framework. Generally, in practical applications, engineers solve the static force balance equation by assuming a fully elastic or quasi-elastic behavior to evaluate the initial stress conditions [8]. But the initial density distribution must still be postulated. The numerical simulation presented in this work (see Section 4.6.1), shows that density inhomogeneities strongly influence the mechanical properties of the sand heap formed by pouring. Additionally, stress and density distributions are strongly influenced by the preparation procedure, i.e the way how grains have been filled. In soil mechanics, it is however generally assumed that for a time greater than a critical value, the initial conditions may no affect the solution so strongly. In our model, we describe the evolution of a granular system inside the yield surface as hypoplastic. The stress and density computed by the EKM in a quasi-static regime can be used as initial condition for the hypoplastic law. In this way, we formulate a continuous transition in terms of stress from the quasi-static limit of the EKM to the rate-independent hypoplastic law. This is also a powerful way to account for the filling history the grains. The density and the stress distribution in the quasi-static limit of the EKM have been influenced by the filling procedure and this information is kept by the density and the stress. Thus the hypoplastic regime is also influenced by the preparation history of the grains. The criteria above which the hypoplastic description may apply, is when the quasi-static regime of the EKM is reached, i.e $f_Y = 0$.

5.3.6 Illustrative example

Consider the same example as in Section (5.2.5). A 2D granular layer in the critical state is characterized by a constant volume fraction and a shear stress given by $\sigma_{12} = \mu_s P_Y$. A simple hypoplastic law, which reproduces this state at yield can be formulated from the results of this part

$$\frac{\partial \sigma_{12}}{\partial t} = B_h \left(\frac{\partial v_1}{\partial x_2} - \frac{\sigma_{12}}{\mu_s P_Y} \left| \frac{\partial v_1}{\partial x_2} \right| \right). \quad (5.3.22)$$

In the stationary limit, it reads

$$\frac{\partial v_1}{\partial x_2} - \frac{\sigma_{12}}{\mu_s P_Y} \left| \frac{\partial v_1}{\partial x_2} \right| = 0, \quad (5.3.23)$$

what gives

$$\sigma_{12} = \mu_s P_Y, \quad (5.3.24)$$

for a positive shearing, i.e $\frac{\partial v_1}{\partial x_2} > 0$.

From critical state to solid behavior Consider an initial state given by $\sigma_{12} = \mu_s P_Y$. If the system is loaded, i.e, $\frac{\partial v_1}{\partial x_2} > 0$, the system stays at yield (according to (5.3.22)) and still flows. During unloading, i.e $\frac{\partial v_1}{\partial x_2} < 0$, the evolution of the shear stress is given by

$$\frac{\partial \sigma_{12}}{\partial t} = A_h \left(1 + \frac{\sigma_{12}}{\mu P_Y} \right) \frac{\partial v_1}{\partial x_2} < 0, \quad (5.3.25)$$

and the stress can reach values inside the yield surface. If the value $\sigma_{12} = -\mu_s P_Y$ is reached, then the system is again at yield. If the strain rate vanishes before that $\sigma_{12} = -\mu_s P_Y$, then a static state is reached inside the yield surface.

5.4 Conclusion: General hydrodynamic model

By completing the EKM with the hypoplastic law formulated in the previous section, one can define a hydrodynamic model able to account for a wide range of granular phenomena. The full model is summarized on pages 104 and 105.

We showed during this work that it includes several well-known behavior such as rate-dependent dilute flow, Bagnold's scaling, slow viscoplastic motion, asymptotic behavior and incremental non-linearity. Mechanisms for

the transition between the different regimes have been defined. The rate-dependent flow of dilute granular systems is captured with the kinetic constitutive equations. The transition to the dense flow has been modeled through a smooth transition to the yield regime. The hypoplastic extension allows the system to reach static states and account for incremental non-linearity.

This model was developed to account for the evolution of granular systems moving from dilute flow to quasi-static regime. The limit surface is not used to make the distinction between reversible and irreversible deformations, like in classical elasto-plasticity theories. It is implicitly defined and linked with the transition from flowing behavior to solid behavior. Irreversible deformations appear also above yield. This is actually more realistic than assuming an elastic behavior inside the yield surface [8]. Here the hypoplastic law is employed to describe the solid-like behavior of our system. In the hypoplastic regime, the information about the grains history is kept by the stress and the density.

This model was initially developed to account for the evolution of a granular system from the rate-dependent dilute regime to quasi-static behavior. However it can be also applied to simulate the transition from a static state to flowing behavior. Consider a static granular system which is loaded. It will first deform until it reaches the limit state where it plastically flows. Inside the hypoplastic framework, these states are expressed as $\frac{\partial \sigma_{ij}}{\partial t} = 0$. At yield, the flow relation

$$\frac{\kappa_{ij}}{\sqrt{\dot{\gamma}^2 + \frac{\zeta_0}{2\eta_0} \kappa_{ll}^2}} = \frac{2}{9\zeta_0} \sqrt{\frac{\rho\eta_0}{3\epsilon_0}} \frac{(\sigma_{ll} + 3P_Y) \delta_{ij}}{P_Y} + \frac{\sigma_{ij}^D \sqrt{\rho}}{\sqrt{3\eta_0\epsilon_0} P_Y}, \quad (5.4.1)$$

holds and it can be inverted to get the stress-stain relations:

$$\sigma_{ij} = -P_Y \delta_{ij} + \frac{2\eta_0 \sqrt{3\rho\epsilon_0} P_Y}{\rho \sqrt{4\eta_0 \dot{\gamma}^2 + 2\zeta_0 \kappa_{ll}^2}} \kappa_{ij}^D + \frac{\zeta_0 \sqrt{3\rho\epsilon_0} P_Y}{\rho \sqrt{4\eta_0 \dot{\gamma}^2 + 2\zeta_0 \kappa_{ll}^2}} \kappa_{ll} \delta_{ij} \quad (5.4.2)$$

from which one can formulate a consistent transition to the flow model, by adding the kinetic terms and including the temperature equation. The initial value of the granular temperature must be given by $T = \frac{4\eta_0 \dot{\gamma}^2 + 2\zeta_0 \kappa_{ll}^2}{3\rho\epsilon_0}$.

Generally, hypoplastic laws are formulated without further thermodynamic considerations. The formulation of thermodynamic consistent hypoplastic models is a current topic of research [136]. Thus the development of a general thermodynamic consistent model which includes a hypoplastic regime requires some additional efforts. In Section 5.2, we directly account for the reversible behavior of granular systems by introducing an elastic energy and an elastic deformation field. It is an interesting solution from a

thermodynamical point of view since it allows to directly quantify the reversible behavior of granular systems. But we argued that in the perspective of the numerical approach, it will significantly increase the problem complexity.

Thus we chose to directly combine the EKM with a hypoplastic law. It is a convenient practical solution to explicitly account for the granular solid-like behavior in a realistic way. The shortcoming is that the initial conditions of a static granular assembly cannot be determined. This is due to the structure of the hypoplastic laws. However, a convenient practical solution is to evaluate the stress state by assuming the initially static medium to be quasi-elastic and to solve the static momentum balance equation [8]. On the other side, some recent experiments show that the stress distribution inside a granular medium depends on how the system was filled [122]. Thus one may argue that the better way to evaluate the static initial condition of a granular system is to simulate how he was filled, what can be done with the hydrodynamic model developed in this work.

Balance equations

$$\begin{cases} \frac{\partial \rho}{\partial t} + \frac{\partial (\rho v_i)}{\partial x_i} = 0, \end{cases} \quad (5.4.3)$$

$$\begin{cases} \frac{\partial (\rho v_i)}{\partial t} + \frac{\partial (\rho v_i v_j)}{\partial x_j} = \rho g_i - \frac{\partial P}{\partial x_i} + \frac{\partial \tilde{\sigma}_{ij}}{\partial x_j}, \end{cases} \quad (5.4.4)$$

Kinetic and yield regime

$$\frac{\partial (\rho T)}{\partial t} + \frac{\partial (\rho v_i T)}{\partial x_i} = \frac{2}{3} \left(\tilde{\sigma}_{ij} \kappa_{ij} - \frac{\partial}{\partial x_i} \left(-\lambda \frac{\partial T}{\partial x_i} \right) \right) - \rho \epsilon T$$

$$\tilde{\sigma}_{ij} = 2\eta \kappa_{ij}^D + \zeta \kappa_{ll} \delta_{ij} \quad (5.4.5a)$$

with

$$\kappa_{ij} = \frac{1}{2} \left(\frac{\partial v_i}{\partial x_j} + \frac{\partial v_j}{\partial x_i} \right) \quad (5.4.5b)$$

$$P = P_K + P_Y \quad \text{with} \quad \begin{cases} P_Y = 0, & \rho \leq \rho_{co} \\ P_Y = T_0 (\rho - \rho_{co}) g(\rho), & \rho > \rho_{co} \end{cases} \quad (5.4.5c)$$

$$\eta = \eta_K \left(1 + \frac{P_Y}{P_K} \right), \quad \zeta = \zeta_K \left(1 + \frac{P_Y}{P_K} \right), \quad (5.4.5d)$$

$$\epsilon = \epsilon_K \left(1 + \frac{P_Y}{P_K} \right), \quad \lambda_K = \lambda_K \left(1 + \frac{P_Y}{P_K} \right) \quad (5.4.5e)$$

and

$$\eta_K = \eta_0 \sqrt{T} g(\rho), \quad \epsilon_K = \epsilon_0 \sqrt{T} g(\rho), \quad (5.4.5f)$$

$$\zeta_K = \zeta_0 \sqrt{T} g(\rho), \quad \lambda_K = \lambda_0 \sqrt{T} g(\rho) \quad P_K = T \rho g(\rho), \quad (5.4.5g)$$

with $g(\rho) = \left(1 - \frac{\rho}{\rho_{cp}} \right)^{-1}$ **Hypoplastic regime, $f_Y < 0$**

$$T = \frac{4\eta_0 \dot{\gamma}^2 + 2\zeta_0 \kappa_{ll}^2}{3\rho \epsilon_0}. \quad (5.4.6)$$

$$f_Y = (\sigma_{ll} + 3P_Y)^2 + \frac{9\zeta_0}{2\eta_0} \sigma_s^2 - \frac{27\zeta_0 \epsilon_0}{2\rho} P_Y^2, \quad (5.4.7)$$

$$\frac{\partial \sigma_{ij}}{\partial t} = f \left(L_{ijkl} \kappa_{kl} - N_{ij} \sqrt{\dot{\gamma}^2 + \frac{\zeta_0}{2\eta_0} \kappa_{ll}^2} \right), \quad (5.4.8)$$

$$L_{ijkl} = A_h \delta_{ij} \delta_{kl} + B_h (\delta_{ik} \delta_{jl} + \delta_{il} \delta_{jk}) \quad (5.4.9)$$

with

$$N_{ij} = \frac{\sigma_{ij}^D \sqrt{\rho}}{2B'_h \sqrt{3\varepsilon_0 \eta_0} P_Y} + \frac{2}{9\zeta_0 (A'_h + \frac{2}{3}B_h)} \sqrt{\frac{\rho \eta_0}{3\varepsilon_0}} \frac{(\sigma_{ll} + 3P_Y) \delta_{ij}}{P_Y}, \quad (5.4.10)$$

$$f = \left(\frac{\rho - \rho_{co}}{\rho_{cp} - \rho} \right)^\alpha, \quad A'_h = A'_0 |\sigma_{ll}|, \quad B'_h = B'_0 |\sigma_{ll}|. \quad (5.4.11)$$

6

Numerical applications

6.1 Numerical methods for filling and compression processes

We emphasized in the introduction that granular materials are involved in many industrial processes used in a wide range of industries. Developing efficient numerical tools to simulate these processes is of crucial importance for research and development purposes. Generally, different regimes and complex phenomena appear during industrial operations. For instance, sand casting implies a filling step during which the material is poured into a mold and compressed. A detailed study of the flow and filling behavior of granular matter during these processes can be found in [137]. The model formulated in this work covers several regimes, from the dilute flow to the quasi-static flow. Thus, it should give a pertinent representation of these processes.

Generally, in soil mechanics applications, quasi-static processes are simulated by solving the static momentum equation combined with some constitutive law, for instance elasto-plastic or hypoplastic. A Lagrangian description is employed. The applied load is decomposed into different load increments. The new strain is calculated at the next iteration by solving the force balance equation. The computational domain can be discretized with finite elements. Since the constitutive relations are generally non-linear, Newton-Raphson iterations can be employed. Several works focus on developing numerical methods to solve hypoplastic problems [138–143]. The numerical performance of these codes is comparable to that of elastoplastic models [8].

A shortcoming of this approach is that the initial density distribution is not known and must be postulated. We showed in our numerical experiment of Section 4.6.1 that filling processes lead to density inhomogeneities, which may significantly influence the mechanical properties of the resulting quasi-

static granular system. In soil mechanics, one assumes that after a certain loading time, the influence of the initial conditions can be neglected, but there is actually no way to check the validity of this hypothesis [8].

It is current practice to solve flow problems with the finite volume method because it ensures flux conservation [144]. The Eulerian description is relevant for systems undergoing very large deformations. Generally, numerical applications focus on only one regime. The mass and momentum conservation is combined with material laws (like those which were presented on Table 4.2 in Section 4.3). However, the model formulated in this work is more general and approximating its solution is a very complex task. The constitutive equations, although deliberately chosen to have a simple form, make the numerical problem very complex (high viscosities in the yield regime, density scaled by a maximal value and different regimes).

Numerical methods have been developed by Schmidt [4] and Niedziela [6] to approximate the solution of the EKM, valid for dilute and dense flow (see summary page 31). They are based on a finite-volume space discretization. In the work of Schmidt [4] a fully implicit nonlinear fractional step method was developed and implemented into the software CoRheoS [4, 6]. At each time step, two coupled equations are solved to compute the pressure and the velocity. It requires to solve a non-linear equation for the pressure, what is done with a variant of the Newton method. This algorithm was successfully applied to simulate several flow problems. The solution can be relatively quickly computed on 2D or 3D domains. The method of Niedziela [145] is based on semi-implicit time-stepping and has also been implemented into CoRheoS. We used it in Section 4 to simulate filling processes with the EKM.

A 3D or 2D numerical integration of the model formulated in this work (see summary pages 104 and 105) presents a big mathematical and computational challenge. It is *a priori* not clear how to approach this complex problem. Thus, it is first reasonable to consider the one dimensional case. Additionally, one may argue that 2D or 3D codes generate a lot of data whose analysis take a long time. The computational times can become also very long. In some processes, effects like shear or compression dominate and one can develop one dimensional models to describe it.

In the following we will first formulate a one dimensional version of our model and develop a numerical method to solve it. Our strategy is to solve the problem by employing an Eulerian framework. A Lagrangian method is not a relevant choice in our case since it will lead to difficulties for large deformations when mesh distortion can occur. In the literature, some works focused on the development of Arbitrarily Eulerian Lagrangian methods (AEL) to couple the advantage of both methods with application to fluid-structure interaction problems or free surface problem [11, 75]. Their application in our

case is not straightforward and requires an intense research. For this reason, we will focus on a Eulerian approach.

6.2 1D Model

6.2.1 Governing equations

Balance equations We first formulate a one dimensional version of the EKM which was introduced Section 3. We focus on a pure compressive or extensive flow. The relevant variables are the velocity v , compression $\kappa_{ll} = \frac{\partial v}{\partial x}$, volume fraction ρ , granular temperature T and the stress σ . In the one dimensional case the balance equations are given by

$$\frac{\partial \rho}{\partial t} + \frac{\partial (\rho v)}{\partial x} = 0, \quad (6.2.1)$$

$$\frac{\partial (\rho v)}{\partial t} + \frac{\partial (\rho v^2)}{\partial x} = \frac{\partial \sigma}{\partial x} - \rho g, \quad (6.2.2)$$

$$\frac{\partial (\rho T)}{\partial t} + \frac{\partial (\rho v T)}{\partial x} = \frac{2}{3} \left(\zeta \kappa_{ll}^2 + \frac{\partial (\lambda \frac{\partial T}{\partial x})}{\partial x} \right) - \rho \epsilon T. \quad (6.2.3)$$

Constitutive equations The stress is given as the sum of the kinetic, yield and dissipative contributions

$$\sigma = -P_K - P_Y + \zeta \kappa_{ll}, \quad (6.2.4)$$

where the kinetic and yield pressure are given by

$$P_K = T \rho g(\rho), \quad P_Y = T_0 (\rho - \rho_{co}) g(\rho). \quad (6.2.5)$$

The bulk viscosity and rate of dissipation are given by

$$\epsilon = \epsilon_0 \sqrt{T} \left(1 + \frac{P_Y}{P_K} \right), \quad \zeta = \zeta_0 \sqrt{T} \left(1 + \frac{P_Y}{P_K} \right). \quad (6.2.6)$$

We recall the expression for the radial distribution function at contact

$$g(\rho) = \frac{1}{1 - \frac{\rho}{\rho_{cp}}}. \quad (6.2.7)$$

At this stage, it is convenient to recall that in the EKM, the sign convention is chosen so that compressive stress is negative. This can be seen by looking

at equation (6.2.4). Generally, in soil mechanics another sign convention is adopted; compressive stresses are taken positive.

To complete the formulation, one needs to include the hypoplastic regime. We will apply in 1D the approach which was detailed in Section 5.3. We first express the equations governing the high density quasi-static limit of the EKM and then formulate a hypoplastic law, which ensures a continuous transition to solid-like behavior.

Transition to hypoplasticity For small deformations, the evolution of the volume fraction is given by

$$\frac{\partial \rho}{\partial t} + \rho \kappa_{ll} = 0. \quad (6.2.8)$$

In the stationary uniform limit, the granular temperature equation gives

$$\frac{2\zeta \kappa_{ll}^2}{3} - \rho \epsilon T = 0. \quad (6.2.9)$$

From this latter equation, it is calculated as

$$T = \frac{2\zeta}{3\rho\epsilon} \kappa_{ll}^2. \quad (6.2.10)$$

Applying (6.2.6), one obtains

$$T = \frac{2\zeta_0}{3\rho\epsilon_0} \kappa_{ll}^2. \quad (6.2.11)$$

By imposing this latter relation into (6.2.4), the stress in the stationary limit is given by

$$\sigma = -\frac{4\zeta_0 \kappa_{ll}^2}{3\rho\epsilon_0} \rho g(\rho) - P_Y + \sqrt{\frac{3\epsilon_0 \zeta_0}{2\rho}} P_Y \frac{\kappa_{ll}}{|\kappa_{ll}|}. \quad (6.2.12)$$

For small compression $|\kappa_{ll}| \ll 1$, it is approximately given by

$$\sigma = -P_Y + \sqrt{\frac{3\epsilon_0 \zeta_0}{2\rho}} P_Y \frac{\kappa_{ll}}{|\kappa_{ll}|}. \quad (6.2.13)$$

By inverting (6.2.13), one can express the flow rule as

$$\frac{\kappa_{ll}}{|\kappa_{ll}|} = \frac{(\sigma + P_Y)}{P_Y} \sqrt{\frac{2\rho}{3\epsilon_0 \zeta_0}}. \quad (6.2.14)$$

By taking the square of this last equation, the expression of the yield surface is found

$$f_Y = (\sigma + P_Y)^2 - \frac{3\epsilon_0 \zeta_0}{2\rho} P_Y^2 = 0. \quad (6.2.15)$$

In this state the system plastically flows at yield.

Hypoplastic regime We formulate an hypoplastic law, whose stationary limit is consistent with this of the EKM. Referring to Section 5.3, it is convenient to take the following law

$$\frac{\partial \sigma}{\partial t} = A_h \left(\kappa_{ll} - \frac{(\sigma + P_Y)}{P_Y} \sqrt{\frac{2\rho}{3\epsilon_0\zeta_0}} |\kappa_{ll}| \right), \quad (6.2.16)$$

where A_h is a material parameter. In the stationary limit, i.e. $\frac{\partial \sigma}{\partial t} = 0$, it leads to

$$\kappa_{ll} - \frac{(\sigma + P_Y)}{P_Y} \sqrt{\frac{2\rho}{3\epsilon_0\zeta_0}} |\kappa_{ll}| = 0, \quad (6.2.17)$$

which yields

$$\frac{\kappa_{ll}}{|\kappa_{ll}|} = \frac{(\sigma + P_Y)}{P_Y} \sqrt{\frac{2\rho}{3\epsilon_0\zeta_0}}. \quad (6.2.18)$$

Again, a limit surface is found from this relation, it is given by

$$(\sigma + P_Y)^2 - \frac{3\epsilon_0\zeta_0}{2\rho} P_Y^2 = 0. \quad (6.2.19)$$

This is consistent with (6.2.15).

Transition between the regimes The criteria for the transition between different regimes can be formulated as:

- transition from flow regime to hypoplastic: $\kappa_{ll} < 0$ and $T = \frac{2\zeta_0}{3\rho\epsilon_0} \kappa_{ll}^2$,
- transition from hypoplastic regime to flow model: $f_Y = 0$ and $\kappa_{ll} > 0$.

The first criteria specifies the transition from a dense compressed system to hypoplastic behavior. This transition allows to reach static states, characterized by $T = 0$ and $\frac{\partial \sigma}{\partial t} = 0$ and to account for incremental non-linearity.

Consider now a system initially in the hypoplastic regime which extends, $\kappa_{ll} > 0$. After a certain time, it will reach a limit state characterized by

$$\sigma = -P_Y - \sqrt{\frac{3\epsilon_0\zeta_0}{2\rho}} P_Y, \quad (6.2.20)$$

which can be explicitly expressed as a function of the density by inserting the value of P_Y

$$\sigma = T_0 (\rho - \rho_{co}) g(\rho) - \sqrt{\frac{3\epsilon_0\zeta_0}{2\rho}} T_0 (\rho - \rho_{co}) g(\rho). \quad (6.2.21)$$

If the system is still extending, its density diminishes since $\frac{\partial \rho}{\partial t} = -\rho \kappa_{ll}$. According to (6.2.21), the pressure will diminish and tends to zero if the cross-over value is reached, i.e $\rho \rightarrow \rho_{co}$. To account for the fluid-like behavior of granular materials, and the pressure induced by collisions between the grains, it is thus necessary to make a transition to the flow model. Finally, the full model is given by

$$\frac{\partial \rho}{\partial t} + \frac{\partial (\rho v)}{\partial x} = 0, \quad (6.2.22)$$

$$\frac{\partial (\rho v)}{\partial t} + \frac{\partial (\rho v^2)}{\partial x} = \frac{\partial \sigma}{\partial x} - \rho g \quad (6.2.23)$$

Flow regime

$$\frac{\partial (\rho T)}{\partial t} + \frac{\partial (\rho v T)}{\partial x} = \frac{2}{3} \left(2\zeta \kappa_{ll}^2 + \frac{\partial (\lambda \frac{\partial T}{\partial x})}{\partial x} \right) - \rho \epsilon T, \quad (6.2.24)$$

$$\sigma = -P + \zeta \kappa_{ll}, \quad (6.2.25)$$

$$\epsilon = \epsilon_K \left(1 + \frac{P_Y}{P_K} \right), \quad \zeta = \zeta_K \left(1 + \frac{P_Y}{P_K} \right), \quad (6.2.26)$$

$$\lambda = \lambda_K \left(1 + \frac{P_Y}{P_K} \right), \quad P_K = T \rho g(\rho), \quad (6.2.27)$$

$$\epsilon_K = \epsilon_0 \sqrt{T} g(\rho), \quad \lambda_K = \lambda_0 \sqrt{T} g(\rho), \quad \zeta_K = \zeta_0 \sqrt{T} g(\rho), \quad (6.2.28)$$

$$P = P_K + P_Y \quad \text{with} \quad \begin{cases} P_Y = 0, & \rho \leq \rho_{co} \\ P_Y = T_0 (\rho - \rho_{co}) g(\rho), & \rho > \rho_{co} \end{cases} \quad (6.2.29)$$

and $g(\rho) = \left(1 - \frac{\rho}{\rho_{cp}} \right)^{-1}$

Hypoplastic regime, $f_Y < 0$

$$T = \frac{2\zeta_0}{3\rho\epsilon_0} \kappa_{ll}^2, \quad (6.2.30)$$

$$\frac{\partial \sigma}{\partial t} = A_h \left(\kappa_{ll} - \frac{(\sigma + P_Y)}{P_Y} \sqrt{\frac{2\rho}{3\epsilon_0\zeta_0}} |\kappa_{ll}| \right). \quad (6.2.31)$$

Material parameters: $\epsilon_0, \lambda_0, \zeta_0, T_0, A_h, \rho_{co}, \rho_{cp}$.

6.2.2 Hypoplastic behavior at loading and unloading

In this section, we present an example to illustrate how the hypoplastic constitutive law accounts for the solid-like behavior. Consider a granular system initially at rest in a pre-constrained state, let say $\sigma = -0.4P_Y$. We integrate the hypoplastic equation along a cyclic strain rate path, composed of loading steps ($\kappa_{ll} > 0$) and unloading steps ($\kappa_{ll} < 0$) and plotted on Figure 6.1. The equation is integrated by applying an explicit Euler method and the results can be seen on Figure 6.2. During the loading step, $\kappa_{ll} < 0$, the hypoplastic law reduces to

$$\frac{\partial \sigma}{\partial t} = A_h \left(1 + \frac{(\sigma + P_Y)}{P_Y} \sqrt{\frac{2\rho}{3\epsilon_0\zeta_0}} \right) \kappa_{ll}, \quad (6.2.32)$$

which takes the form of an elastic law (in a rate form) with a pressure-dependent bulk modulus $K \sim A_h \left(1 + \frac{(\sigma + P_Y)}{P_Y} \sqrt{\frac{2\rho}{3\epsilon_0\zeta_0}} \right)$. The pressure increases until the yield surface value $\sigma = -P_Y - \sqrt{\frac{3\epsilon_0\zeta_0}{2\rho}}$ is reached. If the material is still loaded, $\kappa_{ll} < 0$, the system remains at yield and is still flowing. If the system is unloaded $\kappa_{ll} > 0$, the evolution of stress is governed by

$$\frac{\partial \sigma}{\partial t} = A_h \left(1 - \frac{(\sigma + P_Y)}{P_Y} \sqrt{\frac{2\rho}{3\epsilon_0\zeta_0}} \right) \kappa_{ll}. \quad (6.2.33)$$

Again, this can be seen as an elastic law (in a rate form), with the value of the bulk modulus $K \sim A_h \left(1 - \frac{(\sigma + P_Y)}{P_Y} \sqrt{\frac{2\rho}{3\epsilon_0\zeta_0}} \right)$. The difference of the stiffness between loading and unloading is a well-known property of soils and generally referred to incremental non-linearity. Note that in the presented example, the materials constant are assumed to be independent of the density.

6.3 Numerical method

From a mathematical point of view, the one dimensional hydrodynamic model (fully given on page 112) involves many difficulties. The density is bounded by a maximum value. Viscosities and transport coefficients are varying with the density and the granular temperature. They can become very large in the quasi-static limit. Huge compressibility variations can be expected between the dilute flow regime and the quasi-static one. Additionally, in the hypoplastic regime, the constitutive equation is given in a rate form and must be integrated at each time step.

The involved PDE's are neither always hyperbolic nor parabolic. A wide range of mathematical methods have been developed and can be applied to solve time dependent parabolic or hyperbolic problems [144]. Since we focus here on the full hydrodynamic equations, the majority of these methods cannot be directly applied.

Generally in fluid dynamics, the numerical schemes employed are constructed to ensure flux conservation. This is the approach which is followed here. An explicit time discretization will be combined with a centered finite difference spatial discretization. An explicit time integration has the advantage that no algebraic equations must be additionally solved, but requires small time steps. Explicit schemes are bounded by a time restriction of the type $\tau < Ch^2/\eta$, where h is the scale of the space discretization, C a constant and η the viscosity [146]. Being aware of this restriction, our numerical simulation will be run with small time steps (typically smaller than 10^{-5} s). We notice that similar methods have been developed in compressible fluid dynamics and for shock waves problems [147].

6.3.1 Time discretization

In the following q denotes one of the three variables of the problem, i.e the density ρ , the momentum density ρv or the energy density ρT . The starting point is to discretize the time interval $\Omega_t = (0, t_f)$, where t_f is the final time. The time steps $t^{n+1} - t^n = \Delta t$ are constant. We take $n \in \{0, 1, \dots, m\}$ and the discretized time interval is given by

$$\omega_t = \left\{ t^n = n\Delta t \in \Omega_t, \quad n = 0, 1, \dots, M, \quad \Delta t = \frac{t_f}{M} \right\}.$$

The superscript $n + 1$ is used to denote the value of a variable at the new time step and n denotes the values at the time t^n . The time derivatives are

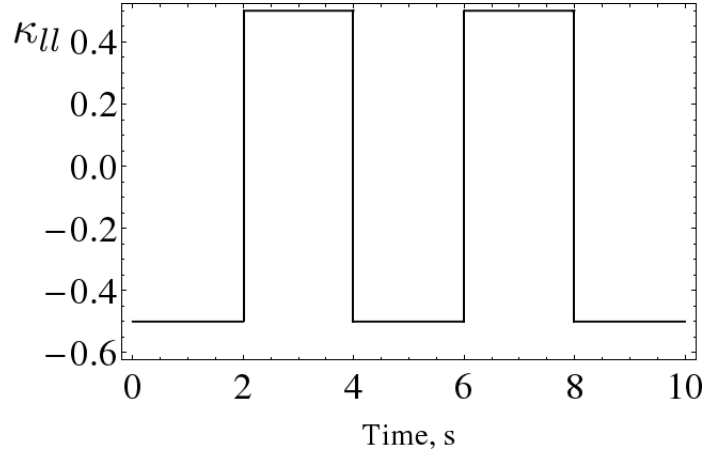


Figure 6.1: Applied compression rate κ_{ll} , in s^{-1} .

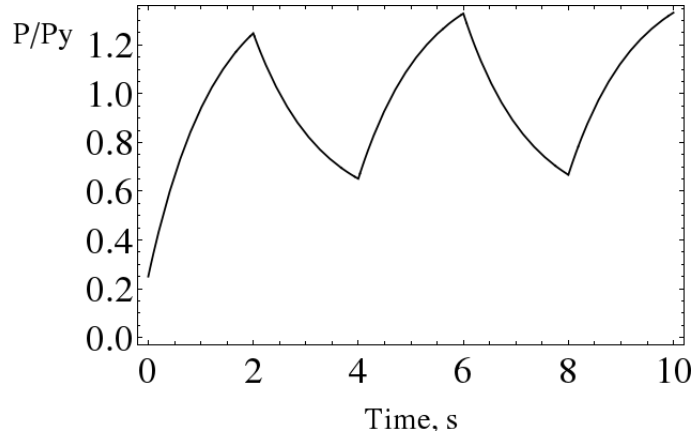


Figure 6.2: Typical variation of the scaled pressure $P/P_Y = -\sigma/P_Y$ during loading and unloading.

approximated at first order by difference quotients formula

$$\frac{\partial q}{\partial t} \approx \frac{q^{n+1} - q^n}{\Delta t}. \quad (6.3.1)$$

Once the relation (6.3.1) is applied, one needs to specify how the other terms involved in the PDE are evaluated. For explicit schemes the value of these terms are taken at the previous time step whereas they are taken at the current time for implicit schemes. Implicit schemes require to solve additionally an algebraic equation. Alternatively, one can integrate some terms implicitly and others explicitly. In this case, the scheme is called semi-implicit. As previously explained, the numerical scheme developed here is explicit.

6.3.2 Space discretization

The computational domain $\Omega_h = (0, L)$ is discretized into N cells of constant size h . The discretized domain ω_h is thus defined by

$$\omega_h = \left\{ x_i = ih \in \Omega_h \quad i = 0, 1, \dots, N, \quad h = \frac{L}{N} \right\}.$$

We will develop a flux conserving scheme where grid points are cell centers located at x_i . The value of the variable q at x_j is denoted by $q_j = q(x_j)$. The quantities $q_{j+1/2}$ and $q_{j-1/2}$ stand for the value at the cell interfaces, which are situated at

$$x_{j+1/2} = \frac{1}{2}(x_j + x_{j+1}), \quad x_{j-1/2} = \frac{1}{2}(x_j + x_{j-1}). \quad (6.3.2)$$

The grid can be seen on Figure 6.3. The two boundary cells of the domain are defined by

$$x_{1/2} = x_1 - \frac{h}{2}, \quad x_{N+1/2} = x_N + \frac{h}{2}. \quad (6.3.3)$$

In the following, the value of the variable q at $x = x_j$ and $t = t^n$ is denoted $q_j^n = q(x_j, t^n)$.

Finite difference The finite difference approximation is based on the simple idea that a spatial derivative can be approximated by the ratio of two differences according to the definition of the derivative. The order of the approximation is obtained by applying a Taylor series development. Spatial derivatives are approximated here with a central scheme

$$\frac{\partial q}{\partial x}|_j \approx \frac{q_{j+1/2} - q_{j-1/2}}{h}. \quad (6.3.4)$$

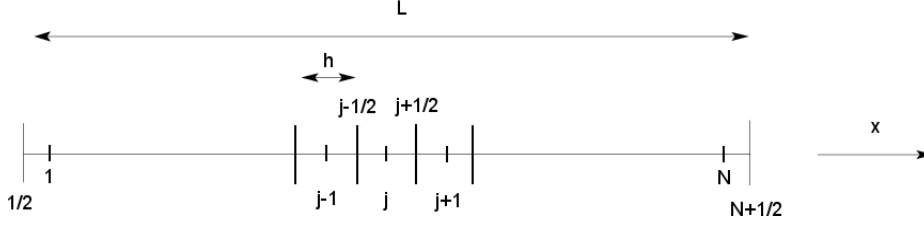


Figure 6.3: Space discretization.

This latter relation will be applied to discretize terms of the conservation equations which involve a spatial derivative, like for instance the pressure gradient $\frac{\partial P}{\partial x}$. The discretization of convective terms requires more attention.

Convective terms The terms of the form $\frac{\partial(qv)}{\partial x}$ in the conservation equations describe the convective transfer of the quantity q . The discretization of this term with centered finite difference (6.3.4) gives

$$\frac{\partial(qv)}{\partial x}|_j = \frac{\{qv\}_{j+1/2} - \{qv\}_{j-1/2}}{h}, \quad (6.3.5)$$

where the bracket $\{qv\}_{j+1/2}$ stands for the value of qv at the boundary between the cell j and $j+1$, $\{qv\}_{j+1/2} = (qv)(x_{j+1/2}, t^n)$. This value is a priori not known and must be specified by the algorithm. It is tempting to take $q_{j+1/2}$ as the average of the q between the two cells but this leads to an unconditionally unstable scheme [144]. A well-known scheme to overcome this difficulty is to employ a donor-cell scheme. If the flux is in the direction of the face, the value at the wall is taken as the value at the center of the control volume. If the flow is in the opposite direction, the value at the wall is approximated with the value of the neighboring control volume. This is written as

$$\begin{cases} \{vq\}_{j-1/2} = q_{j-1}v_{j-1/2} & \text{if } v_{j-1/2} > 0 \\ \{vq\}_{j-1/2} = q_jv_{j-1/2} & \text{if } v_{j-1/2} < 0 \end{cases} \quad (6.3.6)$$

and

$$\begin{cases} \{vq\}_{j+1/2} = \rho_jv_{j+1/2} & \text{if } v_{j+1/2} > 0 \\ \{vq\}_{j+1/2} = \rho_{j+1}v_{j+1/2} & \text{if } v_{j+1/2} < 0, \end{cases} \quad (6.3.7)$$

where the value of the velocity at the boundary is taken as the average of

two values of the two adjacent cells

$$v_{j+1/2} = \frac{v_j + v_{j+1}}{2} \quad \text{and} \quad v_{j-1/2} = \frac{v_j + v_{j-1}}{2}. \quad (6.3.8)$$

The donor cell is a simple flux conserving scheme. If one wants to have a second or higher order spatial accuracy, one may use a high resolution scheme. These schemes can lead to oscillations near discontinuities, but one can apply slope or flux limiters to limit them [147].

6.3.3 Discretization of the balance equations

Mass conservation Applying an explicit time integration and the central finite difference scheme, the discretized mass conservation is given by

$$\rho_j^{n+1} = \rho_j^n + \frac{\Delta t}{h} \left(\{\rho v\}_{j-1/2}^n - \{\rho v\}_{j+1/2}^n \right). \quad (6.3.9)$$

The values $\{\rho v\}_{j-1/2}^n$ and $\{\rho v\}_{j+1/2}^n$ are given by the upwind scheme (6.3.6), (6.3.7). It is convenient to introduce the function θ which checks the velocity direction

$$\theta = \theta(v) = \text{sgn}(v) = \begin{cases} 1, & v \geq 0 \\ -1, & v < 0. \end{cases} \quad (6.3.10)$$

Applying (6.3.10), the discretized mass conservation equation is now given by

$$\begin{aligned} \rho_j^{n+1} = \rho_j^n + \frac{\Delta t}{h} & \left(\frac{1}{2} v_{j-1/2}^n [(1 + \theta_{j-1/2}^n) \rho_{j-1}^n + (1 - \theta_{j-1/2}^n) \rho_j^n] \right. \\ & \left. - \frac{1}{2} v_{j+1/2}^n [(1 + \theta_{j+1/2}^n) \rho_j^n + (1 - \theta_{j+1/2}^n) \rho_{j+1}^n] \right). \end{aligned} \quad (6.3.11)$$

Momentum balance If the same discretization can be applied to the momentum equation, one gets

$$\begin{aligned} \{\rho v\}_j^{n+1} = \{\rho v\}_j^n + \frac{\Delta t}{h} & \left(- \{\rho v^2\}_{j-1/2}^n + \{\rho v^2\}_{j+1/2}^n - \right. \\ & \left. (\sigma_{j+1/2}^n - \sigma_{j-1/2}^n) \right) - \rho_j^{n+1} g \Delta t. \end{aligned} \quad (6.3.12)$$

In this latter expression, the pressure gradient has been discretized as

$$\left\{ \frac{\partial \sigma}{\partial x} \right\}_j^n \approx \frac{(\sigma_{j+1/2}^n - \sigma_{j-1/2}^n)}{h}. \quad (6.3.13)$$

It gives

$$\left\{ \frac{\partial \sigma}{\partial x} \right\}_j^n \approx \frac{\Delta t}{h} \left(\frac{(\sigma_{j+1}^n + \sigma_j^n)}{2} - \frac{(\sigma_{j-1}^n + \sigma_j^n)}{2} \right) = \frac{\Delta t}{h} \left(\frac{\sigma_{j+1}^n - \sigma_{j-1}^n}{2} \right).$$

This last equation shows that the pressure gradient is approximated by taking the difference of the pressure between two grid points. This can lead to an unrealistic approximation of the pressure field. To overcome this, we follow the recommendation of Patankar [144] to solve the momentum equation on a displaced grid. Velocity components are calculated at the interface between two cells

$$\{\rho v\}_{j+1/2}^{n+1} = \{\rho v\}_{j+1/2}^n + \frac{\Delta t}{h} \left(-\{\rho v^2\}_j^n + \{\rho v^2\}_{j+1}^n - (\sigma_{j+1}^n - \sigma_j^n) \right) - \rho_j^n g \Delta t. \quad (6.3.14)$$

With this discretization of the momentum equation, the pressure is evaluated at the interface between adjacent pressure components. The values of $\{\rho v^2\}_{j-1/2}^n$ and $\{\rho v^2\}_{j+1/2}^n$ are then also calculated with the upwind scheme specified by (6.3.6) and (6.3.7). It gives

$$\begin{cases} \{\rho v^2\}_j^n = v_j^n \{\rho v\}_{j-1/2}^n & \text{if } v_j^n > 0 \\ \{\rho v^2\}_j^n = v_j^n \{\rho v\}_{j+1/2}^n & \text{if } v_j^n < 0. \end{cases} \quad (6.3.15)$$

A similar relation applies for $\{\rho v^2\}_{j+1}^n$. According to this last equation, the discretized momentum equation is given by

$$\begin{aligned} \{\rho v\}_{j+1/2}^{n+1} = & \{\rho v\}_{j+1/2}^n \\ & + \frac{\Delta t}{h} \left(\frac{1}{2} v_{j-1}^n \left[(1 + \theta_j^n) \{\rho v\}_{j-1/2}^n + (1 - \theta_j^n) \{\rho v\}_{j+1/2}^n \right] \right. \\ & - \frac{1}{2} v_j^n \left[(1 + \theta_{j+1}^n) \{\rho v\}_{j+1/2}^n + (1 - \theta_{j+1}^n) \{\rho v\}_{j+3/2}^n \right] \\ & \left. - (\sigma_{j+1}^n - \sigma_j^n) \right) - \rho_j^n g \Delta t. \end{aligned} \quad (6.3.16)$$

Temperature equation The temperature equation can be discretized, as previously, by combining a finite difference space discretization with an ex-

explicit time discretization

$$\begin{aligned} \{\rho T\}_j^{n+1} = \{\rho T\}_j^n &+ \frac{\Delta t}{h} \left(-\{\rho v T\}_{j+1/2}^n + \{\rho v T\}_{j-1/2}^n \right) \\ &+ \left\{ \frac{4}{3} \zeta \kappa_{ll}^2 \right\}_j^n \Delta t - \{\rho \epsilon T\}_j^n \Delta t + \left\{ \frac{\partial \lambda \frac{\partial T}{\partial x}}{\partial x} \right\}_j^n \Delta t. \end{aligned} \quad (6.3.17)$$

The convective terms $\{\rho v T\}_{j+1/2}^n$ and $\{\rho v T\}_{j-1/2}^n$ are discretized with the upwind scheme. The heat conduction term can be discretized as

$$\left\{ \frac{\partial \lambda \frac{\partial T}{\partial x}}{\partial x} \right\}_j^n = \frac{\left\{ \lambda \frac{\partial T}{\partial x} \right\}_{j+1/2}^n - \left\{ \lambda \frac{\partial T}{\partial x} \right\}_{j-1/2}^n}{h}. \quad (6.3.18)$$

Again, the spatial derivative of this last equation is discretized with a centered finite difference scheme

$$\left\{ \lambda \frac{\partial T}{\partial x} \right\}_{j+1/2}^n = \lambda_{j+1/2}^n \frac{T_{j+1}^n - T_j^n}{h}, \quad \left\{ \lambda \frac{\partial T}{\partial x} \right\}_{j-1/2}^n = \lambda_{j-1/2}^n \frac{T_j^n - T_{j-1}^n}{h}.$$

By inserting this two latter equations into (6.3.18), one gets

$$\left\{ \frac{\partial \lambda \frac{\partial T}{\partial x}}{\partial x} \right\}_j^n = \frac{1}{h^2} \left(\lambda_{j+1/2}^n (T_{j+1}^n - T_j^n) - \lambda_{j-1/2}^n (T_j^n - T_{j-1}^n) \right). \quad (6.3.19)$$

The discretization of the heat dissipation term and viscous terms gives

$$\{\rho \epsilon T\}_j^n + \left\{ \frac{4}{3} \eta \kappa_{ll}^2 \right\}_j^n = \rho_j^n \epsilon_j^n T_j^n + \frac{4}{3} \eta_j^n \left\{ \kappa_{ll}^2 \right\}_j^n, \quad (6.3.20)$$

with

$$\left\{ \kappa_{ll}^2 \right\}_j^n = \left(\frac{v_{j+1/2}^n - v_{j-1/2}^n}{h} \right)^2 = \left(\frac{v_{j+1}^n - v_{j-1}^n}{2h} \right)^2. \quad (6.3.21)$$

By combining these latter equations, the discretized temperature equation gives

$$\begin{aligned} \{\rho T\}_j^{n+1} = \{\rho T\}_j^n &+ \frac{\Delta t}{h} \left(\frac{1}{2} v_{j-1/2}^n \left[(1 + \theta_{j-1/2}^n) \{\rho T\}_{j-1}^n + (1 - \theta_{j-1/2}^n) \{\rho T\}_j^n \right] \right. \\ &- \left. \frac{1}{2} v_{j+1/2}^n \left[(1 + \theta_{j+1/2}^n) \{\rho T\}_j^n + (1 - \theta_{j+1/2}^n) \{\rho T\}_{j+1}^n \right] \right) \\ &+ \frac{\Delta t}{h^2} \left(\lambda_{j+1/2}^n (T_{j+1}^n - T_j^n) - \lambda_{j-1/2}^n (T_j^n - T_{j-1}^n) \right) \\ &+ \left(\{\rho T\}_j^n \epsilon_j^n + \frac{4}{3} \eta_j^n \left(\frac{v_{j+1}^n - v_{j-1}^n}{2h} \right)^2 \right) \Delta t, \end{aligned} \quad (6.3.22)$$

In the hypoplastic regime, the granular temperature equation is not solved and the granular temperature is updated as

$$T_j^{n+1} = \frac{2\zeta_0}{3\rho_j^n \epsilon_0} \{\kappa_{ll}^2\}_j^n. \quad (6.3.23)$$

Hypoplastic regime The hypoplastic law is integrated as follows

$$\sigma_j^{n+1} = \sigma_j^n + A_h \left(\frac{v_{j+1}^n - v_{j-1}^n}{2h} - \frac{(\sigma_j^n + \sigma_{Y,j}^n)}{P_{Y,j}^n} \sqrt{\frac{2\rho_j^n}{3\epsilon_0\zeta_0}} \left| \frac{v_{j+1}^n - v_{j-1}^n}{2h} \right| \right) \Delta t. \quad (6.3.24)$$

Boundary conditions Two kinds of boundary condition are considered in this work, Dirichlet and homogeneous Neuman. Dirichlet boundary condition requires to set the value of a variable at the boundary. If it is applied to the left boundary, it gives

$$q_{1/2} = \bar{q}, \quad (6.3.25)$$

where \bar{q} is the Dirichlet condition at the boundary. The homogeneous Neuman boundary condition is given by $\frac{\partial q}{\partial x} = 0$. Similarly as in [4], we directly set this condition in diffusive terms. In pressure gradients and convective terms, we approximate this condition by writing

$$q_{1/2} = q_{1+1/2}, \quad (6.3.26)$$

if the condition is applied to the left side of the computational domain. For the right side, it is given by

$$q_{N+1/2} = q_N. \quad (6.3.27)$$

6.4 Implementation

In this section, we explain the implementation approach. The algorithm was implemented using the computer algebra system *Mathematica 8.0*, see Algorithm 1. In the initialization procedure, all the relevant parameters of the problems are set. One must successively specify the material parameters, the size of the computational domain and the initial and boundary conditions. The material parameters of the problem are ζ_0 , T_0 , ϵ_0 , ρ_{co} , ρ_{cp} and A_h . At each time steps, the new values of the density, velocity and temperature are computed. The results are saved each $l\Delta t$, where l is specified by the user. We introduce the variable r which specifies the flow regime (dilute, dense

Algorithm 1: Explicit finite difference conservative scheme

Initialize Material parameters, Initial condition, Geometry

```

for  $n = 1, n = M$  do
  for  $j = 1, j = N$  do
    ①  $t = t + \Delta t$ . If  $t = l\tau \rightarrow$  Store results, If  $t = t_f \rightarrow$  end, else go to ②.
    ② Set boundary conditions.
    ③ Update  $r_j^n$  by checking variable values.
    ④ Update variables values

     $\{\rho\}_j^{n+1}$  given by (6.3.11),
     $\{\rho v\}_{j+1/2}^{n+1}$  given by (6.3.16),
    If  $r_j^n = \text{dilute or dense} \rightarrow \{\rho T\}_j^{n+1}$  given by (6.3.22),
    If  $r_j^n = \text{hpp}$ , update  $\{\rho T\}_j^{n+1}$  with (6.3.23).

    ⑤ Pressure update

    If  $r_j^n = \text{dilute or dense}$ ,  $\sigma_j^n = (P_K + P_Y)_j^n$ ,
    If  $r_j^n = \text{hpp}$ , integrate  $\sigma_j^{n+1}$  with (6.3.24).

    ⑥ Update transport coefficients  $\zeta_j^{n+1} = \zeta_0(1 + \frac{P_{Y,i}^n}{P_{K,j}^n})$ ,
     $\lambda_j^{n+1} = \lambda_0(1 + \frac{P_{Y,i}^n}{P_{K,j}^n})$ ,  $\epsilon_j^{n+1} = \epsilon_0(1 + \frac{P_{Y,i}^n}{P_{K,j}^n})$ .

    ⑦ Update  $T_j^{n+1}$  and  $v_j^{n+1}$ :  $T_j^{n+1} = \frac{\{\rho T\}_j^{n+1}}{\{\rho\}_j^{n+1}}$ 
     $v_j^{n+1} = \left( \frac{\{\rho v\}_{j+1/2}^{n+1}}{\{\rho\}_{j+1/2}^{n+1}} + \frac{\{\rho v\}_{j-1/2}^{n+1}}{\{\rho\}_{j-1/2}^{n+1}} \right) / 2$ .
  end
end

```

or hpp, for hypoplastic). The value of the pressure, loss energy rate, bulk viscosity must also be updated at each time step.

6.5 Numerical tests

In this part, we perform a qualitative validation of the code by running some numerical tests. We will show that the developed model can cover several flow regimes. Analytical solutions of the model can only be obtained in simple cases, due to the complexity of the equations. We restrict ourselves to testing if the density, velocity, pressure or granular temperature are physically consistent in three numerical experiments. This also allows us to investigate in which case no satisfying solution is found, so that further works can focus on developing more appropriate numerical methods for these specific cases. Once tested, the code can be later employed to do more quantitative analysis and comparison to experiments.

Simulation parameters The following simulations are run with a time step of 10^{-6} s. The length of the system is $L = 0.3$ m and divided into 30 cells. The following values of the parameters are chosen

$$\rho_{co}/\rho_b=0.6, \quad \zeta_0/\rho_b=0.0001 \text{ m}^2 \text{ s}^{-1}, \quad T_0/\rho_b=1.5 \text{ m}^2 \text{ s}^{-1}, \quad \epsilon_0/\rho_b = 500 \text{ s}^{-1}, \\ \rho_b = 1600 \text{ kg m}^{-3}, \quad \rho_{cp}/\rho_b=0.64, \quad A_h = 200 \text{ MPa}.$$

6.5.1 Stationary kinetic flow

Initial and boundary condition As first test, we study a pure kinetic flow. We consider a system which is filled on its left side and which is allowed to flow on the right side. The grains are filled until a kinetic stationary regime is reached. The system is initially at rest and contains no material. Thus, we set the following initial conditions

$$v|_{t=0} = 0, \quad \rho|_{t=0} = 0, \quad T|_{t=0} = 0. \quad (6.5.1)$$

At $x = L$ we model an outflow boundary condition by specifying the following conditions

$$\frac{\partial v}{\partial x}|_{x=L} = 0, \quad \frac{\partial T}{\partial x}|_{x=L} = 0. \quad (6.5.2)$$

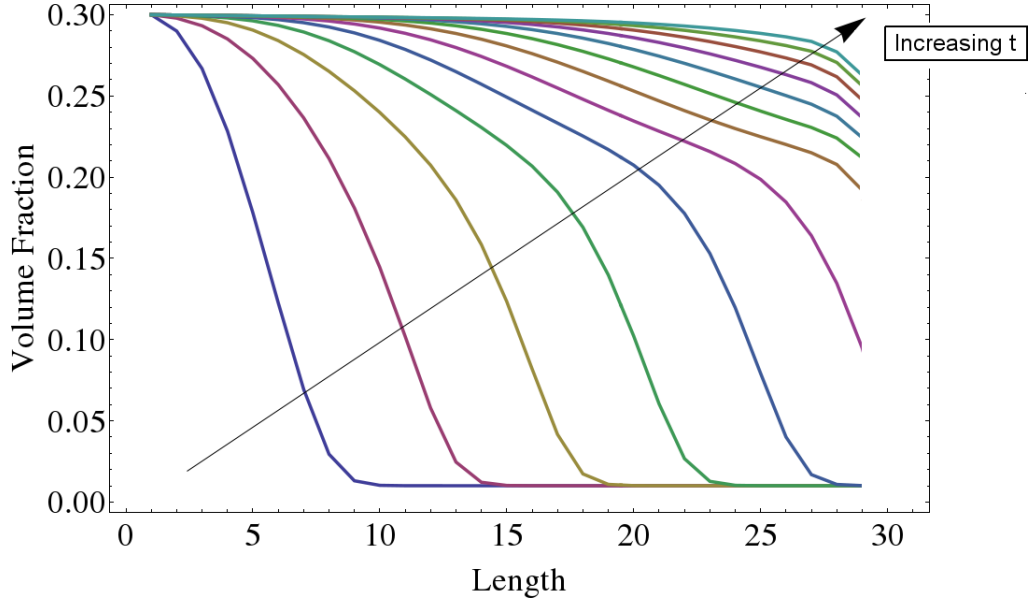


Figure 6.4: Volume fraction distributions at different time steps of the kinetic flow. The blue curve of the left corresponds to the beginning of the flow. The green curve on the top corresponds to the stationary limit reached at the end of the simulation. Length in m.

The material is filled at $x = 0$. To mimic this condition, we impose a Dirichlet boundary condition to the density and velocity and set the gradient to zero

$$\rho|_{x=L} = \rho_{inflow}, \quad \frac{\partial T}{\partial x}|_{x=L} = 0 \quad v|_{x=L} = v_{inflow}. \quad (6.5.3)$$

Results The density profiles obtained are plotted on Figure 6.5.1 for inflow velocity of 0.01 ms^{-1} . After a certain time the stationary condition is reached. The volume fraction profile progressively increases until it becomes stationary. Near the outflow boundary, the volume fraction remain constant after a certain time, around a value which is near to ρ_{inflow} .

6.5.2 Filling simulation

As a second example, we consider the filling of some granular materials into a box. Gravity is set to zero and we apply the same inflow boundary condition as previously. The system is initially at rest. To mimic these conditions, we apply the same initial conditions as in the previous part. At $x = L$ we set a

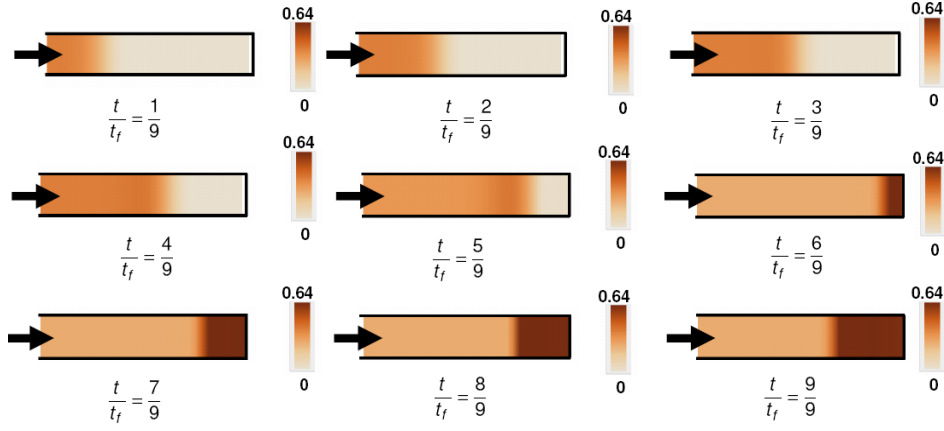


Figure 6.5: Volume fraction distributions ρ at different steps of the filling process.

wall boundary condition by the following conditions

$$v|_{x=0} = 0 \quad \frac{\partial \rho}{\partial x}|_{x=0} = 0 \quad T|_{x=0} = 0. \quad (6.5.4)$$

Results The results can be seen on Figure 6.5. During the first steps of the filling, the volume fraction is below the cross-over value ρ_{co} . Thus a pure kinetic flow happens. At greater volume fractions, yield flow appears. In these regions, the quasi-static limit is reached, the system slowly compresses under critical conditions and the pressure only depends on the volume fraction. To get a more precise representation of these states, the volume fraction profiles during the early filling stage, where the yield regime is not reached, are plotted on Figure 6.6. The blue curve on the right side corresponds to an early stage of the process, whereas the brown on the right corresponds to the state just before yield is reached. Between $t/t_f = 5/9$ and $t/t_f = 6/9$, the grains of the right side moves from the kinetic to the yield regime. The evolution of the volume fraction during this period can be seen on Figure 6.7.

We also found that the value of the filling conditions significantly influences the stability of the numerical solution. For greater values of the input velocities (from $v = 10v_{inflow}$) but also very small ones (for $v = 0.01v_{inflow}$), strong oscillations in the solution are observed. Additionally, in these cases, the volume fraction was observed to become greater than its maximal value. Further investigations should focus on developing numerical scheme more adapted to these specific cases.

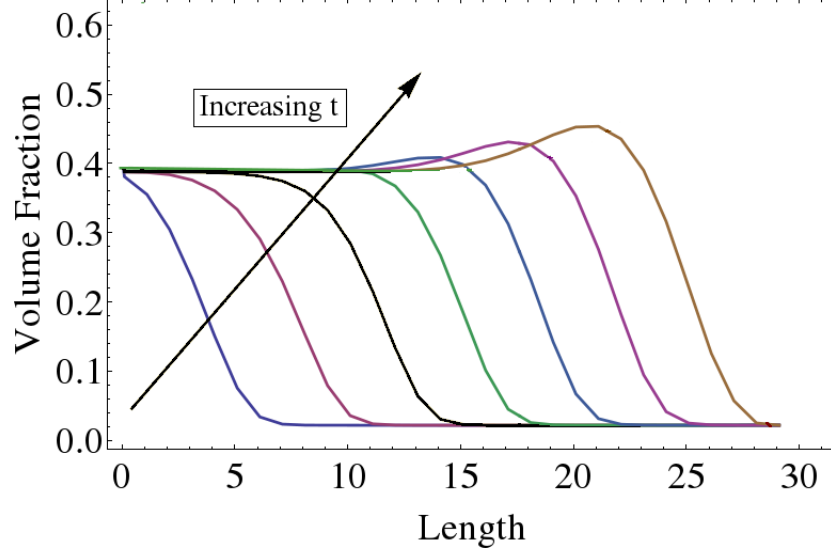


Figure 6.6: Plot of the volume fraction ρ/ρ_b profiles between $t/t_f = 1/9$ and $t/t_f = 5/9$. Length in m.

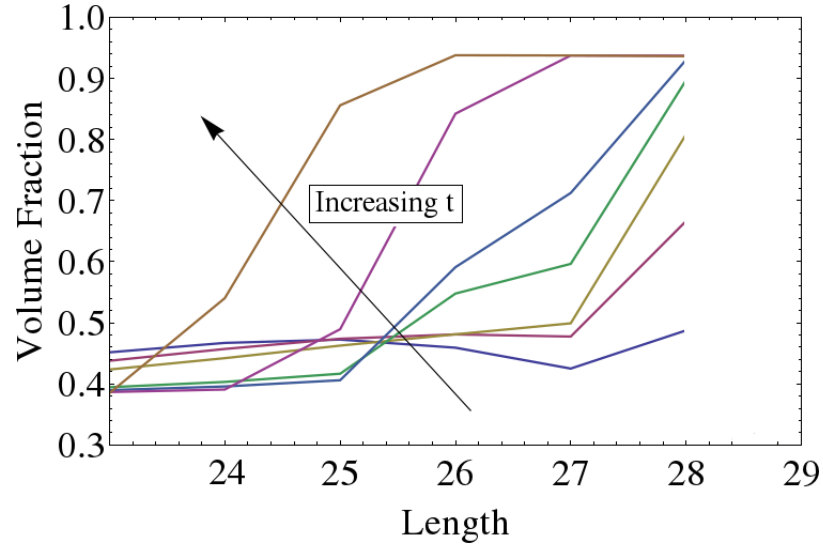


Figure 6.7: Plot of the volume fractions ρ/ρ_b scaled with the maximal value ρ_{cp}/ρ_b between $t/t_f = 5/9$ and $t/t_f = 6/9$. Length in m.

6.5.3 Sand flowing on an inclined plane

In this section, we model a column of sand initially on a inclined plane. As initial conditions, we consider a dense sand system initially at rest having a constant initial volume fraction $\rho/\rho_b = 0.61$ and an initial pressure of $\sigma = -0.4P_Y$. It is easy to check that with this initial value, the stress is inside the yield surface. The angle of the inclined plane is set to 30° . On the left side, we set an outflow boundary condition to allow the system to flow.

The volume fraction plots can be seen on Figure 6.8. In the early stage of the process, the system moves from its initial hypoplastic steady state to yield. This happens very quickly, since at $t = t_f/6$, the system is already flowing in the kinetic regime. A small perturbation appears and can be seen from $t = 2/12t_f$ to $t = 5/12t_f$, which is induced by the extensional flow. At the end of the process, the block of sand has been transformed into a dilute layer flowing on the plate. These results show that one can apply the EKM (with hypoplastic regime) to model the transition from the solid state to flow regime. If the system is initially at rest, the stress state can be reasonably assumed to be inside the yield surface.

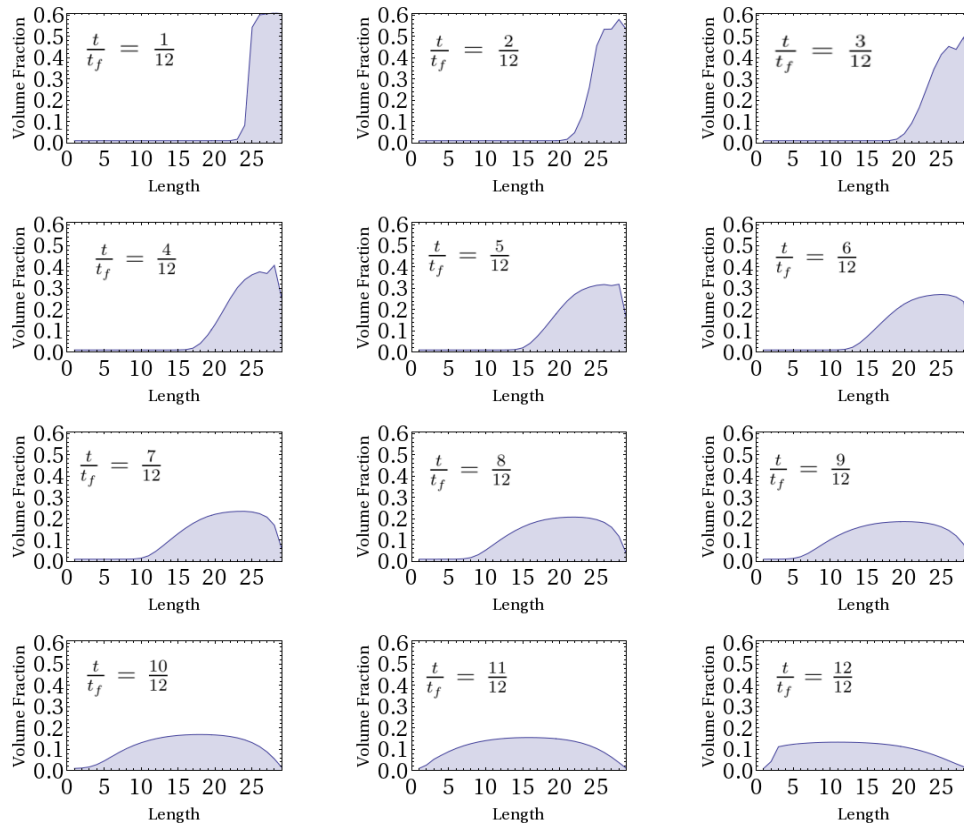


Figure 6.8: Plot of the volume fraction profiles during the flow of a sand column. Length in m

7

Conclusion

In this work, we developed hydrodynamic models to describe dry granular systems. We show that a general granular hydrodynamic model with relatively simple constitutive equations can recover a lot of non-trivial effects and flow regimes. Several flow regimes or properties which have been simply deduced from our model, have been attributed to more complicated features of granular flows in the literature. For instance, we demonstrated that a compressible hydrodynamic model built to account for dilute and dense flow can reproduce the formation of sand piles with predictive angle of repose and the correct pressure distribution. This work synthesizes and build some link between recent advanced theories made by engineers and physicists. Additionally, we show pioneered numerical results, where the three regimes, i.e the dilute, dense flow and rate-independent quasi-static, can be simultaneously simulated.

We started from a hydrodynamic model valid for dilute flow and extended its applicability to the quasi-static regime. In the first part, we introduced a continuum mechanical model valid for dilute and dense granular flows, called Extend Kinetic Model (EKM). It is composed of the mass, momentum and granular temperature equations. In the dilute regime, the constitutive relations are chosen to be similar to those proposed by Bocquet to model shear bands [65]. The viscosities and transport coefficients vary with the square root of the granular temperature and diverges at maximum packing. The kinetic pressure reduces to that of a gas at low volume fraction and diverges at maximum packing. Since the validity of kinetic models is questionable at larger dissipation, we modified the constitutive relations to account for the dense flow regime. Like in the work of Latz and Schmidt [3,4], a rate-independent pressure was introduced above a cross-over volume fraction. Viscosities and transport coefficients were extended so that they diverge at vanishing granular temperature, with the dependence found by Savage [5].

We called this hydrodynamic model EKM, for Extended Kinetic Model.

In the second part, a rich diversity of behavior was found by studying the flow regimes of the EKM. In the literature constitutive relations have been formulated from experiments based on the study of steady uniform flows. We underlined that the EKM covers some of these well-identified behavior. We recalled in a simple way that it covers Bagnold's scaling in the dilute flow regime. The study of frictional properties in the rapid dense shear flow regime, showed how the constitutive equations can be modified to be consistent with the frictional law observed by Pouliquen et al [31].

We intensively analyzed the high-density quasi-static regime. We found that in this regime, the EKM reduces to a critical-state plastic model. In the steady uniform limit, the granular temperature is proportional to the square of the strain rate. By substituting its value into the stress-strain relation, the stress-strain relation exhibits a viscoplastic behavior. We pointed out that similar laws have been proposed by fluid rheologists to model the slow frictional motion of powders. By inverting the stress-strain rate relation, we can identified the flow rule and the yield surface. Thus, the EKM implicitly contains a rate-independent plastic regime, which occur in the limit of vanishing granular temperature.

Following this, we identified the asymptotic behavior, a well-known feature of granular materials. The isochoric critical state is solution of the hydrodynamic equations. This allows us to define the critical internal friction angle as a function of the material parameters. Dilative asymptotic states and compressive asymptotic states, which are generally observed in experiments, were also identified as solution of the EKM. Additionally, we established the dependence of the friction coefficient on the rate of dilation.

As an illustrative example, we performed a 2D filling simulation using the finite volume software CoRheoS. We modeled the filling of some granular system into a plate with the EKM. As in the simulation of Latz and Schmidt [3, 4], one can reproduce the formation of sand piles and its slope vary from a few degrees to the internal friction angle in the critical state. Remarkably, we showed that the pressure distribution inside the pile exhibits a dip at the center. This phenomena has already been experimentally identified and recognized as a striking feature of granular materials. Its explanation is often discussed in the literature and still subject to debates. In our numerical simulation, the inhomogeneous density distribution implied by the filling process creates a pressure dip. This tends to validate the hypothesis previously formulated in the literature that small density variations create the pressure dip. Further investigations should focus on a numerical study of the influence of the filling process on the quasi-static stress distributions. It is a crucial information to know that an extended kinetic model with simple

constitutive relations can reproduce this phenomena. In the literature, the pressure dip has been often attributed to more complicated features.

Furthermore, we identified the shortcomings of the EKM. The choice of the constitutive relations requires a non-vanishing granular temperature to avoid a divergence of the transport coefficients. Static states were identified as asymptotic static limits for diverging transport coefficients but cannot be reached in numerical simulations. In the quasi-static regime, the system is constrained to flow at yield. Additionally, numerical instabilities can appear since viscosities are becoming very large. We also emphasized that a stress discontinuity may appear is the system moves from loaded to unloaded states. Furthermore, the critical state can be approached by a dilute system becoming denser, but there is no way to model the evolution from a static state to the critical state.

In the third part, we made investigations to overcome these shortcomings. Three different scenarios were investigated. The simplest one consists of adding a rigid solid behavior. In these zones, the strain rate is set to zero and no stress is computed. This is a basic simplification which neglects the initial quasi-elastic regime. It is easy to implement and can also be seen as an interesting practical solution to avoid numerical instabilities.

A second possibility is to include a quasi-elastic regime into the EKM. We proposed to combine the EKM with the hyperelastic law of Jiang and Liu [7]. We showed that an initial elastic strain can be calculated which ensures a continuous transition between both regimes. A possible solution is to describe the material behavior as quasi-elastic inside the yield surface and plastic at yield, as currently done in the classical elasto-plasticity framework. However the yield surface of the EKM does not coincide exactly with the unstable zone of the elastic energy of Jiang and Liu, and further investigations must be performed to develop a consistent model.

Alternatively, one can include a hypoplastic regime inside the EKM. Hypoplastic laws are based on the formulation of only one rate-equation between the derivative of the stress and of the strain. Despite this simple formalism, they reproduce effects like yield, critical states, Reynolds dilatancy and history dependence. We designed a hypoplastic law which reproduces in its limit state the same properties of the EKM in its quasi-static limit to ensure the consistency of both descriptions. In this model the limit state is employed to make a distinction between flowing and solid-like behavior. It is not used to distinguish reversible and irreversible like in plasticity theories. The hypoplastic law has a similar form to that of Wolffersdorff [59]. However, the 4th order tensor L_{ijkl} was chosen to have a simpler form, and further investigations must be made to qualitatively evaluate the influence of this choice. We underlined also that other choices of hypoplastic law are

possible.

The EKM completed with the hypoplastic regime presents a closed set of equations to describe granular systems from dilute flow to static state. It includes Bagnold scaling in the dilute collisional regime, slow viscoplastic motion and quasi-static behavior. It is a relevant choice to describe industrial processes where several regimes occur, like flow in silos or mixing processes. Although it may not contain the size-grain effects observed in granular systems due to the nature of the hydrodynamic approach, it contains a lot of effects which play a major role in many industrial applications.

In the last part, we developed a numerical method to solve a one dimensional version of the full hydrodynamic model. From a mathematical point of view, approximating the solution of our model is a very complex task. It implies non constant viscosities and transport coefficients. Huge compressibility variation can appear between the different regimes. We developed a flux-conservative numerical scheme, based on the centered finite differences with explicit time integration. Convective terms are evaluated with a Donor-Cell scheme [147] and the momentum equation is solved on a staggered grid. The algorithm was implemented into the computer algebra system *Mathematica 8.0*.

Finally we present a basic validation of the code on some typical problems. We performed a filling experiment where kinetic, dense and critical plastic flows occur. We can also qualitatively reproduce a sand column flowing on an inclined plane. These results are very promising and further investigations must be performed to give a more quantitative validation. The numerical method employed fails for problem involving shocks. This may be overcome by employing some high resolution scheme with total variation diminishing limiters. Further development should focus on granular flow problems involving shock waves and adapt the numerical method to efficiently treat these cases.

Appendix A

Some properties of the granular solid

A.1 Basic properties

Reynolds dilatancy First defined by Reynolds in 1885 [9], dilatancy designs the volume changes associated with shear distortion in a granular system. It can be qualitatively understood by considering layers of compact spheres as in the Figure A.1. To sustain shear, grains must roll or slide over each other, what leads to an expansion of the overall volume. Reynolds dilatancy is a common phenomena observed in soil mechanics and a detailed review can be found in [17]. This phenomena depends strongly on the initial

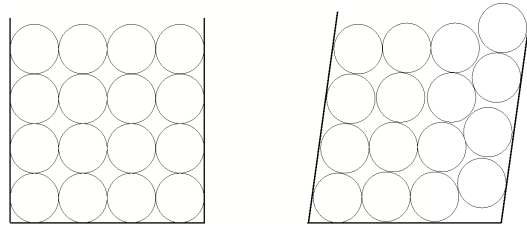


Figure A.1: Layers of compact spheres under shear forces.

condition of the grains: if the system have been set up in a loose state of packing, a reduction of the volume can be observed. This property is called contractancy.

Contact mechanics and effective elastic moduli Granular Matter is composed of many grains which are in contact and can be deformed. Con-

tact mechanics is focused on stresses and deformations which occur when solids are in contact. The pioneering work of Hertz [148] about frictionless contacts of two elastic bodies is still a reference for mechanical engineers. The Hertz model has been extended to complicated geometries and used to derive constitutive laws. The main result of the Hertz theory is presented here, and a detailed review can be found in [46]. Consider two elastic spheres of radius R which are in contact, as shown in Figure A.2. If these two bodies are pressed together with a force F , deformations occur near the point of contact. Hertz showed that the radius of the circular contact area a , where deformation occur, depends on the displacement δ which is given as

$$\delta = \frac{a^2}{R}. \quad (\text{A.1.1})$$

The relation between force and displacement is non-linear

$$F \sim \sqrt{R}\delta^{3/2}. \quad (\text{A.1.2})$$

When grains deform, an elastic energy W_e is accumulated, which can be evaluated by integrating the product of the force and the displacement over the volume of the sphere

$$W_e \sim \sqrt{R}\delta^{5/2}. \quad (\text{A.1.3})$$

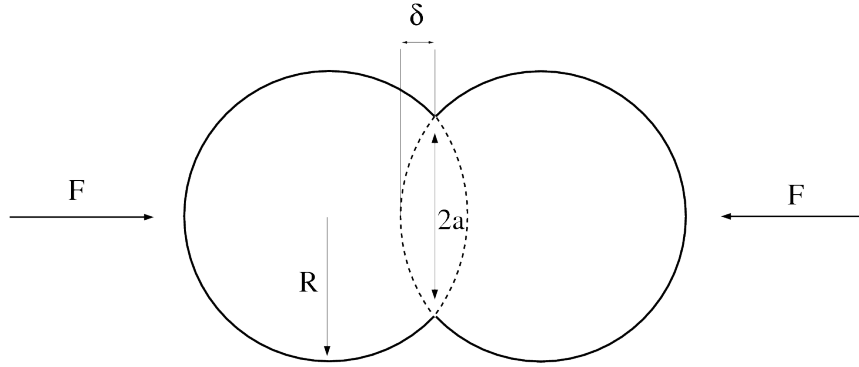


Figure A.2: Two elastic spheres of radius R in contact.

Although the two spheres are elastic, the applied forces do not vary linearly with the displacement. An increase of them leads to an increase of the contact area and of the stiffness of the material.

The case of spheres subject to tangential forces is more complicated but has been studied by Mindlin [149]. He found that the work depends on the loading path. Different behaviors are observed if the system is first sheared

and then compressed or the contrary. The Effective Medium Theory is based on the Hertz-Mindlin description. Expressions of the effective shear and bulk modulus have been proposed. These parameters are found to vary with the pressure in $P^{1/3}$. However, some disagreements have been observed with experiments where dependences in $P^{1/2}$ are measured. Several explanations based on micro-mechanical considerations have been proposed. The presence of shell oxide layers between the grains is a possible reason [150]. This issue is still controversial.

Granular Random packings Random packings have been intensively studied in the last few years. This topic is still a major challenge of the condensed matter physics. The study of packings provide reliable information about the microscopic structure of materials like glasses, simple liquids, amorphous solids or granular systems. Random compaction has been studied by shaking spheres vertically in a box. Experimental and numerical investigations have allowed the calculation of relevant parameters. Finney [151], following the work of Bernal [152], performed computer simulations for packings containing particles of different geometries. He showed that a random packing of spheres cannot have a volume fraction greater than 0.64. The maximal volume fraction of particles randomly packed is called the random-close-packing, $\hat{\rho}_{cp}$. For hexagonal packings, it reaches the value of 0.74. This is the greatest possible packing that can be obtained for spherical particles. In 2D, it reaches the value of 0.84.

The definition of the random loose packing $\hat{\rho}_{lp}$ is more difficult. It is sometimes assumed to be the loosest possible packing which remains mechanically stable. Onoda et al. [153] identified it as the lowest possible density than can be obtained in a vanishing gravitation field. Immersing glass spheres in a liquid, whose density was modified to minimize the effect of gravity, they found a value of 0.56.

Incremental non-linearity For any plastic material, the stiffness is larger when the material is unloaded than when it is loaded [92]. This can qualitatively illustrated on the Figure A.3. If a plastic material is loaded until the point P, the stress change is then greater when the material is unloaded than still loaded. As a consequence, $d\sigma$ cannot be linear on $d\epsilon$. This property is generally called incremental non-linearity.

Critical state plasticity An advanced theory about the behavior of soils under shearing was developed in 1968 and is called the "Soil critical state theory" [56]. It starts from the observation that when a granular system is

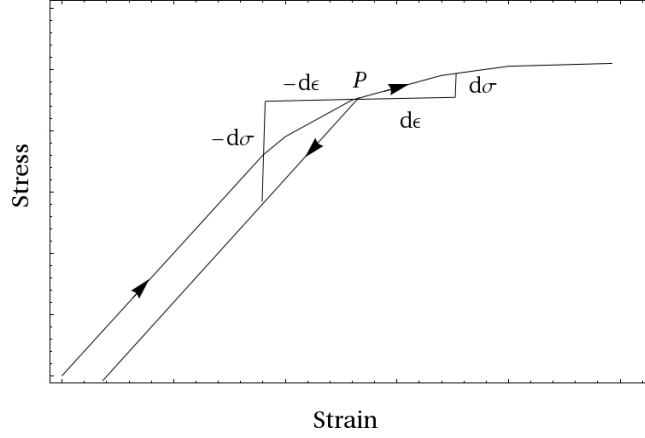


Figure A.3: Typical stress-strain relation for loading and unloading of a plastic material

continuously and slowly sheared until it flows, it reaches a stationary state independent of the initial conditions, called critical state. In soil mechanics, it is current practice to characterize soils with their stress state and void ratio e , defined as the ratio between the volume of void space and the solid volume.

During a triaxial test, the mean pressure P is generally kept constant and a shear strain is applied. The deviator stress is given by $q = \sigma_1^p - \sigma_3^p$, where the superscript p stands for the principal stresses. Starting from a dense system, it reaches a maximum before it tends to the critical value q_c . Then, the system dilates until the void ratio e_c is reached. In dilute systems, q increases monotonically and contracts to reach the critical void ratio e_c . This is illustrated in Figure A.4. The critical state doesn't depend on the initial concentration and is fully characterized by the two values q_c and e_c which depend on the pressure.

A.2 Hypoplastic law of Wolffersdorff

One of the most employed hypoplastic law was formulated by Wolffersdorff [59]. It incorporates the Matsuoka/Nakai yield surface and pressure and density dependences. It starts from the rate equation

$$\frac{\partial \sigma_{ij}}{\partial t} = L_{ijkl} \kappa_{kl} + N_{ij} \sqrt{\kappa_{ij}^D \kappa_{ij}^D + \kappa_{ll}^2},$$

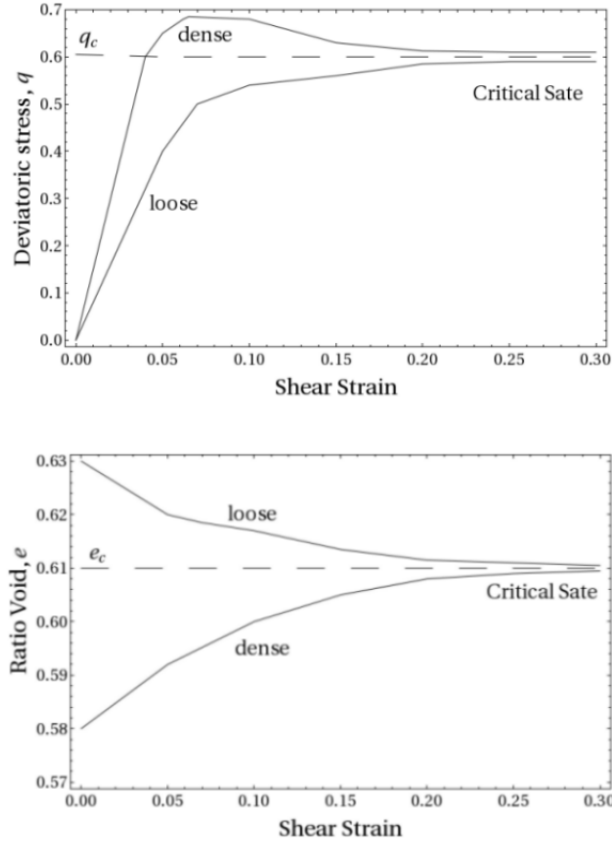


Figure A.4: Typical variation of the shear stress and bulk density with the shear strain for dense and dilute soils, subjected to shear deformations. q in MPa. Picture inspired from [154].

where L_{ijkl} specifies the linear dependence on the stress rate and strain state and N_{ij} the non-linear one. Both are a function of the effective stress tensor σ_{ij} and the density. Determining the expression of the involved tensor is sometimes called "calibration" or "parameter identification" and requires the set up of one or several triaxial tests. A recent set of coefficients was proposed

$$L_{ijkl} = \frac{f_b f_e}{\hat{\sigma}_{mn} \hat{\sigma}_{mn}} \left(F^2 \delta_{ij} \delta_{kl} + a^2 \hat{\sigma}_{ij} \hat{\sigma}_{kl} \right),$$

$$N_{ij} = f_b f_e \frac{F a}{\hat{\sigma}_{kl} \hat{\sigma}_{kl}} \left(\hat{\sigma}_{kl} + \hat{\sigma}_{kl}^D \right),$$

where $\hat{\sigma}_{kl} = \sigma_{kl}/\sigma_{ll}$. The coefficients a and F can be related to the friction angle ϕ in the critical state and determine the critical state surface

$$a = \sqrt{\frac{3}{8}} \frac{(3 - \sin(\varphi))}{\sin(\varphi)},$$

$$F = \sqrt{\frac{1}{8} \tan^2 \psi + \frac{2 - \tan^2 \psi}{2 + \sqrt{2} \tan \psi \cos(3\theta)}} - \frac{1}{2\sqrt{2}} \tan \psi,$$

with $\tan \psi = \sqrt{3 \hat{\sigma}_{ij}^D \hat{\sigma}_{ij}^D}$ and $\cos(3\theta) = -\sqrt{6} \frac{\hat{\sigma}_{ij}^D \hat{\sigma}_{jk}^D \hat{\sigma}_{ki}^D}{[\hat{\sigma}_{mn} \hat{\sigma}_{mn}]^{1.5}}$, where θ is the Lode angle. Coefficients f_b is the barotropy factor which describes a pressure dependence and results from the consistency equation implied by (5.3.1). f_d and f_e are called pycnotropy factors because they model the density dependence and are both exponential functions

$$f_d = \left(\frac{e - e_d}{e_c - e_d} \right)^\alpha,$$

$$f_e = \left(\frac{e_c}{e} \right)^\beta,$$

$$f_b = \frac{h_s}{n} \left(\frac{1 + e_i}{e_i} \right) \left(\frac{e_{i0}}{e_{c0}} \right)^\beta \left(\frac{-3\sigma_{ll}}{h_s} \right)^{1-n} \left[3 + a^2 - a\sqrt{3} \left(\frac{e_{i0} - e_{d0}}{e_{c0} - e_{d0}} \right)^\alpha \right]^{-1},$$

where e_c is the critical void ratio, e_{c0} is the critical void ratio at zero stress, e_d the void ration at maximal density, e_{d0} the void ration at maximal density at zero stress, e_{i0} and e_i characteristic void ratio at minimum density, h_s the granular stiffness, n , α and β additional constants. The characteristic void ratio obey

$$\frac{e_i}{e_{i0}} = \frac{e_c}{e_{c0}} = \frac{e_d}{e_{d0}} = \exp \left(- \left(\frac{\sigma_{ll}}{h_s} \right) \right).$$

This constitutive law has been used in many numerical simulations and gives quantitative agreements with triaxial, biaxial and oedometric tests [59].

Appendix B

Pressure profile in sand piles

In the Jiang-Liu hyperelastic model [7] (see also part 5) the stress-strain relation is given by

$$\sigma_{ij}(\varepsilon_{kl}) = -\frac{\partial W}{\partial \varepsilon_{ij}} = B\Delta^{3/2}\delta_{ij} + \frac{A\varepsilon_s^2\delta_{ij}}{2\sqrt{\Delta}} - 2A\sqrt{\Delta}\varepsilon_{ij}^D. \quad (\text{B.0.1})$$

This relation completed with the static force balance equation provide a close set of equation that can be employed to calculate static stress distributions. In [129], we considered a 2D triangular domain subjected to its own weight. As boundary conditions, grains are glued at the bottom of the sand pile $\partial\Omega_2$ and the normal stress equals to zero on the free surface of the pile $\partial\Omega_1$. The boundary value problem is given by

$$\left\{ \begin{array}{ll} \frac{\partial \sigma_{ij}}{\partial x_j} = \rho g_i & \text{in } \Omega \\ \sigma_{ij}n_j = 0 & \text{in } \partial\Omega_1 \\ u_i = 0 & \text{in } \partial\Omega_2 \\ \sigma_{ij} = B\Delta\sqrt{\Delta}\left(1 + \frac{\varepsilon_s^2}{2\Delta^2\xi}\right)\delta_{ij} - \frac{B\sqrt{\Delta}}{\xi}\varepsilon_{ij}^D & \text{in } \Omega \\ \varepsilon_{ij} = \frac{1}{2}\left(\frac{\partial u_i}{\partial x_j} + \frac{\partial u_j}{\partial x_i}\right) & \text{in } \Omega \end{array} \right.$$

This problem has been solved by the author by implementing a Newton-Raphson method into the finite element freeware FreeFem++ [137] and the obtained pressure distribution can be seen on Figure B.1 and B.2.

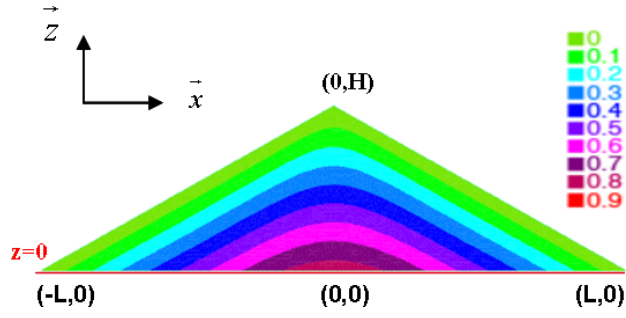


Figure B.1: Normalized pressure $\sigma_{zz}/\rho g H$.

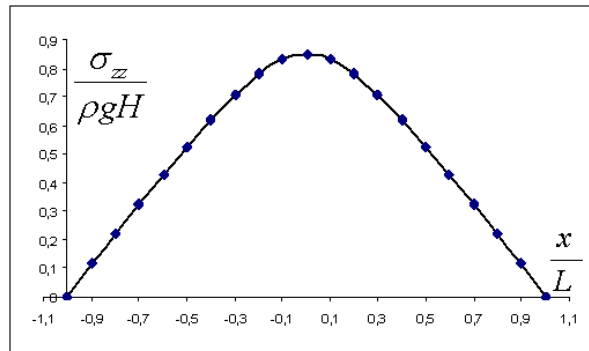


Figure B.2: Normalized pressure $\sigma_{zz}/\rho g H$ at the bottom of the pile.

Notation

Acronyms

EKM	Extended Kinetic Model
CoRheoS	Complex Rheology Solver
PDE	Partial Differential Equation

List of Symbols

A	First elastic constant of the Jiang-Liu hyperelastic law.....	82
B	Second elastic constant of the Jiang-Liu hyperelastic law	82
A_h	Material parameter introduced in the hypoplastic law	98
B_h	Material parameter introduced in the hypoplastic law	98
C_{ijkl}	4th-order stiffness tensor	84
c_p	Specific heat at constant pressure	18
e	Void ratio	95
f_Y	Yield surface	44
g	Plastic potential	44
g_i	Gravitation field	22
$g(.)$	Radial distribution function	24
\tilde{N}_{ij}	2nd-order tensor introduced in the elasto-plastic law	85
N_{ij}	2nd-order tensor of the hypoplastic law	95
L_{ijkl}	4th-order tensor of the hypoplastic law	95
P	Pressure	29
\tilde{P}	Dissipative pressure	47
P_t	Total pressure	47
P_K	Kinetic pressure	24
P_Y	Yield pressure	29
q_i	Heat flux	23
R	Ratio of viscous heating and dissipation	25
T	Granular temperature	23

T_0	Material parameter of the EKM	29
u_i	Displacement vector	81
v_i	Velocity vector	15
W	Elastic strain energy density	81
β	Rate of dilation	43
$\dot{\gamma}$	Shear rate	25
ε_{ij}	Total strain	23
ε_{ij}^D	Deviatoric strain	82
ε_s	Second deviatoric strain invariant	82
η	Shear viscosity	23
Θ	Function introduced to specify the existence of an elastic strain ..	87
θ	Dilatancy angle	43
ϵ_K	Kinetic loss energy rate	24
η_K	Kinetic shear viscosity	24
η_Y	Yield shear viscosity	29
η_0	Viscosity coefficient	24
ϵ	Loss energy rate	24
ϵ_K	Kinetic Loss energy rate	24
ϵ_Y	Yield Loss energy rate	29
ϵ_0	Dissipation coefficient	24
κ_{ij}	Strain rate	23
κ_{ij}^D	Deviatoric strain rate	23
λ	Thermal conductivity	23
λ_K	Kinetic thermal conductivity	24
λ_Y	Yield thermal conductivity	29
λ_0	Material constant	24
μ	Internal friction coefficient	48
μ_s	Static friction coefficient	36
ζ_K	Kinetic bulk viscosity	24
ζ_Y	Yield bulk viscosity	29
ζ_0	Bulk viscosity coefficient	24
ξ	Elastic constant in the Liu model	82
ρ	Volume fraction	15
ρ_c	Critical density	49
ρ_{co}	Cross over density	29
ρ_{cp}	Random close density	24
ρ_b	Bulk density	89
σ_s	Shear stress	35
$\sigma_{s,K}$	Kinetic shear stress	54

σ_{ij}	Cauchy stress tensor	23
$\tilde{\sigma}_{ij}$	Dissipative stress tensor	22
σ_{ij}^D	Deviatoric stress tensor	42
ϕ	Internal angle of friction	50
χ	Parameter introduced in the elasto-plastic model	85
Δ	Elastic compression	82

Bibliography

- [1] N. V. Brilliantov and T. Pöschel. *Kinetic theory of granular gases*. Oxford Graduate Texts. Oxford University Press, Berlin, 2003.
- [2] G. I. Tardos. A fluid mechanistic approach to slow, frictional flow of powders. *Powder Technology*, 92(1):61–74, 1997.
- [3] A. Latz and S. Schmidt. Hydrodynamic modeling of dilute and dense granular flow. *Granular Matter*, 12:387–397, 2010.
- [4] S. Schmidt. *On numerical simulation of granular flow*. PhD thesis, University of Kaiserslautern, Department of Mathematics, 2009.
- [5] S. B. Savage. Analyses of slow high-concentration flows of granular materials. *Journal of Fluid Mechanics*, 377:1–26, 1998.
- [6] D. Niedziela and A. Latz. Numerical simulation of sand-air mixture for the casting industry. 2008.
- [7] Y. Jiang and M. Liu. A brief review of granular elasticity. *Phys. Rev. E*, 22(3):250–260, Dec 2007.
- [8] D. Kolymbas. *Introduction to hypoplasticity*. Balkema, Rotterdam, 2000.
- [9] O. Reynolds. On the dilatancy of media composed of rigid particles in contact, with experimental illustrations. *Phil. Mag. Series 5*, 20:469–481, 1996.
- [10] C. A. Coulomb. Essai sur une applicaton des règles de maximis et minimis à quelque problèmes de statique, relatifs à l’architecture. *Mem. Academ. Roy*, 1776.
- [11] C. W. Hirt, A. A. Amsden, and J. L. Cook. An arbitrary lagrangian-eulerian computing method for all flow speeds. *Journal of Computational Physics*, 14(3):227 – –253, 1974.

- [12] P. G. de Gennes. Granular matter: a tentative view. *Rev. Mod. Phys.*, 71(2):374–382, Mar 1999.
- [13] R. M. Nedderman. *Static and kinematics of granular materials*. Cambridge University, 1992.
- [14] P. Lettieri, R. Di Felice, R. Pacciani, and O. Owoyemi. CFD modelling of liquid fluidized beds in slugging mode. *Powder Technology*, 167(2):94–103, 2006.
- [15] J. M. Valverde, M. A. S. Quintanilla, A. Castellanos, and P. Mills. Experimental study on the dynamics of gas-fluidized beds. *Phys. Rev. E*, 67:016303, Jan 2003.
- [16] N. Borderies, P. Goldreich, and S. Tremaine. A granular flow model for dense planetary rings. *Icarus*, 63:406, 1985.
- [17] J. Duran. *Sands, Powders, and Grains: An Introduction to the Physics of Granular Materials*. Partially Ordered Systems. Springer, 2000.
- [18] H. A. Janssen. Getreidedruck in silozellen. *Z. Ver. Dtsch. Ing 39.*, pages 1045–1049, 1895.
- [19] C. J. Brown and J. Nielsen. *Silos: fundamentals of theory, behavior, and design*. E & FN Spon, 1998.
- [20] S. Friedmann, N. Taberlet, and W. Losert. Rock-avalanche dynamics: insights from granular physics experiments. *International Journal of Earth Sciences*, 95:911–919, 2006. 10.1007/s00531-006-0067-9.
- [21] C. Ancey. Plasticity and geophysical flows: A review. *Journal of Non-Newtonian Fluid Mechanics*, 142(1-3):4–35, mar 2007.
- [22] R. A. Bagnold. *The Physics of Blown Sand and Desert Dunes*. Dover Publications, Inc, Mineola, New York, 1941.
- [23] P. Mériaux, P. Royet, and C. Folton. *Surveillance, entretien et diagnostic des digues de protection contre les inondations: Guide pratique à l’usage des propriétaires et des gestionnaires*. Cemagref, 2003.
- [24] P. Shiva and C. Kroener. Shock waves in rapid flows of dense granular materials: theoretical predictions and experimental results. *Phys Rev E Stat Nonlin Soft Matter Phys*, 2008.

- [25] P. Eshuis, K. Weele van der, D. Meer van der, Bos. R., and D. Lhose. Phase diagram of vertically shaken granular matter. *Physics of Fluids*, 19(12):123301, 2007.
- [26] L. B. Loeb. *The Kinetic Theory of Gases*. Dover phoenix editions. Dover Publications, 2004.
- [27] O. Pouliquen. Les milieux granulaires entre fluide et solide, 2001. Cours donné à l'ENSTA et l'IUSTI.
- [28] P. Kadanoff. Built upon sand: Theoretical ideas inspired by granular flows. *Review of Modern Physics*, 71(1):435–444, Jan 1999.
- [29] C. S. Campbell. Rapid granular flows. *Annual Review of Fluid Mechanics*, 22(1):57–92, 1990.
- [30] J.-P. Bardet. *Experimental soil mechanics*. Dover phoenix editions. Prentice Hall, 1997.
- [31] O. Pouliquen. Flows of dense granular media. *Annual Review of Fluid Mechanics*, 40:1–24.
- [32] R. Patrick, P. Philippe, B. Fabrice, S. Bourlès, X. Thibault, and D. Bideau. Analysis by X-ray micro tomography of a granular packing undergoing compaction. *Phys. Rev. E*, 68:020301, Aug 2003.
- [33] J. Crassous. Diffusive wave spectroscopy of a random close packing of spheres. *The European Physical Journal E: Soft Matter and Biological Physics*, 23:145–152, 2007. 10.1140/epje/i2006-10079-y.
- [34] T. S. Komatsu, S. Inagaki, N. Nakagawa, and S. Nasuno. Creep motion in a granular pile exhibiting steady surface flow. *Phys. Rev. Lett.*, 86(9):1757–1760, Feb 2001.
- [35] G. W. Baxter. Stress distributions in a two dimensional granular material. In R. P. Behringer and J. T. Jenkins, editors, *Powders and Grains 97*. Balkema, Rotterdam, 1997.
- [36] P. Dantu. Étude expérimentale d'un milieu pulvérulent. *Ann. Ponts Chauss.*, IV:193–202, 1967.
- [37] D. Howell, R. P. Behringer, and C. Veje. Stress fluctuations in a 2D granular couette experiment: A continuous transition. *Physical Review Letters*, 82(26):5241–5244, jun 1999.

- [38] R. Kuwano and R. F. Jardine. On the applicability of cross anisotropic elasticity to granular materials at very small strains. *Géotechnique*, 52:727–750, 2002.
- [39] B. Andreotti. Sonic sands. *Reports on Progress in Physics*, 75(2):026602, 2012.
- [40] R. Kaianauskas, R. Baleviius, D. Markauskas, and A. Maknickas. Discrete element method in simulation of granular materials. In G. M. L. Gladwell, R. Moreau, and P. Eberhard, editors, *IUTAM Symposium on Multiscale Problems in Multibody System Contacts*, volume 1 of *IUTAM Bookseries*, pages 65–74. Springer Netherlands.
- [41] G. G. W. Mustoe. A generalized formulation of the discrete element method. *Engineering computations*, 9:181–190, 1992.
- [42] G. H. Shi. On discontinuous deformation analysis. *First international forum on discontinuous deformation analysis*, 1996.
- [43] S. Schmidt, A. Latz, D. Niedziela, R. Weiler, and S. Ripperger. Comparison of the discrete element method with a finite volume approach for predicting bulk flows and for designing silos. In *Proceeding of the 6th World Congress on Particel technology (WTC6)*.
- [44] F. Bertrand, L.-A. Leclaire, and G. Levecque. DEM-based models for the mixing of granular materials. *Chemical Engineering Science*, 60(89):2517 – 2531, 2005.
- [45] L. D. Landau and E. M. Lifschitz. *Fluid mechanics*, volume VI of *Lehrbuch der theoretischen Physik*. Akademie-Verlag, Berlin, 1978.
- [46] L. D. Landau and E. M. Lifschitz. *Theory of Elasticity*, volume VII of *Lehrbuch der theoretischen Physik*. Akademie-Verlag, Berlin, 1978.
- [47] J. Sliseris and K. Rocens. Optimal design of composite plates with discrete variable stiffness. *Composite Structures*, 98(0):15 – 23, 2013.
- [48] J. Sliseris, G. Frolovs, K. Rocens, and V. Goremikins. Optimal design of GFRP-plywood variable stiffness plate. *Procedia Engineering*, 57(0):1060 – 1069, 2013. Modern Building Materials, Structures and Techniques.
- [49] R. E. Rosensweig. *Ferrohydrodynamics*. Dover Books on Physics. Dover Publications, 1997.

- [50] O. Pouliquen and Y. Forterre. A non-local rheology for dense granular flows. *Philosophical Transactions of the Royal Society A: Mathematical, Physical and Engineering Sciences*, 367(1909):5091–5107, 2009.
- [51] D. Kolymbas. *Constitutive modelling of Granular Materials*. Springer, Berlin, 2000.
- [52] F. Nicot and F. Darve. On the elastic and plastic strain decomposition in granular materials. *Granular Matter*, 8:221–237, 2006. 10.1007/s10035-006-0012-4.
- [53] D. Kolymbas. *The misery of constitutive modelling*, pages 11–24. Constitutive Modelling of Granular Materials. Springer, 2000.
- [54] M. J. Boussinesq. Essai théorique sur l’équilibre des massifs pulvérulents comparé à celui des massifs solides, et sur la poussée des terres sans cohésion. *Mem. Academ. Sci*, 1874.
- [55] W. Ehlers. A single-surface yield function for geomaterials. *Archive of Applied Mechanics*, 65:246–259, 1995.
- [56] A. N. Schofield and P. Wroth. *Critical state soil mechanics*. Number vol. 1968,ptie. 2 in European civil engineering series. McGraw-Hill, 1968.
- [57] C. Truesdell. Hypoelasticity. *J. Rat. Mech. Analysis*, 4:83–133, March 1955.
- [58] B. Cambou, F. Dubujet, F. Emeriault, and F. Sidoroff. Homogenization for granular materials. *Eur. J. Mech. A/Solids*, 14(2):255–276, 1995.
- [59] P.-A. von Wolffersdorff. A hypoplastic relation for granular materials with a predefined limit state surface. *Mechanics of Cohesive-frictional Materials*, 1(3):251–271, 1996.
- [60] W. Wu and A. Niemunis. Failure criterion, flow rule and dissipation function derived from hypoplasticity. *Mechanics of Cohesive-frictional Materials*, 1(2):145–163, 1996.
- [61] P. Nott. Classical and Cosserat plasticity and viscoplasticity models for slow granular flow. *Acta Mechanica*, 205:151–160, 2009. 10.1007/s00707-009-0166-3.

- [62] J. Tejchman. *Shear Localization in Granular Bodies with Micro-Polar Hypoplasticity*. Springer Series in Geomechanics and Geoengineering. Springer, 2008.
- [63] E. Khain and B. Meerson. Symmetry-breaking instability in a prototypical driven granular gas. *Physical Review E*, 66(2):021306, Aug 2002.
- [64] V. Garzó and J. W. Dufty. Dense fluid transport for inelastic hard spheres. *Physical Review E*, 59(5):5895–5911, May 1999.
- [65] L. Bocquet, W. Losert, D. Schalk, T. C. Lubensky, and J. P. Gollub. Granular shear flow dynamics and forces: Experiment and continuum theory. *Physical Review E*, 65(1):011307, dec 2001.
- [66] D. Gidaspow. *Multiphase Flow and Fluidization: Continuum and Kinetic Theory Description*. Acad. Press, 1994.
- [67] L. Bocquet, J. Errami, and T. C. Lubensky. Hydrodynamic model for a dynamical jammed-to-flowing transition in gravity driven granular media. *Physical Review Letters*, 89(18):184301, Oct 2002.
- [68] Groupement De Recherche Milieux Divisés CNRS. On dense granular flows. *The European Physical Journal E: Soft Matter and Biological Physics*, 14:341–365, 2004. 10.1140/epje/i2003-10153-0.
- [69] O. Pouliquen. On the shape of granular fronts down rough inclined planes. *Physics of Fluids*, 11(7):1956–1958, 1999.
- [70] L. Srinivasa Mohan, P. R. Nott, and K. K. Rao. Fully developed flow of coarse granular materials through a vertical channel. *Chemical Engineering Science*, 52(6):913 – 933, 1997.
- [71] W. Zhonghua and A. S. Mujumdar. CFD modeling of the gas-particle flow behavior in spouted beds. *Powder Technology*, 183(2):260 – 272, 2008.
- [72] I. S. Aranson and L. S. Tsimring. Continuum theory of partially fluidized granular flows. *Phys. Rev. E*, 65:061303, Jun 2002.
- [73] D. Volfson, L. S. Tsimring, and I. S. Aranson. Partially fluidized shear granular flows: Continuum theory and molecular dynamics simulations. *Phys. Rev. E*, 68(2):021301, Aug 2003.

- [74] L. D. Landau and E. M. Lifschitz. *Statistical Physics*, volume 5 of *A Course of Theoretical Physics*. Pergamon Press, Berlin, 1969.
- [75] C. Leppert. *Mehrphasenmodell für granulare Medien zur numerischen Untersuchung des Phasenübergangs bei der Entleerung von Silos*. PhD thesis, TU Braunschweig, Institut für Statik, 2007.
- [76] Y. Jiang and M. Liu. Granular solid hydrodynamics. *Granular Matter*, 11:139–156, 2009.
- [77] M. Mayer and M. Liu. Propagation of elastic waves in granular solid hydrodynamics. *Phys. Rev. E*, 82:042301, Oct 2010.
- [78] S. Mahle, Y. Jiang, and M. Liu. The critical state and the steady-state solution in granular solid hydrodynamics. *ArXiv e-prints*, June 2010.
- [79] S. Mahle, Y. Jiang, and M. Liu. Granular solid hydrodynamics: Dense flow, fluidization and jamming. *ArXiv e-prints*, October 2010.
- [80] Y. Jiang and M. Liu. Compaction in granular solid hydrodynamics. *ArXiv e-prints*, November 2009.
- [81] G. Gudehus, Y. Jiang, and M. Liu. Seismo- and thermodynamics of granular solids. *Granular Matter*, 13:319–340, 2011. 10.1007/s10035-010-0229-0.
- [82] Y. Jiang and M. Liu. From elasticity to hypoplasticity: Dynamics of granular solids. *Phys. Rev. Lett.*, 99(10):105501, Sep 2007.
- [83] Y. Jiang and M. Liu. Energetic instability unjams sand and suspension. *Phys. Rev. Lett.*, 93(14):148001, Sep 2004.
- [84] D. O. Krimer, M. Pfitzner, K. Bräuer, Y. Jiang, and M. Liu. Granular elasticity: General considerations and the stress dip in sand piles. *Phys. Rev. E*, 74(6):061310, Dec 2006.
- [85] K. Bräuer, M. Pfitzner, D. O. Krimer, M. Mayer, Y. Jiang, and M. Liu. Granular elasticity: Stress distributions in silos and under point loads. *Phys. Rev. E*, 74(6):061311, Dec 2006.
- [86] Y. Jiang and M. Liu. Incremental stress-strain relation from granular elasticity: Comparison to experiments. *Phys. Rev. E*, 77(2):021306, Feb 2008.

- [87] J Spahn, H Andrä, M Kabel, and R Müller. A multiscale approach for modeling progressive damage of composite materials using fast fourier transforms. *Computer Methods in Applied Mechanics and Engineering*, 2013.
- [88] C. Hirsh. *Numerical computation of internal and external flows. Vol. 1 : Fundamentals of numerical discretization*. Wiley, 1990.
- [89] P. Tanseng. *Implementation of Hypoplasticity for Fast Lagrangian Simulations*. Logos Berlin, 2006.
- [90] A. Latz. Enthalpy equation: Temperature changes at constant pressure. ITWM Report, August 2006.
- [91] P. Jop, Y. Forterre, and O. Pouliquen. Crucial role of side walls for granular surface flows: consequences for the rheology. *Journal of fluid mechanics*, 541:167–192, 2005.
- [92] A. F. Bower. *Applied Mechanics of Solids*. CRC PressINC, 2010.
- [93] I. Goldhirsch. Rapid granular flows. *Annual Review of Fluid Mechanics*, 35:267–293, 2003.
- [94] P. K. Haff. Grain flow as a fluid-mechanical phenomenon. *Journal of Fluid Mechanics*, 134:401–430, 1983.
- [95] S. B. Savage. The mechanics of rapid granular flows. volume 24 of *Advances in Mechanics*, pages 289–366. Elsevier, 1984.
- [96] J. Jenkins and M. Richman. Kinetic theory for plane flows of a dense gas of identical, rough, inelastic, circular disks. *Physics of Fluids*, 28(12):3485, 1985.
- [97] A. Levy and H. Kalman. *Handbook of conveying and handling of particulate solids*. Handbook of powder technology. Elsevier, 2001.
- [98] S. Ogawa, A. Umemura, and N. Oshima. On the equations of fully fluidized granular materials. *Zeitschrift für Angewandte Mathematik und Physik (ZAMP)*, 31:483–493, 1980. 10.1007/BF01590859.
- [99] S. Luding. Towards dense, realistic granular media in 2d. *Nonlinearity*, 22(12):R101, 2009.
- [100] L. Lacaze and R. R. Kerswell. Axisymmetric granular collapse: A transient 3d flow test of viscoplasticity. *Phys. Rev. Lett.*, 102:108305, March 2009.

- [101] S. Sundaresan. Modeling the hydrodynamics of multiphase flow reactors: Current status and challenges. *AIChE Journal*, 46(6):1102–1105, 2000.
- [102] S. B. Savage. Granular flows down rough inclines — review and extension. In J. T. Jenkins and M. Satake, editors, *Mechanics of granular materials: new models and constitutive relations*, 1983.
- [103] K. Kamrin and M. Z. Bazant. Stochastic flow rule for granular materials. *Phys. Rev. E*, 75:041301, Apr 2007.
- [104] P. A. Shirvanian, J. M. Calo, and G. Hradil. Numerical simulation of fluid particle hydrodynamics in a rectangular spouted vessel. *International Journal of Multiphase Flow*, 32(6):739–753, 2006.
- [105] W. Shuyan, H. Zhenghua, S. Dan, L. Yikun, W. Lixin, and W. Shuai. Hydrodynamic simulations of gas-solid spouted bed with a draft tube. *Chemical Engineering Science*, 65(4):1322–1333, 2010.
- [106] A. Srivastava and S. Sundaresan. Analysis of a frictional kinetic model for gas particle flow. *Powder Technology*, 129(13):72 – 85, 2003.
- [107] A. de Ryck, H. P. Zhu, S. M. Wu, A. B. Yu, and P. Zull. Numerical and theoretical investigation of the surface flows of granular materials on heaps. *Powder technology*, 203:125–132, 2010.
- [108] Y. Forterre. Kapiza waves as a test for three-dimensional granular flow rheology. *Journal of Fluid Mechanics*, 563:123–132, 2006.
- [109] Y. Jiang and M. Liu. Granular solid hydrodynamics (GSH): from quasi-static motion to rapid dense flow. *ArXiv e-prints*, 2012.
- [110] E. B. Pitman and D. G. Schaeffer. Stability of time dependent compressible granular flow in two dimensions. *Communications on Pure and Applied Mathematics*, 40:421–447, 1987.
- [111] R. Jackson. Some mathematical and physical aspects of continuum models for the motion of granular materials. In *Theory of Disperse Multiphase Flow*, 1982.
- [112] P. A. Vermeer. Non-associated plasticity for soils, concrete and rock. In H. J. Herrmann, J. P. Hovi, and S. Luding, editors, *Physics of dry granular media - NATO ASI Series E350*, pages 163–197, Dordrecht, 1998. Kluwer Academic Publishers.

- [113] D. C. Drucker and W. Prager. Soil mechanics and plastic analysis for limit design. *Quarterly of Applied Mathematics*, 10(2):157–165, Nov 1952.
- [114] D. Masin. Asymptotic behaviour of granular materials. *Granular Matter*, pages 1–16, 2012.
- [115] H. Matsuoka and T. Nakai. Stress-strain relationship of soil based on the smp. *9th International Conference on Soil Mechanics and Foundation Engineering*, pages 153–162., 1997.
- [116] C. S. Desai and H. J. Siriwardane. A concept of correction functions to account for non-associative characteristics of geologic media. *International Journal for Numerical and Analytical Methods in Geomechanics*, 4(4):377–387, 1980.
- [117] G. R. McDowell. A simple non-associated flow model for sand. *Granular Matter*, 4:65–69, 2002. 10.1007/s10035-002-0106-6.
- [118] M. Lambrecht and C. Miehe. Two non-associated isotropic elastoplastic hardening models for frictional materials. *Acta Mechanica*, 135:73–90, 1999. 10.1007/BF01179047.
- [119] V. Garzó and J. W. Dufty. Dense fluid transport for inelastic hard spheres. *Physical Review E*, 59(5):5895–5911, May 1999.
- [120] D. R. Lowe. Grain flow and grain flow deposits. *Journal of Sedimentary Research*, 46(1):188–199, 1976.
- [121] Jun Ai. *Particle scale and bulk scale investigation of granular piles and silos*. PhD thesis, The University of Edinburgh, 2010.
- [122] L. Vanel, D. Howell, D. Clark, R. P. Behringer, and E. Clément. Memories in sand: Experimental tests of construction history on stress distributions under sandpiles. *Phys. Rev. E*, 60(5):R5040–R5043, Nov 1999.
- [123] J.-P. Bouchaud, M. E. Cates, and P. Claudin. Stress distribution in granular media and nonlinear wave equation. *Journal de Physique I*, 5(2):639–656, June 1995.
- [124] J. Wittmer, M. Cates, and P. Claudin. Stress propagation and arching in static sandpiles. *Journal de Physique I* 7, 1, pages 39–80, 1997.

- [125] P. W. Humrickhouse. *Hyperelastics model for granular materials*. PhD thesis, University of Wisconsin, Nuclear Engineering and and Engineering Physics, 2009.
- [126] L. Fusi and A. Farina. Modelling of bingham-like fluids with deformable core. *Comput. Math. Appl.*, 53(3–4):583–594, February 2007.
- [127] J. D. Goddard. Nonlinear elasticity and pressure-dependent wave speeds in granular media. *Proc. R. Soc. Lond. A*, 430(1878):105–131, Juli 1990.
- [128] G.D. Scott. *Nature (London)* 194 956, 1962.
- [129] C. Zemerli, A. Latz, and H. Andrä. Constitutive models for static granular systems and focus to the Jiang-Liu hyperelastic law. Technical Report 215, Fraunhofer (ITWM), 2012.
- [130] K. Kamrin. Nonlinear elasto-plastic model for dense granular flow. *International Journal of Plasticity*, 26:167–188, 2010.
- [131] J. D. Goddard. Parametric hypoplasticity as continuum model for granular media: from stokesium to mohr-coulombium and beyond. *Granular Matter*, pages 145–150, 2009.
- [132] Y. Jiang, H. Zheng, Z. Peng, L. Fu, S. Song, Q. Sun, M. Mayer, and M. Liu. Expression for the granular elastic energy. *Phys Rev E Stat Nonlin Soft Matter Phys*, 85(5-1):051304, 2012.
- [133] W. Wu and E. Bauer. A simple hypoplastic constitutive model for sand. *International Journal for Numerical and Analytical Methods in Geomechanics*, 18(12):833–862, 1994.
- [134] A. E. Green. Hypo-Elasticity and Plasticity. *Proceedings of The Royal Society A: Mathematical, Physical and Engineering Sciences*, 234:46–59, 1956.
- [135] R. Chambon, J. Desrues, W. Hammad, and Charlier R. CloE, a new rate-type constitutive model for geomaterials theoretical basis and implementation. *International Journal for Numerical and Analytical Methods in Geomechanics*, 18:253–278, 1994.
- [136] S. Toll. The dissipation inequality in hypoplasticity. *Acta Mechanica*, 221:39–47, 2011.

- [137] C. S. Bierwisch. *Numerical simulations of granular flow and filling*. PhD thesis, Fakultät für Mathematik und Physik der Albert-Ludwigs-Universität Freiburg im Breisgau, 2009.
- [138] K. Nübel and C. Karcher. FE simulations of granular material with a given frequency distribution of voids as initial condition. *Granular Matter*, 1:105–112, 1998. 10.1007/s100350050016.
- [139] J. Tejchman and W. Wu. Numerical simulation of shear band formation with a hypoplastic constitutive model. *Computers and Geotechnics*, 18(1):71–84, 1996.
- [140] J. Tejchman, I. Herle, and J. Wehr. FE-studies on the influence of initial void ratio, pressure level and mean grain diameter on shear localization. *International Journal for Numerical and Analytical Methods in Geomechanics*, 23(15):2045–2074, 1999.
- [141] D. Roddeman. FEM-implementation of hypoplasticity. Technical report, Institut für Geotechnik und Tunnelbau, Universität Innsbruck, 1997.
- [142] W. Fellin, M. Mittendorfer, and A. Ostermann. Adaptive integration of constitutive rate equations. *Computers and Geotechnics*, 36(5):698–708, 2009.
- [143] W. Fellin and A. Ostermann. Consistent tangent operators for constitutive rate equations. *International Journal for Numerical and Analytical Methods in Geomechanics*, 26(12):1213–1233, 2002.
- [144] S. V. Patankar. *Numerical heat transfer and fluid flow*. Hemisphere Publishing Corp., Washington, DC, 1980.
- [145] D. Niedziela. *On numerical simulations of viscoelastic fluids*. PhD thesis, University of Kaiserslautern, Department of Mathematics, 2006.
- [146] C. Hirsch. *Numerical Computation of Internal and External Flows: The Fundamentals of Computational Fluid Dynamics*. Number Bd. 1 in Butterworth Heinemann. Elsevier Science, 2007.
- [147] R. J. Leveque. *Numerical Methods for Conservation Laws*. Lectures in Mathematics ETH Zürich. Birkhäuser Verlag, 1992.
- [148] H. Hertz. *On Contact Between Elastic Bodies*, 92:156–171, 1882.

- [149] S. Ellák, J.-N. Roux, J. H. Snoeijer, M. van Hecke, and W. van Saarloos. Elastic wave propagation in confined granular systems. *Phys. Rev. E*, 72:021301, Aug 2005.
- [150] P.-G. de Gennes. Static compression of a granular medium: the soft shell model. *EPL (Europhysics Letters)*, 35(2):145, 1996.
- [151] J. Finney. Randoms packing and the structure of the liquid state. *Proc. Roy. Soc.*, 1970.
- [152] J. D. Bernal. *Proc. Roy. Soc. Instn.* 37, 355, 1959.
- [153] G. Y. Onoda and E. G. Liniger. Random loose packings of uniform spheres and the dilatancy onset. *Phys. Rev. Lett.*, 64(22):2727–2730, May 1990.
- [154] R. M. Iverson, M. E. Reid, and R. G. Lahusen. Debris-flow mobilization from landslides. *Annual Review of Earth and Planetary Sciences*, 25(1):85–138, 1997.

LEBENS LAUF

- 1985 Geboren in Tassin-la-Demi-Lune, Frankreich
- 2003 Wissenschaftliches Abitur,
Lycée du Parc, Lyon, Frankreich
- 2003 – 2005 Vorbereitungsstudium für die Aufnahmeprüfungen der
französischen Grandes Ecoles, Physik und Chemie,
Lycée du parc, Lyon, Frankreich
- 2008 Master im Maschinenbau mit einer Spezialisierung in
Verbrennungstechnik und Raketenantrieb
an der ENSTA-Bretagne (ehemalig-ENSIETA)
Brest, Frankreich
- 2008 – 2009 Befristeter Mitarbeit am Fraunhofer “Institut
für Chemische Technologie” (ICT), Karlsruhe, Deutschland
- 2009 – 2012 Doktorand am Fraunhofer “Institut für
Techno- und Wirtschaftsmathematik” (ITWM),
Kaiserslautern, Deutschland
- seit 2013 Wissenschaftlicher Mitarbeiter am
Fraunhofer ITWM, Kaiserslautern, Deutschland

CURRICULUM VITAE

- 1985 Born in Tassin-la-Demi-Lune, France
- 2003 Baccalauréat, Scientific section,
Lycée du Parc, Lyon, France
- 2003 – 2005 Two years secondary school preparation,
in advanced Physics and Chemistry
for the competitive entrance to French
Graduate Engineering schools, Lycée du Parc, Lyon
- 2008 Master degree in mechanical engineering
from ENSTA Bretagne (ex-ENSIETA) with
a specialization in propulsion and pyrotechnics,
Brest, France
- 2008– 2009 Research employee at the
“Fraunhofer Institute for Chemical Technology” (ICT),
Karlsruhe, Germany
- 2009 – 2012 PhD Student at Fraunhofer “Institute
for Industrial Mathematics” (ITWM),
Kaiserslautern, Germany
- since 2013 Scientific employee at Fraunhofer ITWM,
Kaiserslautern, Germany

